Journal Pre-proofs

Chlorine and Felsic Magma Evolution: Modeling the Behavior of an Under-Appreciated Volatile Component

James D. Webster, Alexander A. Iveson, Michael C. Rowe, Paul M. Webster

PII: S0016-7037(19)30745-8
DOI: https://doi.org/10.1016/j.gca.2019.12.002
Reference: GCA 11549

To appear in: *Geochimica et Cosmochimica Acta*

Received Date: 15 February 2018
Revised Date: 5 July 2019
Accepted Date: 1 December 2019

Please cite this article as: Webster, J.D., Iveson, A.A., Rowe, M.C., Webster, P.M., Chlorine and Felsic Magma Evolution: Modeling the Behavior of an Under-Appreciated Volatile Component, *Geochimica et Cosmochimica Acta* (2019), doi: https://doi.org/10.1016/j.gca.2019.12.002

Chlorine and Felsic Magma Evolution: Modeling the Behavior of an Under-Appreciated Volatile Component

James D. Webster*
Alexander A. Iveson†
Michael C. Rowe$
Paul M. Webster°

*Department of Earth and Planetary Sciences
AMNH, Central Park West at 79th Street
New York, NY 10024-5192 USA

†Department of Earth Sciences
Science Labs
Durham University
Durham DH1 3LE
UK
alexander.a.iveson@durham.ac.uk

$School of Environment
The University of Auckland
23 Symonds Street
Auckland, NZ 1142

°1325 West Estes Ave.
Chicago, Illinois
60626-5411 USA

†Corresponding Author

Submitted to **GCA**, February 16th, 2018
Revised version resubmitted July 5th, 2019

Abstract

Research on magmatic Cl has proven useful for understanding melt evolution, degassing, and other igneous processes. Magmatic Cl behavior varies strongly with its solubility in melt, and Cl solubility and its partitioning between melts and fluids vary with the Cl content of the system, melt composition, pressure, and the abundance of oxidized magmatic sulfur. Given these relationships and given that they differ from other magmatic volatiles, Cl can provide unique insights on magma evolution. We present a new method of interpreting melt Cl concentrations that are normalized to their calculated Cl solubilities, and the most accurate results apply to solubilities computed at 200 MPa due to insufficient experimental data for other pressures. We apply the new method to compositional data for more than 3500 dacitic to rhyolitic melt inclusions and matrix glasses, representing 64 felsic igneous systems, to demonstrate how the behavior of Cl during magmatic, magmatic-hydrothermal, and degassing processes can be more accurately interpreted.

Variations in Cl for most of the 64 systems agree with modeled Cl behavior indicative of melt evolution dominated by fractional crystallization of fluid(s)-saturated melts, and the majority of these systems were apparently saturated in fluid(s) well before melt inclusion entrapment. Comparison of Cl solubility-normalized Cl concentrations of these glasses with modeled results identifies magmas saturated in hydrosaline liquid ± vapor at pressures as high as 600 MPa. Modeling of pressure reductions from 600 down to 20 MPa distinguishes other magmas that exsolved hydrosaline liquid as magmas ascend to shallower depths. This new approach also supports computation of Cl concentrations of magmatic fluids at 200 MPa, for each of the > 3500 glasses, and shows how the Cl contents of fluids vary with the (fluid/melt) mass ratio. For example, Cl contents of magmatic fluids range from 0.3 to nearly 70 wt.% at fluid/melt mass ratios of $2x10^{-3}$, and from 0.3 to a maximum of only 11 wt.% Cl for fluid/melt mass ratios of $4.2x10^{-2}$.

Compositional trends in the glass data show either increasing Cl contents of residual melt, essentially no change of Cl in melt, or decreasing Cl contents of aliquots of residual melt with progressive melt evolution. This method identifies melts that have assimilated magmatic or externally sourced hydrosaline liquids. Plots of (measured Cl in melt/modeled solubility of Cl in melt; Cl[Me/Mo]) versus the Larsen melt differentiation index show minimal dispersion for the least-evolved dacitic melts and increasing dispersion with melt evolution to rhyolitic compositions. Increased dispersion may be a consequence and indication of equilibrium or non-equilibrium degassing and/or assimilation of hydrosaline liquid.

1. INTRODUCTION

This study describes the development of a geochemical tool for interpreting the Cl contents of MI and rapidly quenched matrix glasses to improve our understanding of volatile behavior during magma differentiation. We show how normalizing the measured Cl concentration of a quenched glass to the modeled solubility of Cl for its bulk melt composition at geologically relevant pressure and temperature conditions reduces ambiguity and provides a useful frame of reference for understanding magmatic Cl behavior. Identifying pulses of fluid-saturated magma, both intrusive and eruptive (Wallace et al., 1995), is essential for understanding a host of magmatic-hydrothermal processes. Accurate interpretation of buoyancy-driven fluid ascent and fluid accumulation at apices of plutons; component exchange between hydrothermal fluid, melt, and minerals; the deposition of genetically related magmatic-hydrothermal mineralization; and the explosive fragmentation and eruption of volatile-enriched melts requires unambiguous recognition of the presence of exsolved magmatic fluids. As magmatic fluid inclusions (FI) are rare in volcanic rocks and not particularly abundant in plutonic phenocrysts, geochemical observations rather than textural features (e.g., the presence of primary magmatic FI) have proven most useful for recognizing the presence of magmatic

fluids and interpreting their physical as well as chemical effects. Chlorine along with H_2O, CO_2, S, Li, B, and Cu (± K, Rb, Cs, Ba, U, and Pb) behave as variably fluid-mobile components at magmatic temperatures and have been variably applied in this regard. Studies of melt inclusions (MI) from felsic magmas (Devine et al., 1984; Wallace et al., 1999; Lowenstern 1993; Stix and Layne, 1996; Dunbar and Hervig, 1992a;b; Davidson and Kamenetsky, 2007) have determined geochemical relationships involving these components that reflect their sequestration by vapor ± hydrosaline liquid (or brine) and provide information on the timing, distribution, and consequences of magmatic fluid exsolution (e.g., Johnston, 1978; Lowenstern, 1994; Gerlach et al. 1994; Signorelli and Carroll, 2000; Davidson and Kamenetsky, 2001; Webster and Rebbert, 2001; Humphreys et al., 2010; Balcone-Boissard, 2016; Iacovino et al., 2016). Data derived from melt inclusions from more mafic systems have also been reviewed and interpreted using similar methods by Webster et al. (2018), and references therein.

Chlorine concentrations in increasingly evolved, residual fractions of felsic melt increase with magma differentiation (e.g., Katmai and Taupo, Wallace [2005]; Augustine [Webster et al., 2010]) and/or through exchange and transfer with fluids (Villemant and Boudon, 1999; Villemant et al., 2008). Although most non-alkaline mafic magmas contain less Cl than H_2O, CO_2, or S (Carroll and Webster, 1994; Wallace, 2005), modeling shows that Cl contents of some fluid-saturated felsic melts increase to levels exceeding those of CO_2 or S due to the stronger sequestration of the latter volatile components by vapor (and due to sulfide liquid or sulfide/sulfate mineral formation). With continued fractionation of fluid-saturated magma, the Cl concentrations of residual melt eventually increase, level off, or decrease due to Cl loss to the fluid(s). A consequence of this complexity is that some publications on magmatic Cl include ambiguous references to “high” versus “low” Cl in MI and the melts they represent. Equivocal characterizations like these hinder the interpretation of

volatile behavior during magma evolution because they describe relative rather than absolute concentrations. This is particularly problematic for Cl because its solubility in melt and its partitioning between melts, minerals, and fluids vary so strongly with melt composition and magmatic Cl contents (e.g. Doherty et al., 2014; Dalou et al., 2015; Iveson et al., 2017). A small number of studies have applied experimental solubility limits for Cl to track hydrosaline liquid exsolution for felsic magmas (Webster et al., 2015; Balcone-Boissard, 2016), but most others have not accounted for the fundamental control of melt composition on Cl dissolution in silicate melts and coexisting fluids. Modeled Cl solubilities represent maximum values that are fixed in the melt through thermodynamic equilibrium with a coexisting hydrosaline liquid or brine (with or without a coexisting aqueous or aqueous-carbonic vapor phase) at a fixed pressure, temperature, and melt composition.

This study models Cl dissolution in melts and fluids to elucidate its behavior as magmas evolve through the compositional range of dacite to rhyolite via fractional crystallization, magma mixing, and the exsolution and/or assimilation of Cl-bearing fluids. To achieve this, we apply the ratio (measured wt.% Cl concentration of melt/modeled wt.% Cl solubility of melt, henceforth referred to as the Cl[Me/Mo] ratio) to > 3500 intermediate-silica to felsic MI and matrix glasses (MG). The glasses span a compositional range from dacitic, pantelleritic, comenditic, and trachytic melts to more-evolved rhyolitic melt compositions, including some plutonic equivalents, representing a range of tectonic settings. The application of this ratio in particular allows Cl behavior to be interpreted independently from the strong influence of melt composition. We address some magmatic systems that are sufficiently enriched in Cl such that geobarometric constraints on the pressures at which Cl-enriched, hydrosaline liquids (HSLs) exsolve from aluminosilicate melt can be derived. This approach identifies the stage(s) of magma evolution at which Cl-bearing fluid or

fluids exsolve, and permits estimation of Cl concentrations of exsolved aqueous fluids for any MI composition as a function of the (fluid/melt) ratio. This approach is also applicable to plutonic MI that have lost their magmatic H_2O contents after the time of entrapment, i.e., even if H_2O loss occurs during MI crystallization in nature or while reheating in the laboratory.

2. BACKGROUND INFORMATION

2.1 Phase terminology and fluid phase relations

In this paper we refer to aluminosilicate component-dominated fluids as melts, and to noncrystalline multicomponent volatile-bearing phases as fluids. Vapors are relatively low-density fluids that are dominantly aqueous or aqueous carbonic in composition. Higher-density fluid phases include silicate melt and saline liquid. A hydrosaline liquid (HSL), also referred to as a brine, is an electrolyte-enriched aqueous or aqueous-carbonic fluids. Fluid-unmixing processes at pressures and temperatures less than those of the fluid critical point include boiling, which involves vapor exsolution from HSL, and condensation, which involves the exsolution of HSL from vapor (Fig. 1). With respect to this terminology, the Cl solubility in silicate melt, *sensu stricto*, is determined experimentally through the equilibration of silicate melts with an HSL, or an HSL plus vapor; whereas the measured abundances of Cl in melts saturated only with vapor are referred to as Cl concentrations.

Phase relations of HSL and/or vapor have been investigated experimentally for simple, melt-free H_2O-M_xCl_y±CO_2 systems at pressures ≤ 400 MPa where M represents Na, K, Ca, Mg, or Fe (Bodnar et al., 1985; Webster and Mandeville, 2007; Heinrich, 2007; Steele-MacInnis et al., 2015; Lecumberri-Sanchez et al., 2015; Aranovich, 2017) but data for complex fluid compositions are quite limited. In Cl-enriched systems, HSL is rarely accompanied by Cl-poor vapor above ca. 200 MPa for geologically reasonable magmatic temperatures and low CO_2 contents. However, the reader should be aware that with the addition of CO_2, the systems H_2O-NaCl and H_2O-$CaCl_2$, for example,

include vapor plus HSL at considerably higher pressures (i.e., as high as 900 MPa) (Bowers and Helgeson, 1983a;b; Shmulovich and Graham, 2004; Heinrich, 2007; Aranovich, 2017).

Fluid phase assemblages that include an HSL have also been addressed through study of natural eruptive systems (Lowenstern, 2000). Investigations of subaqueous emissions in volcanic crater lakes and subaerial fluids (i.e., salt melts) of volcanic craters as well as analyses of FI and MI in phenocrysts of eruptive magmas have confirmed the presence of brines in numerous volcanic systems (Guglielminetti, 1986; Frezzotti, 1992; Roedder, 1992; Chiodini et al., 1993; Lowenstern, 1994; Shinohara, 1994; Giggenbach and Glover, 1995; Korzhinsky et al., 1996; Taran et al., 1997; Wahrenberger, 1997; Kasai et al., 1998; Shmulovich and Churakov, 1998; Christensen, 2000; Varekamp et al., 2000; Frezzotti, 2001; Chiodini et al., 2001; Giggenbach et al., 2003; Davidson and Kamenetsky, 2006; Kamenetsky, 2006; Webster and Mandeville, 2007; Werner et al., 2008). The presence of highly saline FI in felsic magmas emplaced in the crust, such as mineralized porphyritic systems (Cline and Bodnar, 1991), also provides strong evidence of magmatic HSL exsolution for shallowly emplaced, non-eruptive systems.

2.2 Data sources and evaluation

Herein, we outline an approach that constrains the state of magmatic-fluid saturation for a given melt composition and the presence or absence of magmatic HSL in the phase assemblage. This study is based on the chemical compositions of more than 3500 individual natural glasses, all of which contain at least 63 wt.% SiO_2 (anhydrous basis) representing 64 individual magmatic systems. Most data (n = 3542) represent MI or MG analyses that were extracted from the published sources listed in Table 1; this report also includes new MI analyses of the authors (n = 62; Supp. Data Table). The latter data were obtained by EPMA methods consistent with the analytical protocols outlined in the

relevant literature source accompanying the data, with further information on the samples available in the Supp. Data Table.

The scrutinized and filtered data should be representative of the melts from their respective magmas. We have, for example, excluded glasses with analytical totals > 101 wt.% or < 90 wt.% and those with maximum SiO_2 concentrations > 82 wt.%. In addition, one study reports Cl concentrations of rhyolitic MI in the range of 1.6 to 3.2 wt.% (Saunders et al., 2010), and these particular data were rejected because application of the Cl solubility model of Webster et al. (2015) determines that the felsic melts would have required HSL exsolution at petrologically unrealistic pressures of > 3 GPa. Thus, Figure 2 illustrates the compositional range of the filtered database glasses in terms of their SiO_2 contents and total alkali (Na_2O+K_2O) contents on an anhydrous basis. The data shown in Fig. 2 are subject to inherent sampling biases based on the research objectives of the 64 separate investigations. Furthermore, F-enriched rhyolites are overrepresented compared to the volumetric significance of F- and/or alkali-enriched magmas on Earth. The database should only be used to interpret ranges of Cl in magmas and not the relative significance of Cl in the different magmas.

Due to EPMA-based analytical challenges of determining accurate alkali concentrations of hydrous silicate glasses in small-diameter MI (Morgan and London, 1996; Humphreys et al., 2006), some data, particularly from the smaller MI, could have artificially low Na_2O and K_2O values due to alkali migration during electron-beam analysis. Figure 3 plots the Cl concentrations versus the molar (A/CNK = $Al_2O_3/CaO+Na_2O+K_2O$) ratios of all glasses of this study. The overall dataset includes some inordinately large values of the molar A/CNK within an overall, weakly developed, hyperbolic relationship. This relationship is significant in this context because EPMA analyses returning inaccurately low concentrations of Na_2O and K_2O increase the molar A/CNK artificially.

Previous experimental research on hydrous granitic melts demonstrates that maximum values of the molar A/CNK are limited to ca. 1.16 to 1.3 at 700 to 800°C and 200 MPa (Acosta-Vigil et al., 2003) because higher A/CNK values would cause saturation of the melts in corundum, cordierite, or one of the Al_2SiO_5 polymorphs. This ca. 1.16 to 1.3 range is restricted to felsic melts containing low concentrations of the fluxing components F, B_2O_3, and P_2O_5, because experiments show that alumina solubility in felsic melts increases with increasing concentrations of these components (Webster et al., 1997; Acosta-Vigil et al., 2003). It follows that the molar A/CNK will increase with increasing F, B, or P contents in aluminosilicate-saturated melts. Figure 3, for instance, displays samples with molar A/CNK values approaching 2.4, and many of these glasses represent highly evolved granitic glasses with F and/or P_2O_5 contents that exceed 0.1 wt% (some of which approach 8 wt.%) (Webster and Duffield, 1994; Webster et al., 1997; Audétat, 2015; Mercer et al., 2015; Thomas and Davidson, 2016). Given their elevated concentrations of fluxing components, we assume that the high A/CNK values of these particular samples may reflect accurate EPMA results for the alkali elements and that the A/CNK values are correct. However, some high-(A/CNK) glasses contain low concentrations of F, B_2O_3, or P_2O_5 that are typical of most granites (i.e., ca. < 0.1 wt.% of each) and hence their values of the molar A/CNK should not be controlled by the presence of F, B and/or P. In this regard, Figure 3 identifies felsic melts (enclosed by two rectangles) that have relatively large molar A/CNK values but have bulk compositions that are generally low in F, B, and/or P. Therefore, we note that these glass compositions may have suffered from issues with alkali analysis, but the data have not been rejected from the overall dataset as this is not known with certainty. More importantly, the influence of changes in the Na and K contents on Cl solubilities in melts (addressed below) is small in comparison with the imprecision of the computed Cl solubility values, so the effect on our modeling is minor even with retention of these potentially erroneous data points.

2.3 Experimental background for MI data interpretation and fluid-melt modeling

Chlorine dissolution in fluid-saturated silicate melts varies strongly with pressure as well as fluid and melt composition; the Cl content of the bulk system has a particularly dominant effect (Malinin et al., 1989; Webster, 1992a;b; Métrich and Rutherford, 1992; Signorelli and Carroll, 2002; Webster and DeVivo, 2002; Chevychelov and Suk, 2003; Carroll, 2005; Baker and Alletti, 2012; Zajacz et al., 2012). However, the observed influences of pressure on Cl solubility in melt are contradictory, and hence, not well resolved (Webster et al., 2015; Lukanin 2015; 2016). Experiments with granites and phonolites report increasing Cl contents in the melts with decreasing pressure when saturated in vapor ± HSL (Shinohara et al. 1989; Shinohara 1994; Métrich and Rutherford 1992; Chevychelov and Chevychelova 1997; Signorelli and Carroll 2000; 2002). Alletti et al. (2009) observed increasing Cl partitioning ($D_{Cl}^{fluid/melt}$) in favor of the fluid for experiments involving Etna basalt with pressure decreases from 200-1 MPa; this likely reflects decreasing Cl in melt at lower pressures. Conversely, Chevychelov and Suk (2003) determined higher Cl concentrations in fluid-saturated basaltic, dacitic, albitic, and orthoclase-rich melts at 100 MPa and 300 MPa but lower Cl contents in the melts at pressure < 100 MPa. Experiments on phonolitic melts also show complex behaviors as a function of the Cl concentrations and pressures involved (Alletti et al., 2014). The Cl contents of fluid-saturated phonolitic melts containing > 0.5 wt% Cl increase as pressures is reduced from 250 to 100 MPa (with roughly equivalent Cl contents in the coexisting fluids), but the Cl contents of melts with < 0.5 wt% Cl vary little through this change in pressure (again with constant Cl contents of the coexisting fluids). However, with further reductions in pressure of 100 to 10 MPa, the Cl contents of the phonolitic melts decrease, hold constant, or increase depending on the bulk Cl concentration of the system (Alletti et al., 2014). Other experiments with HSL- (± vapor)-saturated basaltic (Malinin et al., 1989), granitic (Webster 1992a;b; Webster and Rebbert 1998; Webster et al.

1999; Webster 2004), rhyodacitic (Doherty et al., 2014), and phonolitic melts (Webster et al., 2003) show decreasing Cl solubility in melt with reductions in pressure. Given these contradictions, some of the models in the following sections of this study follow observations showing decreasing Cl dissolution in fluid-saturated melts (i.e., increasing $D_{Cl}^{fluid/melt}$) with decreasing pressure. Other models, however, address increasing Cl dissolution in melt (i.e., decreasing $D_{Cl}^{fluid/melt}$) with pressure reduction for comparison.

In order to generate ratios of Cl[Me/Mo] for this study, the solubilities of Cl in all melts represented by the MI and MG (matrix glasses) were computed using the model of Webster et al. (2015) for geologically relevant temperatures and a range of pressures equivalent to those of the mid to shallow crust. The temperatures were chosen to be appropriate for melts of these compositions at the pressures of interest even though Cl solubility in melt only varies modestly with changing temperature (Webster et al., 2015). For example, rhyolitic and granitic melt temperatures are assumed to range from 700° to 900°C and dacitic melt temperatures from 900° to 1050°C. The pressures used in the modeling range from 20 to 600 MPa. The solubility calculations also require data on the F, K, Na, Ca, Fe, Mg, Ti, P, and Al contents of the glasses, but some of the data sets sampled do not include EPMA data for F and/or P. For these few data sets, we estimated geologically representative values for use in the modeling. The F ± P values chosen were based on the concentrations of these components in other melts of similar bulk compositions and for similar tectonic environments. In this regard, it is worthy of note that the F ± P concentrations that we estimated were all low, and hence, the potential influence of any related inaccuracies on the computed Cl solubilities is negligible.

A more problematic issue is accounting for the role of magmatic sulfur. Chlorine solubility in felsic to mafic melts varies strongly with the presence or absence of relatively oxidized S in the melts

and fluids (Botcharnikov et al., 2002; 2004; Webster et al., 2009; 2014; Beermann, 2010). The Cl solubility modeling used herein does not account directly for the strong influence of S in reducing Cl solubility in HSL-saturated melts at such oxidizing conditions (i.e., log fO_2 of ca. ≥ NNO). These prior studies observed a maximum reduction in Cl solubilities of 25 to 35 rel.% with the addition of S (primarily as the oxidized S^{6+} species) to their experiments. Moreover, Beermann (2010) determined that this influence decreased for basaltic melt as f_{O2} was reduced from ca. NNO+3 to NNO+1. Consequently, for comparison we have normalized the measured Cl contents of each MI and MG to their respective Cl solubilities for two conditions: melts plus fluids containing negligible oxidized S (abbreviated NOS), and melts plus fluids assumed to contain oxidized S (abbreviated OS). The fO_2, fluid saturation state, and S contents of magmatic fluids are unknown and unreported for many of the data sets given in Table 1, so our display and discussion of modeled Cl solubilities for OS conditions may not fully constrain the likelihood of saturation in a S-bearing HSL for any given magma. For OS conditions, we therefore reduced Cl solubilities by 30% relative to their S-free equivalent following Webster et al. (2015) to demonstrate the potentially strong influence of oxidized S on the exsolution of an HSL in felsic magmas in general (Table 2).

The MI and MG of this study that achieve Cl[Me/Mo] ratios of unity indicate equilibrium for Cl exchange between silicate melt, HSL, and phenocrysts ± vapor for the pressure-temperature values applied to their respective magmatic systems. Many felsic magmas at shallow-crustal pressures are considered to have been fluid saturated at the time of MI entrapment (Audétat and Lowenstern, 2014; see Table 2). Given the loss of volatiles from melt to fluid, it follows that many of these MI represent partially degassed magma. Melt inclusions that are incorporated into their host minerals when magmas are saturated in one or more fluid phases cannot provide constraints on the maximum volatile concentrations prior to fluid exsolution, due to the sequestration of volatiles from melt by

fluid(s). Thus, the calculated Cl contents of fluids reported herein represent minima due to potential prior volatile exchange with fluid(s) for many of these samples, and especially the matrix glasses.

To support modeling of Cl dissolution in natural felsic melts and fluids, we describe a mass balance-based approach for determining the distribution of Cl between these phases that is based on the maximum Cl solubilities in melts. This new method is available in an Excel spreadsheet (PartitionCl200MPa) for making the necessary calculations, and is provided at the journal website for interested readers. Prior models have supported prediction of Cl contents of magmatic fluids as the magmas undergo crystallization and/or decompression as closed or open systems (Sisson and Layne, 1993; Edmonds et al., 2008; Johnson et al., 2011), but only Lukanin (2015, 2016) has attempted to account for the strong influence of the Cl content of the system on $D_{Cl}^{fluid/melt}$ for high-silica, metaluminous granitic melts.

3. RESULTS OF SOLUBILITY MODELING: CL BEHAVIOR IN DACITIC, RHYODACITIC, TRACHYTIC, COMENDITIC, PANTELLERITIC, AND RHYOLITIC MAGMAS

3.1. Chlorine and glass compositions

Most of the > 3500 MI and MG are metaluminous and rhyolitic, but the glass compositions range from sub-alkaline dacites to alkaline trachytes and pantellerites and comendites and also include alkali-poor to alkali-enriched rhyolites. Tectonically, the vast majority of glasses come from eruptive systems including volatile-enriched subduction-related magmas, back-arc basins (Manus basin), and tephra of continental rhyolitic systems. Other MI represent hot-spot related oceanic granites (e.g., Ascension Island); rift-related granites; tin-mineralized porphyritic granites; and other Cu-, W-, Mo-, Ag-, base metal-, ± Nb-mineralized porphyritic granites.

The Cl concentrations of these magmatic systems (Fig. 4) vary systematically with progressive melt evolution (i.e., increasing Larsen indices [wt.% (K_2O + 1/3 SiO_2) – (CaO + MgO + FeO)]).

The Larsen index (Larsen, 1938) is useful for characterizing evolving melt compositions, particularly with regard to Cl behavior, as it accounts for the decreasing concentrations of Ca, Mg, and Fe (all of which exert a major control on Cl solubility in silicate melts) during melt evolution. It also neglects Na which is the most likely alkali element to potentially suffer from electron beam-induced migration during hydrous glass analyses (Humphreys et al. 2006). These data represent a projection through aluminosity-alkalinity compositional space, and the filtered data demonstrate that alkaline melts contain the highest Cl concentrations while the lowest Cl contents are found in metaluminous and peraluminous compositions. The molar A/CNK ranges from ca. 0.4 to values > 2 for all data (Fig. 3), and metaluminous and peraluminous compositions with molar A/CNK of 0.9 to 1.18 represent ca. 65% of this data set. The highly alkaline pantelleritic MI have been highlighted in Figure 4 because Cl solubility is higher in alkaline and peraluminous melts as compared with metaluminous melts (Métrich and Rutherford, 1992; Carroll, 2005; Webster et al., 2015; Dolejs and Zajacz, 2018) and because the magmas represented by these MI evidently had ample Cl available for dissolution. The Cl in melts represented by the glasses in this dataset varies from low tens of ppm to as much as 1.1 wt.% (Fig. 4); 95% of the glasses contain < 0.5 wt.% Cl and peak Cl contents occur with rhyodacitic-melt Larsen indices of ca. 20-23. Continued differentiation of melt to the most-evolved rhyolitic compositions (greater Larsen indices) causes strongly decreased maximum Cl contents, and minima for Cl also decrease with progressive evolution from dacitic to rhyolitic compositions.

Alkaline glasses containing ≥ 0.5 wt.% Cl include: pantellerites from Pantelleria, Italy (with molar A/CNK < 0.55; Neave, 2010; Gioncada and Landi, 2010; Lanzo et al., 2013); Ascension Island granites (A/CNK of 0.56 to 0.72, Webster and Rebbert, 2001); pantelleritic to comenditic rhyolites of Baitoushan/Paektu volcano (A/CNK of 0.65 to 0.75; Horn, 1997; Horn and Schmincke, 2000;

Iacovino et al., 2016); comenditic rhyolites of Vulcano, Italy (A/CNK ≈ 0.5, Frezzotti et al., 2004); Manus Basin rhyolites (Yang and Scott, 2002; 2005; Sun et al., 2007); and tholeiitic MOR-sourced dacites of the Juan de Fuca ridge and East Pacific Rise (Wanless et al. 2011). Other systems with ≥ 0.5 wt.% Cl include alkaline to metaluminous rhyodacites and rhyolites of the Izu Bonin arc (Straub and Layne, 2003) and Augustine volcano, AK, USA (Tappen et al., 2009; Webster et al., 2010). In addition, some glasses from the metaluminous to peraluminous rhyolites of Oruanui, New Zealand (Saunders et al., 2010); Healy caldera, Kermadec arc, rhyolites (Saunders et al., 2010); peraluminous granites of the Caucasus (R. Thomas, personal comm.), and of the Oslo rift, Norway (Hansteen and Lustenhouwer, 1990); Zr-, Nb-, and REE-mineralized alkaline granites of Namibia (Schmidt et al., 2002); Chalk Mountain rhyolite (associated with the Colorado Climax Mo deposit, USA; Audétat, 2015); and meta- to peraluminous, Cu-Ag- and base metal-mineralized granites of the Cerro de Paso district, Peru (Rottier et al., 2016) contain > 0.5 wt.% Cl.

3.2. System composition and Cl behavior of silicate melts; using the Cl[Me/Mo] ratio

The bulk compositions of each glass were used to compute their respective Cl solubilities at 20 MPa for both sulfur conditions; NOS and OS magmatic conditions (Fig. 5) (Webster et al., 2015). This pressure was selected to represent magmatic processes occurring at shallow-crustal conditions. Our interpretation of MI compositions with 20 MPa Cl solubility data involves the assumption that there was time for MI entrapment during the crystallization and degassing of the magmas involved, which may not be true for all the systems at this pressure. The measured Cl concentrations of each MI and MG sample have then been normalized to their calculated Cl solubilities. A comparison of Figures 4 and 5 shows important differences that arise when the Cl[Me/Mo] ratios are employed to display these data, instead of the simple total Cl concentration. These differences include: (1) the majority of maxima in the Cl solubility-normalized ratios increase more *progressively* with melt

evolution than simple Cl concentrations (i.e., the dispersion in the trends decreases when accounting for Cl solubility), and (2) many of the individual data sets, when expressed as Cl[Me/Mo], assume a more distinctly positive slope (e.g., see the pantelleritic glasses in particular). At fluid-absent conditions, the latter relationship reflects increasing Cl contents of melts that are associated with crystallization of predominantly Cl-free to Cl-poor minerals and the simultaneous decrease in modeled Cl solubility due to decreasing concentrations of CaO, MgO, and FeO in residual melt aliquots during progressive melt evolution. These cations exert the strongest influence on Cl solubility in melts (Malinin et al., 1989; Webster and De Vivo, 2002; Chevychelov and Suk, 2003; Webster et al., 2015).

Interpreting glass data modeled at 20 MPa

Conversely to fluid-absent conditions, Cl behavior is strongly influenced by the presence of fluid(s). Thus, the application of solubility-normalized Cl ratios to igneous glasses provides a means of constraining magmatic fluid-phase assemblages. To illustrate this, we have modeled Cl behavior at 20 MPa for all samples to consider the fluid saturation condition of magma at equilibrium NOS conditions during ascent to very shallow-crustal eruptive depths. Any glass composition lying on the solid horizontal lines in Figure 5 represents HSL-saturated melts (with or without a vapor) with fixed Cl contents at 20 MPa pressure, if they had ascended to this depth and pressure. All glasses lying above the line represent fractions of silicate melt that exsolved and equilibrated with HSL at some pressure $\geq$ 20 MPa (within the quoted error of ca. 10 rel.% for computing Cl solubility, Webster et al., 2015). For example, the Cl solubility-normalized ratios are $\geq$ 1 for ca. 200 of the individual volcanic glasses at NOS conditions (Fig. 5), indicating magmatic HSL saturation - with or without vapor - as magma ascended through ca. 600 meters depth (i.e. pressure of 20 MPa). The volcanic systems involved include (Table 1): Augustine volcano, AK (System 3); the Taupo volcanic zone

of NZ (System 46); Lipari, Italy (System 22); Mt. Jang, Korea (System 30); evolved and F-enriched topaz-/tin-rhyolites of Taylor Creek, NM, USA (System 47) and Spor Mountain, UT, USA (System 45); Pantelleria, Italy (System 36); Baitoushan/Paektu volcano, China-North Korea (System 4); Manus Basin rhyolites (System 26); and Healy caldera of the Kermadec arc (System 14). Some prior studies of these systems have also considered a role for HSL ± vapor in the differentiation of these magmas. For example, the evidence for magmatic HSL at Pantelleria in Figure 5 is compatible with prior interpretations of solid inclusions of salt found in phenocrysts of its eruptive materials (Lowenstern, 1994). Moreover, Iacovino et al. (2016) considered the role of CO_2- and S-charged HSL plus vapor in the commenditic Paektu magma as it evolved at apparent pressures of 20 to 60 MPa. Integration of their interpretation, with the constraints in Figure 5, indicates that the elevated S contents must have reduced the Cl solubility in melt and supported the presence of the HSL; HSL should not be stable for this melt composition at 20 MPa and NOS conditions.

Interpreting glass data modeled at 100 MPa

To focus on plutonic glasses at NOS conditions, we have adjusted the pressure used to model Cl solubility behavior to 100 MPa (Fig. 6A). Under these conditions, there are three barren or mineralized, plutonic systems: the alkaline granites of the Oslo rift, Norway (System 61); Tyrone, NM, quartz monzonite (System 63); and the Cu-Ag- and base metal-mineralized intrusions of Cerro de Paso, Peru (System 54) that exhibit sufficiently evolved melt compositions and also contain enough Cl that they would have saturated in an HSL ± vapor at equilibrium conditions (i.e., Cl[Me/Mo] ≥ 1). If we consider and account for the estimated error on the calculated Cl solubilities in these melts (10 % rel.) three additional plutonic systems show Cl[Me/Mo] ratios < 1 but > 0.9. They include the Dexing Cu-Mo porphyry, China (System 58); the Deva Cu-Au porphyry of Romania (System 57); Ascension Island (System 53) that are suggestive of HSL ± vapor saturation

at magmatic conditions. This approach can also be applied to plutonic MI that have lost their magmatic H_2O contents after the time of entrapment (i.e., due to H_2O loss during MI crystallization in nature or during reheating in the laboratory). In contrast to H_2O, Cl is essentially immobile via diffusive re-equilibration through phenocryst host crystals during melt inclusion-host component exchange at magmatic temperatures (Bucholz et al., 2013).

Effect of oxidized S on Cl solubility

As discussed previously in Section 2.3., the application of our approach to real systems at OS conditions is limited, currently, by insufficient experimental data on the minimum S^{6+} required in melt and the minimum S^{6+} and S^{4+} required for coexisting fluids to reduce Cl solubility in melt. A larger restriction is that most of the MI and MG of these data sets contain very low S contents, indicative of prior sequestration of S by magmatic fluids, sulfide liquids, and/or sulfide or sulfate minerals. Thus, it is difficult to model the S contents of the magmatic fluids and to apply experimental observations regarding S and Cl interactions in melts and/or fluids to natural systems at present. Although the following data interpretation is highly theoretical, we consider it to be instructive nevertheless.

Shifting from modeled NOS to OS conditions (i.e. decreasing the Cl solubility values by 30% relative, after Webster et al., 2015), shows that ca. 680 of the volcanic glasses modeled for 20 MPa and ca. 80 of the MI glasses from plutons at 100 MPa are characterized by Cl[Me/Mo] ratios that equal or exceed unity for OS conditions (Figs. 5 and 6A). These ca. 750 glasses include the 16 volcanic and plutonic systems noted above for NOS conditions, which now are displaced to even larger ratios (implying higher pressures of HSL ± vapor exsolution). The glasses also represent an additional 11 magmatic systems, most of which are eruptive: Soufriere Hills volcano, Montserrat (System 44); Mt. Mazama, OR, USA (System 31); Bandelier Tuff, NM, USA (System 22);

Hideaway Park topaz rhyolite, Red Mtn., CO, USA (System 16); Dikii Greben, Kamchatka, Russia System 11); unidentified eruptives of the Eastern volcanic front, Kamchatka, Russia (System 49); Mayor Island, NZ (System 25); Bataan, Philippines (System 5); Llallagua, Bolivia (System 23); Merapi, Indonesia (System 27); Mt. Hood, OR, USA (System 29); and the Tyrone NM, USA, quartz monzonite (System 63). The essential observations here are the strong influence of oxidized sulfur on Cl solubility in melts, and the need for accurate knowledge of magmatic S contents and oxygen fugacities in order to interpret the fluid phase equilibria of degassing magmas with this new geochemical tool.

Presence of HSL in previous studies

Prior petrologic research on these igneous systems has interpreted physical and geochemical evidence to suggest the presence and impact of highly saline liquid, with or without vapor, during magma evolution (Table 2). The chemical evidence that was presented includes relatively fixed and apparently buffered Cl concentrations in melts that may represent the "hypothetical solubility limits" for Cl, and physical evidence includes coexisting MI and highly saline FI in the same growth zones of phenocrysts and/or the presence of salt crystals entrapped in phenocrysts. These volcanic and plutonic systems include: Augustine volcano, AK, USA; the Taupo volcanic zone, NZ; Mt. St. Helens, WA, USA; Mt. Mazama, OR, USA; Ascension Island; Pantelleria, Italy; Baitoushan/Paektu volcano, Korea; the Izu arc front; Merapi, Indonesia; the Climax-related Chalk Mountain rhyolite, CO, USA; Oslo rift, Norway; Dexing Cu-Mo-Au porphyry, China; Deva Cu-Au porphyry, Romania; and Cerro de Pasco, Peru. Our new constraints on magmatic HSL saturation, *at NOS conditions only*, that are based on the melt Cl[Me/Mo] ratios are consistent with previously published interpretations on the presence of HSL in eruptive magmas of Augustine volcano, the Taupo

volcanic zone, Pantelleria, and the Baitoushan/Paektu volcano, and for plutons of Ascension Island, the Oslo rift, Dexing Cu-Mo-Au porphyry, Deva Cu-Au porphyry, and Cerro de Pasco.

3.3. Pressure and Cl behavior: geobarometric constraints

The influence of decreasing pressure, resulting from magma ascent-driven decompression, on Cl solubility in HSL- ± vapor-saturated melts has previously been assessed for MI and MG of Augustine and Vesuvius volcanoes to estimate pressures of magmatic fluid-melt volatile exchange for some of their eruptive magmas (Webster et al., 2015; Balcone-Boissard, 2016). Our modeling permits this approach for the other systems of this study. The shift of the Cl[Me/Mo] ratios and HSL saturation state of the melts at NOS and OS conditions as a function of pressure are illustrated by the shifts in the HSL-saturation lines for 100, 400, and 600 MPa in Figures 6A, 6B, 6C, respectively, compared to that for 20 MPa in Figure 5. The modeled Cl solubilities in melt increase and hence the Cl[Me/Mo] ratios decrease, at higher pressure. Comparison of the individual solubility-normalized Cl ratios of the MI and MG with the 1:1 curves identifies those melts whose Cl contents and bulk compositions are consistent with saturation of the source magmas with HSL ± vapor. For example, at 600 MPa and NOS conditions (Fig. 6C), glasses from 2 systems overlap with and 3 others lie above the line indicating saturation in HSL ± vapor at or greater than this pressure, respectively. This contrasts with the 13 ± 3 systems that are consistent with HSL ± vapor saturation at 20 MPa as noted previously. For OS conditions at 600 MPa (Fig. 6C), glasses from 5 systems overlap with the 1:1 line. Glasses from 4 others lie above the line suggesting HSL ± vapor saturation at ≥ 600 MPa.

If it is known, or assumed, that the MI of interest represents magma saturated in fluid (a HSL, in this case), then overlap of the Cl[Me/Mo] ratio of an MI composition with the 1:1 Cl solubility line provides the pressure of entrapment of that MI. This approach is analogous to that used extensively

to interpret pressures of MI entrapment using H_2O-CO_2 solubility plots (Wallace et al., 1999; Newman and Lowenstern, 2000; Moore, 2008).

4. DISCUSSION: APPLICATIONS TO TRACING MAGMATIC EVOLUTION PROCESSES

Here, we discuss modeled relationships in the Cl[Me/Mo] ratio versus Larsen indices of the glasses that provide insights into the petrologic processes of fractional crystallization, magma mixing, degassing, and/or HSL assimilation at fluid-absent to fluid-saturated, generally closed-system NOS conditions. This modeling follows similar approaches in numerous prior studies involving MI. Wallace et al. (1995; 1999), for example, calculated how CO_2 contents of MI should vary as a function of fractional crystallization and compared the results with modeled behaviors of various incompatible trace elements to track the evolution of vapor-saturated high-silica magmas. Similarly, Webster and Rebbert (2001) modeled how the abundances of fluid-mobile versus fluid-immobile trace elements in evolving melts, represented by Ascension Island MI, should vary for felsic melts saturated in Cl-enriched fluids. This approach was summarized in a more general fashion by Audétat and Lowenstern (2014).

The Cl[Me/Mo] ratios of felsic magmas show a variety of trends as well as fluctuating ranges in dispersion or scatter when plotted relative to the Larsen index. Some of these systems exhibit minimal variability and are consistent with increasing Cl[Me/Mo] as residual fractions of melt undergo differentiation. Given that experimental data on Cl partitioning between fluid and melt for pressures other than 200 MPa are limited, the results that follow are most relevant to Cl dissolution in, and exsolution from, melts and fluids of intermediate to felsic magmas at this pressure.

4.1. Fractional crystallization

Three magmatic systems with glasses exhibiting low to moderate dispersion, whose least-evolved and lowest-Larsen index glass compositions are dacitic, and that represent other, similar

systems in this data set include the Manus Basin (Table 1; System 26); Hekla, Iceland (Table 1; System 15); and East Pacific Rise seafloor glasses (Table 1; System 28) (Fig. 7A). The individual, least-evolved melt composition for each contains 0.04, 0.23, and 0.27 wt.% Cl for the Hekla, East Pacific Rise, and Manus Basin systems, respectively, and their Cl[Me/Mo] ratios increase with progressive evolution toward rhyodacitic compositions (Fig. 7A).

Figure 7B compares these MI or MG glass-based, melt-evolution trends with 4 curves that model the variations in the Cl[Me/Mo] versus Larsen index as a result of fractional crystallization of the primary mineral phases present in each of these 3 fluid-free magmatic systems (details of the modeling calculations are given in Appendix A). In contrast to many of the other 64 magmatic systems presenting evidence that Cl and other components were exchanged between melt and fluid(s) (Table 2), none of the prior studies on the East Pacific Rise, Manus basin or Hekla magmas described evidence of magmatic fluid saturation so it appears that fractional crystallization occurred at fluid-absent conditions. We note that Wanless et al. (2011) described a potential role for the assimilation of seawater-sourced HSLs to generate the more Cl-enriched fractions of East Pacific Rise melts, but these magmas were apparently not fluid-saturated during late-stage evolution. It is clear that the slope of each curve increases with increasing Cl content of the system and with increasing Larsen index. The modeled curves 1, 2, and 3 (Fig. 7B) are consistent with the compositional evolution of the glasses from these magmatic systems. Curve 4 (Fig. 7B) is included to illustrate the consequences of eutectic and near-eutectic crystallization of highly evolved granitic melts, i.e., an extremely steep slope. The change in Larsen index of curve 4 (Fig. 7B) is small due to the limited changes in Si, K, Ca, Mg, and Fe. Thus, the increasing Cl[Me/Mo] ratios for the *fluid-absent modeling* of differentiation in these magmas is a consequence of both increasing Cl

concentrations in residual aliquots of evolving melt and the reduced modeled Cl solubility in increasingly evolved melt.

4.2. Magma mixing

Anderson (1976) observed that magma mixing is a widespread, if not universal igneous phenomenon of wide-ranging petrologic importance. Many prior studies of eruptive magmas have presented petrologic and geochemical evidence of mixing and mingling processes (Mandeville et al., 1996; Atlas et al., 2005; Witham, 2011). Most such systems, however, involve the mixing of mafic and felsic end members to generate andesitic melts, and for this study the andesitic to mafic compositional range is out of scope. Moreover, many of these systems have also undergone post-mixing, fractional crystallization which masks the chemical consequences of mixing processes to a variable extent.

Figure 8 presents modeled curves (details of the modeling calculations are given in Appendix B) for hybrid melts that express the changes in Cl[Me/Mo] of melts versus Larsen index resulting from mixing of several rhyolitic melts with more primitive melts. For comparison, the figure includes MI data for several eruptive phases of the Taupo-Oruanui volcanic zone, NZ (Table 1; System 46). Prior research on the ranges in mineral compositions in individual pumice clasts and on chemical and isotopic changes in the rhyolitic pumices have been interpreted as indications of magma mixing that occurred shortly before eruption (Wilson et al., 2006; Liu et al., 2006). The mixed Oruanui magmas were both felsic, however, and consequently cover only a small range in Larsen indices. Similarly, Saunders et al. (2010) discussed textural and geochemical features of the melt inclusions and their host minerals that may be evidence of magma mixing (involving late-stage felsic magmas) or partial melting, and Begue (2014) considered the role of mixing between rhyodacitic and evolved silicic magmas.

Comparison of the modeled trends for fluid-absent fractional crystallization (Fig. 7B) and the mixing of magmas (Fig. 8) shows similar trends. It follows that these modeled relationships are not currently useful for distinguishing the effects of fractional crystallization versus those resulting from mixing of melts or magmas.

4.3. Component exchange between melt and fluid(s) in magmas

As noted previously, glasses from many magmatic systems show evidence of melt-fluid exchange processes involving fluid-mobile components (e.g. Norling et al., 2016). Prior studies of changing Cl concentrations versus those of incompatible, lithophile trace elements in some systems have also been applied to estimate the extent of crystallization of fluid-saturated magmas (Dunbar and Hervig, 1992b; Johnson et al., 2011). In addition to Cl, other components including B, S, and Cu are variably sequestered from progressively evolving fractions of melt by a pre-eruptive fluid phase or by vapor plus HSL, and they provide geochemical evidence of magmatic fluid saturation (e.g. Audetat et al. 2008; Pokrovski et al. 2013) . Here, we address magmatic systems showing increasing dispersion in plots of Cl[Me/Mo] with increasing Larsen indices for rhyodacitic to rhyolitic melts, and we consider the role of magmatic fluids in generating such dispersion. Many of the published data sources for these systems ascribe magma evolution to be a consequence of cooling and crystallization-driven differentiation, so decompression crystallization was dominant for many of these fluid-saturated systems.

4.3.1 Cl relationships in fluid(s)-saturated magmatic systems exhibiting low to moderate dispersion

Flat to positive slopes in the Cl[Me/Mo] ratio versus Larsen index are shown in Figure 9A for several sets of submarine glasses and/or MI. The Manus glass data of Yang and Scott (2005) and Beier et al. (2015) overlap as a single trend, but they differ from those of Sun et al. (2007); the trends in all data are mutually consistent however. For these samples, the slope of the trends shown by

individual datasets increases with increasing Cl content of the system and/or with increasing Larsen index. The only outliers for these 11 systems include De Rosa et al. (2003) for Lipari and Self and King (1996) for Agung; neither study constrained the presence or absence of a magmatic fluid prior to MI entrapment or eruption.

Data trending toward steeply positive slopes with increasing Larsen index are displayed in Figure 9B, and some can be fit with near-vertical lines. Among these systems, saturation of their melts in Cl-bearing fluids prior to entrapment of MI has been considered previously for F-enriched magmas of Ascension Island (Roedder and Coombs, 1967; Webster and Rebbert, 2001); the Chalk Mtn. rhyolite which is considered to be geochemically representative of the Climax Mo system (Audétat, 2015); and Cerro el Lobo, Mexico (Webster et al., 1996). In contrast, the MI data for White Island display decreasing Cl[Me/Mo] with increasing melt evolution, and this behavior is mirrored by other systems (Fig. 9C). Among the data sets showing this behavior, the authors discuss the role of pre-entrapment and pre-eruptive fluid phase or phases for the Bandelier Tuff; Mayor Island; Quilotoa, Ecuador; and granites of Ehrenfriedersdorf, Germany. Comparison of the curves in Figure 9 shows that magmatic systems presenting geochemical ± textural evidence of fluid saturation prior to MI entrapment can display horizontal slopes varying from positive to negative orientations in plots of the melt Cl[Me/Mo] ratio versus Larsen index.

Results of modeling the differentiation of felsic magmas through plots of the Cl[Me/Mo] ratio versus Larsen index of melt as a function of fluid-absent and fluid-present fractional crystallization are shown in Figure 10A (details given in Appendix A). This figure compares the evolutionary trends of MI from Pantelleria, Italy; Ruapehu, NZ; and Satsuma-Iwojima, Japan, with modeled data. The calculations address fluid-absent and fluid-present conditions, account for up to 40 wt.% crystallization of the phenocrysts present in each system, and involve reductions in pressure from

200 to 10 MPa as crystallization proceeds. Figure 10A assumes decreasing $D_{Cl}^{fluid/melt}$ with decompression (Section 2.3; consistent with Shinohara et al. 1989; Shinohara 1994; Métrich and Rutherford 1992; Chevychelov and Chevychelova, 1997; Signorelli and Carroll, 2000; 2002; Alletti et al., 2009); and additional details on the complexity of modeling $D_{Cl}^{fluid/melt}$ versus pressure are included in Appendix C.

At fluid-absent conditions (solid curves, Fig. 10A), the Cl[Me/Mo] ratio increases with differentiation (i.e., Larsen Index) as demonstrated previously (Fig. 7). The modeling also shows that the Cl[Me/Mo] ratio increases with progressive crystallization and concurrent fluid exsolution of Pantelleria or Satsuma-Iwojima magmas (red and blue dashed curves, respectively; with fluid mass up to 5.5 wt.% of the bulk system). Figure 10A also includes a comparison of Cl sequestration by fluid(s) at open- and closed-system conditions with little difference displayed for Cl-enriched pantelleritic melts or with lower Cl contents in Satsuma-Iwojima melts. We note that it is not possible to conclude whether the Pantelleria or Satsuma-Iwojima magmas evolved via fluid-absent versus fluid-present crystallization with this approach given the spread in the MI data. The effect of evolving melt composition on increasing the Cl[Me/Mo] ratio, for Pantelleria or Satsuma-Iwojima magmas, is reinforced by the reduced $D_{Cl}^{fluid/melt}$ at lower pressures during magma ascent which works to retain Cl in these fluid-saturated magmatic melts. The Ruapehu MI, on the other hand, are definitely consistent with the differentiation of fluid-saturated magma. The MI overlap with the modeled results (green dashed curve; Fig. 10A) for evolving melts that have progressively lost Cl to fluid for Larsen index values $\geq$15.

Further modeling of Cl exchange between melts and aqueous fluids during fractional crystallization-driven differentiation of fluid-present magmas is shown in Figures 10B,C,D. However, in contrast to the results in Figure 10A (which models *decreasing* $D_{Cl}^{fluid/melt}$ with

decreasing pressure), the results in Figure 10B,C,D are based on experimental observations showing decreasing Cl solubility (i.e. *increasing* $D_{Cl}^{fluid/melt}$) in fluid-saturated melts with decreasing pressure (Webster, 1992 a;b; Webster and Rebbert, 1998; Webster et al., 1999; Webster et al., 2003; Webster, 2004; Doherty et al., 2014; Webster et al., 2017). This apparent contradiction in Cl partitioning behavior with changing pressure (as outlined in Section 2.3) arises from strong differences in published experimental results, and is discussed extensively in Appendix C. Modeling that assumes $D_{Cl}^{fluid/melt}$ increases with decreasing pressure, consistent with Webster et al. (2017; and references therein), generates curves showing small reductions in the Cl[Me/Mo] ratio of the melt, due to reduced Cl contents of melt, for magma evolution at fixed pressure, and much greater decreases in the Cl[Me/Mo] ratio with decreasing pressure. Each decompression curve (dashed/dotted lines; Figs. 10B,C,D) is characterized by an initially negative slope that then evolves into a horizontal line. In addition, all fluid-saturated melts show increasing loss of Cl from melts to fluids with increasing fluid mass and fluid/melt ratio.

A general consequence of this behavior is that aqueous fluid(s) may sequester significant quantities of Cl from degassing melts, and hence, this can reduce the likelihood of saturation in HSL ± vapor. Prior research determined that saturation in HSL ± vapor at 200 MPa occurs at weight (Cl/H_2O) ratios of ≥ 0.05, ≥ 0.15, ≥ 0.35, and ≥ 0.55 for granitic, phonolitic, andesitic, and basaltic melts, respectively (Webster, 2004). Comparison of curves 5, 10, and 13 in Figure 10B shows strongly increasing negative slopes with increasing Larsen index, i.e., as melts evolve from dacite to rhyodacite to rhyolite compositions. This is consistent with the observation of Humphreys et al. (2009) that closed-system, decompression crystallization at Soufriere Hills, Monserrat, led to decreasing Cl in the melt due to the preferential partitioning of Cl in favor of the fluid(s).

Open-system magma evolution involving successive loss of fluid from melt is associated with overall lower Cl loss to fluid, compared with closed-system evolution in which melt and fluid remain in equilibrium. This is because of the relationship showing $D_{Cl}^{fluid/melt}$ decreases strongly with lower Cl contents in the bulk system. Curves 2 and 4 (Figs. 10 B,C) demonstrate enhanced Cl loss to oxidized and S-enriched fluids (compared with curves 3 and 5 for NOS conditions, respectively) resulting from increasing $D_{Cl}^{fluid/melt}$ with increased S in the system. These modeled results are compared with MI compositions from Healy caldera and Mayor Island (Fig. 10D), and both data sets agree with the modeling of Cl sequestration from melt by fluid(s) during progressive evolution of fluid-saturated magmas. Furthermore, if Cl loss to fluid(s) caused these trends, MI compositions are not consistent with magma evolution at relatively fixed pressure given the slopes shown by the MI data. Chlorine behavior therefore suggests that the MI of both systems may have been trapped through a range of decreasing pressures.

As described previously (Fig. 9), other felsic magmas exhibit steeply negative trends of melt evolution requiring Cl loss to fluids and strong magma decompression, similar to some of those in Figure 10B. They include Ascension Island, Atlantic Ocean; lower eruptive units of the Bandelier Tuff, New Mexico; topaz rhyolites of the Honeycomb Hills and Spor Mountain, Utah; Mt. Jang, Korea; Mayor Island, NZ; and mineralized granites of Ehrenfriedersdorf, Germany. Conversely, the shallow to horizontal slopes shown by glasses from White Island, Karymsky, Quilotoa, and Izu Bonin are more consistent with fractional crystallization of fluid-saturated magmas at relatively fixed pressure conditions.

4.3.2 Cl relationships in magmatic systems exhibiting moderate to strong dispersion

Other magmatic systems involve more scatter in their glass compositional data than those considered previously, and some of these show a dramatic increase in the degree of dispersion in the

Cl[Me/Mo] with increasing magma evolution. MI data for Ascension Island are shown in Fig. 11A and are accompanied by data from Soufriere Hills, Merapi; Santorini, Greece; Shiveluch, Russia; Mt. Hood, Oregon; Paektu/Baitoushan, Korea (Fig. 11B); and Augustine volcano, Alaska (Fig. 11C). Most of these data sets involve multiple sources representing multiple eruptive units. Prior research on most of these systems has determined the presence of pre-eruptive magmatic fluids (Table 2)., however, no textural or chemical evidence for fluid saturation of Santorini magmas prior to eruption has been described.

Before discussing the more highly-dispersed data, it is important to recognize that the minor dispersion in the Cl[Me/Mo] of systems like Ascension Island (Fig. 11A) and Shiveluch (Fig. 11B) at low Larsen values (e.g., ≤ 20) indicates no quantifiable exchange of Cl between melt and HSL or vapor at the earlier stages of differentiation. Likewise, data from Merapi, Paektu/Baitoushan, Mt. Hood, and Santorini show minimal dispersion for their least-evolved, rhyodacitic to rhyolitic compositions and higher dispersion in the most-evolved rhyolitic melts. We interpret the trends in Figure 11A,B to indicate that the earlier stages of magma evolution were driven by fractional crystallization at fluid-absent conditions and that the more-evolved melts were influenced by gains in Cl which forced the Cl[Me/Mo] ratios to variably higher values (as shown by outlined data and the black dotted arrows in Fig. 11B). The scatter in the values of Cl[Me/Mo] of rhyolitic melts is inconsistent with the loss of Cl or decreasing Cl[Me/Mo] ratios given the overall trends of geochemical evolution of the melts. The increasing dispersion results primarily from Cl[Me/Mo] ratios that increase above the main trends of magma evolution. This is clearly demonstrated by the Ascension Island and Merapi MI (Fig. 11A).

Other data sets of this study do not provide the same level of information regarding the broader trend of melt evolution from dacitic to more-evolved compositions, with the highly scattered MI

data for the > 12 eruptive units of Augustine volcano (Fig. 11C) being a good example. Interpreting the behavior of Cl in this system is complicated by the extreme variability in the Cl[Me/Mo] ratios of the evolved rhyolitic melts, and the lack of less-dispersed data for Larsen values < 11. These highly dispersed data may reflect a loss of Cl with progressive magma evolution (thinner dotted arrows) along the hypothetical trend represented by the upper bold curve (in Fig. 11C), or they may indicate a gain of Cl as expressed by the thin dotted arrows along the hypothetical primary magma evolutionary trend of the lower bold curve. The degree of dispersion could be due to irregular extents of Cl sequestration from melts by fluid at equilibrium conditions but with varying fluid/melt mass ratios as expressed previously in the modeling of Figure 10B,C. Otherwise, mixing or mingling of Cl-enriched melt (i.e., similar to MI near the upper dashed curve) with Cl-deficient melt (MI near the lower dashed curve) may theoretically generate increased dispersion in volcanic glass data. However, although mixing/mingling processes have played a significant role in the evolution of some Augustine magmas (e.g., materials erupted in 1986 [Roman et al., 2006] and 2006 [Larsen et al., 2010]) these processes involved the combination of relatively primitive melt compositions that plot at low Larsen indices (e.g., < 12) and could not have generated the increasing dispersion in Augustine melts with larger Larsen values.

Importantly, dispersion in the Larsen index versus Cl[Me/Mo], potentially generated by processes of Cl enrichment in residual fractions of differentiated melt, may also be an expression of disequilibrium via kinetically limited volatile diffusion through melt (Barnes et al., 2014). Slow diffusion of Cl may limit Cl loss during degassing. Baker et al. (2005) and Baker and Balcone-Boissard (2009) addressed variable transport rates of Cl and F versus H_2O through fluid-saturated magma due to rapid growth of fluid bubbles, disequilibrium volatile exchange between melt and fluid, and differing rates of diffusion for these volatile components through melt. Watson (1991),

Bai and Koster van Groos (1994), and Balcone-Boissard (2009) data show Cl diffuses more slowly than H_2O and CO_2 in highly polymerized felsic melts. Such processes should lead to compositional trends similar to curves 1, 9, and 12 in Figure 10 B,C, because the relatively slow and limited Cl sequestration from melt by fluid (compared to that of H_2O which diffuses more rapidly and hence is more rapidly lost to fluid at/near equilibrium) may be outweighed by increasing Cl in melt with fractional crystallization.

4.3.3 Processes and consequences of silicate melts interacting with saline materials

Silicate melts gain chloride ions through processes ranging from relatively slow chemical interactions involving equilibrium or near-equilibrium assimilation of HSL, to the assimilation of Cl-enriched hydrous minerals, to comparatively rapid and kinetically limited exchange of components between melt and Cl-bearing fluids. The large variability in Cl[Me/Mo] shown by some of these 64 magmatic systems may well result from the gain of Cl through such processes. In this situation, the results of Cl enhancement may be expressed as variably dispersed data lying above the primary melt evolution curves for the more-evolved compositions (Fig. 11B) or data above and near the lower dashed primary evolution curve of Figure 11C.

Prior research has demonstrated that the assimilation of a seawater-sourced brine, the exchange of components between melt and a seawater-sourced HSL, and/or the assimilation of Cl-enriched metasomatized igneous rocks of the seafloor can increase Cl contents of magmas, and three systems of this study (e.g., the Manus back-arc basin, MOR dacites of the East Pacific Rise, and Healy Caldera of the Kermadec arc) involve marine environments (Fournier, 1987; Michael and Schilling, 1989; Coombs et al., 2004). Some rare oceanic basalts contain highly elevated concentrations of Cl as a result; Lassiter et al. (2002) measured up to 2.5 wt.% Cl in MI representing seawater HSL-contaminated basaltic melts. Other extreme Cl over-enrichments in melt (Wanless et al. 2010) can

result from the assimilation of small quantities of either Cl-rich HSLs stored in ocean crust or assimilation-contamination of ocean crust that has been hydrothermally altered by aqueous HSLs (Michael and Schilling, 1989; le Roux et al., 2006). Kent et al. (2002), for example, measured up to 0.8 wt.% Cl in mafic to intermediate matrix glasses of the Lau Basin back-arc system, and the Cl enrichments were interpreted to result from crustal assimilation of altered, Cl-rich oceanic crust (Kent et al., 2002). The glasses of the Manus back-arc basin (Fig. 9A) and MOR dacites of the East Pacific Rise (Fig. 7) of this study show clear magmatic evolutionary trends and minimal scatter, but the Healey caldera MI are dispersed (Fig. 9C) and may reflect Cl sequestration to magmatic fluids. Alternatively, the Healey MI trend may be a result of seawater boiling and HSL assimilation.

Given that melts incorporate Cl from brines, we can outline the results of modeling the assimilation of up to 3 wt.% of an HSL (composed of either H_2O-NaCl or H_2O-$CaCl_2$) into a silicate melt (details on the modeling parameters are provided in Appendix B). Specifically, taking a rhyodacitic Manus basin matrix glass composition as a starting point (with a Larsen index ~16 and initial Cl[Me/Mo] ratio ~0.5), the assimilation of 3 wt.% of an NaCl-HSL causes an increase in the Cl[Me/Mo] ratio to ~1.3 (an almost 3-fold increase), with a much smaller commensurate decrease in the Larsen index of < 0.5 units. Assimilation of a $CaCl_2$-HSL causes a similar dramatic Cl[Me/Mo] increase, along with a slightly larger decrease in the Larsen index (as CaO is included in the definition of the index, unlike Na_2O) but still < 2 units. The model, therefore, shows that the resultant Cl[Me/Mo] of melts can increase dramatically, and generate negative, near-vertical slopes simply through the dissolution of small quantities of brine.

Brine has been shown to exsolve in other, i.e. non-marine, magmatic systems due to decompression during magma ascent and/or fractional crystallization at equilibrium conditions (Figs. 5, 6 and Table 2). The resultant brine is available for subsequent interactions with other

fractions of melt either via complete assimilation or disequilibrium exchange of Cl as magma convects and/or as saline fluids ascend through magma. Brines should ascend because they have lower densities than melt (Shmulovich and Churakov, 1998). It follows that assimilation processes may explain the steeply negative and dispersed trends shown by glasses from Mt. Jang, for some MI of the topaz rhyolitic systems, for Climax/Chalk Mountain MI, and for most MI of the Bandelier Tuff (Fig. 9B,C). In this regard, Audétat (2015) discussed the presence and mineralizing consequences of HSL plus vapor percolating through the Climax magmatic system. More broadly, it bears repeating that these magmas, like those of Augustine volcano, do not cover a wide range in Larsen values, and hence, do not express extensive trends of magma evolution, so interpreting their primary magmatic processes with confidence is more problematic than we have attempted with other systems like Ascension Island, Mt. Hood, or Paektu/Baitoushan (Figs. 9 and 11).

If the steeply negative slopes in Cl[Me/Mo] versus Larsen values for systems addressed in Figures 9, 10, and 11 (and for other similar systems not explicitly dealt with in these figures) indicate partial to complete assimilation of a saline fluid, then this interpretation conflicts with the data of Figures 5 and 6 demonstrating that few of the glasses are actually consistent with the exchange of Cl between these melts and an HSL under equilibrium conditions. At equilibrium, the stable presence of an exsolved magmatic HSL requires that the coexisting melt contains its maximum Cl content (i.e., its solubility limit), and the process of HSL exsolution requires sufficient time for the diffusion of Cl through both the melt and fluid phases in order to achieve equilibrium between vapor, HSL, and melt. Slow magma ascent and decompression increase the likelihood that a vapor stays in equilibrium with coexisting melt and cause the activity of Cl in the melt to vary proportionally to that in the vapor. However, given that most of these glass compositions do not contain their maximum Cl solubility values for any of the pressure-composition conditions addressed, we note

that there is a strong potential for disequilibrium processes to play a role in the development of the Cl/Me/Mo] versus Larsen index trends displayed by these data. A full treatment of the length- and timescales of such disequilibrium processes associated with rapid magma ascent and decompression is beyond the scope of this modeling, but the reader should be aware of the role disequilibrium conditions may play in HSL-silicate melt interaction.

4.3.4 Modeled Cl concentrations of magmatic fluids

Based on a comparison of published experimental Cl partitioning data representing basaltic, andesitic, phonolitic, rhyodacitic, and haplogranitic melts (Webster et al., 1992; 1999; 2009; 2014; Kravchuk and Keppler, 1994; Webster and De Vivo, 2002; Botcharnikov et al., 2004; 2007; Mathez and Webster, 2005; Zajacz et al., 2012; Iveson et al., 2017; 2019) at 200 to 220 MPa and varying temperatures (Fig. 12A), we observe similar arcuate curvature in the fits to the concentration of Cl in the fluid versus concentration of Cl in the melt data. The slope of a curve at any point provides a value for $D_{Cl}^{fluid/melt}$. The correspondence in curvature is strongest for Cl in the haplogranitic, phonolitic, rhyodacitic, and andesitic melts, and the curves also have the common feature that the near-vertical portions of the curves correlate with the maximum Cl solubilities in each melt. We apply this similarity in curvature, and the observation that each curve is a function of its Cl solubility in the melt, to model fluid-melt partitioning behavior for Cl for melt compositions as two compositional steps. One ranges from haplogranite to rhyodacite (Fig. 12B) and the second from rhyodacite to andesite composition (Fig. 12C). To perform the modeling, we extracted 200- to 220-MPa, Cl partitioning data (wt.% Cl in fluid, wt.% Cl in melt, and bulk melt compositions) from these 12 experimental studies of granitic to andesitic melts and calculated the Cl solubilities for each melt with the model of Webster et al. (2015). Overall, the experimental data involve a temperature range of ca. 800°C for granitic systems up to 1200° for andesitic systems, and this modeling therefore

accounts for the differing liquidus temperatures of the melt compositions involved (granitic melts – 800°C; rhyodacitic melts – 815-850°C, 900-924°C, and 950-1000°C; andesitic melts – 1000°C and 1050-1200°C). The Cl contents of the run-product fluids were computed by mass balance and/or were measured directly. It is important to understand that among the published experimental studies, some modeled results on Cl partitioning do not account for the cations chemically complexed or associated with the chloride ions dissolved in the fluid(s) (they involve H_2O and Cl, only); whereas direct analyses of Cl in run-product fluids (also containing alkali and other dissolved cations) do include and account for the presence of dissolved cations. Thus, in order to be consistent with the alkali element-bearing fluids of the latter, we adjusted the mass-balance computed Cl contents of fluids in some experimental data to account for the presence of cations in chemical association with the chloride ions (see Webster et al., 2014; and references therein). We assumed an averaged fluid mass of 31 for the average molecular mass of the 1:1 cation combination of Na and K. This approach is based on the assumption that these two cations dominate the chemical associations involving the chloride ion in fluids in equilibrium with these intermediate-SiO_2 to felsic melts at/near 200 MPa.

This approach to modeling $D_{Cl}^{fluid/melt}$ thus supports the calculation of accurate Cl contents of magmatic vapor, of an integrated assemblage of vapor + HSL, or of an HSL that are geologically relevant to high-silica rhyolite to dacite NOS melts at pressures near 200 MPa and evolving as closed systems (see Appendix C for further details). These models represent the first data to quantitatively account for the very strong influence of the Cl content of the bulk system on the Cl concentration of the fluid and on $D_{Cl}^{fluid/melt}$ for this spectrum of felsic melt compositions. Despite the diversity of magmatic evolution processes discussed for individual systems in the previous sections we still consider it illustrative to apply this method to glasses from all 64 magmatic systems together. Some systems may not have been fluid saturated at the time of MI entrapment, but conversely many glasses

represent fluid-saturated melts and hence have already lost Cl to a fluid or fluids. It therefore follows that these modeled Cl concentrations in magmatic fluids do not represent the maximum likely contents for each fluid-saturated system given the prior sequestration of Cl from melt by fluid(s). Moreover, some of those systems that were apparently saturated in fluid(s) did so at pressures < 200 MPa, but nevertheless we report calculated Cl contents of fluids at/near 200 MPa. For the latter, the reported concentrations of Cl reflect what the fluid composition would have been if fluid had been stable at that pressure.

We have selected NOS fluid(s)/melt ratios for modeling of 2.0×10^{-3}, 2.0×10^{-2}, and 4.17×10^{-2}. For the smallest fluid(s)/melt ratio, the estimated Cl concentrations of the fluids (i.e., vapor, brine or integrated vapor plus brine) range from 0.3 to nearly 70 wt.%. This very wide range in Cl contents decreases significantly with increasing fluid(s)/melt ratios; e.g., the fluid(s) contain 0.3 to ≤ 18 wt.% Cl for fluid(s)/melt ratios of 2.0×10^{-2}, and the modeled fluid(s) contain 0.3 to only 11 wt.% Cl when the mass of fluid(s) increases to fluid(s)/melt ratios of 4.17 x 10-2.

A key observation in this work is that although the first-exsolved mass of fluid(s) may be small, such first fluids may nevertheless be highly charged with Cl. With closed-system magma evolution in which the Cl-bearing fluid(s) is retained, the bulk Cl content of the system is maintained and hence the values of $D_{Cl}^{fluid/melt}$ and the Cl content of the system are maintained at the higher values observed in Figure 10. Conversely, if the earliest, Cl-enriched fluids are lost from magma via open-system degassing, then this reduces the bulk Cl content of the system and hence the values of $D_{Cl}^{fluid/melt}$ decrease (because $D_{Cl}^{fluid/melt}$ correlates so strongly with the Cl content of the bulk system), and as a result the Cl contents of subsequent magmatic fluids decrease to comparatively lower levels. Interestingly, at higher fluid(s)/melt ratios in equilibrium with the granitic MI compositions of this study (including MI data from several porphyry copper systems), the modeled fluid compositions

range from ca. 0.5 to 7 wt.% Cl or 0.8 to 11 wt.% $NaCl_{equivalent}$. This range in concentration is interesting because prior research on fluid inclusions from Cu-mineralized granite porphyries show that they typically contain a similar range of 2-10 wt.% $NaCl_{equivalent}$ (Sillitoe, 2010). Given this overlap, it follows that prior studies of the magmatic fluids of Cu-mineralized granitic porphyries (Sillitoe, 2010) must therefore provide information specifically about fluid inclusions trapped during mid- to late-stage fluid evolution, involving larger fluid masses at these stages. These prior studies on Cl concentrations of mineralizing fluids (Sillitoe, 2010) do not account for the significantly higher Cl contents present in the initial, smaller masses of first-exsolved magmatic fluids, as modeled here. In addition, this prior research does not address the potential role of such Cl-enriched early fluids in processes of ore-metal dissolution and transport in and around magma. Note also that the modeled Cl contents of magmatic fluids bears only on magmas at NOS conditions; the Cl contents calculated for mineralizing fluids will increase by 10 rel.% if the influence of S in more-oxidized magmas is taken into account.

It is also useful to evaluate the Cl concentrations of magmatic fluids, calculated with our approach for equilibrium Cl exchange between melt and ca. 1 wt.% of aqueous vapor at 200 MPa at closed-system conditions, and to compare the results with prior modeling of the Cl contents of magmatic and eruptive fluids. We model for NOS conditions, and hence, do not account for the potential influence of oxidized magmatic sulfur. In Figure 13, we compare our fluid Cl contents calculated for each MI at 200 MPa (even though most individual glass compositions represent entrapment pressures near or somewhat different from 200 MPa) with prior published estimates on Cl in magmatic vapors of Soufriere Hills, Montserrat, Bishop Tuff, Mt. St. Helens, and Mt. Mazama. For the latter studies, values or ranges in $D_{Cl}^{fluid/melt}$ were provided in the prior publications, and these values of $D_{Cl}^{fluid/melt}$ were used to compute the previously published fluid Cl contents. Mann et al.

(2013), for example, addressed the effects of decompression crystallization on Cl contents of vapor during Montserrat magma ascent through pressures of 170 to 60 MPa by applying two values of $D_{Cl}^{fluid/melt}$ to 1 wt.% magmatic vapor. The consistency between the former and our results is closer for the higher value in the range of $D_{Cl}^{fluid/melt}$ used, i.e., 25. For Mt. Mazama, Wright et al. (2012) modeled closed-system Cl exchange between melt and 1 wt.% vapor, and their use of $D_{Cl}^{fluid/melt}$ of 9 results in good agreement with our modeled Cl contents in vapor. Using the $D_{Cl}^{fluid/melt}$ value of 10 recommended by Edmonds et al. (2008) for magma at greater depth, higher pressure, and closed-system conditions, we calculate Cl contents in 1 wt.% vapor that are compatible with our modeled values. Lastly, the agreement slips somewhat when we compare Cl contents of vapor, calculated with values of $D_{Cl}^{fluid/melt}$ of 9 ± 4 estimated from Bishop Tuff MI compositions by Wallace et al. (1995; 1999), with our method. The former Cl contents of vapor range from 1 to 2 wt.% whereas our results range from 0.4 to 1 wt.%.

4.3.5. Influence of CO_2 on HSL evolution

Given the complexity of multicomponent volatile phases and their partitioning relationships (e.g. Baker and Alletti, 2012), a full discussion of the effects of variable fluid CO_2 concentrations on Cl solubility and Cl fluid-melt partitioning is also beyond the scope of this investigation. However, we note that the flushing of CO_2-enriched vapor through a stored magma is also likely to play a significant role in facilitating HSL generation in some evolving systems. Brine may condense from vapor if CO_2-enriched fluid passes through a fluid-saturated magma and interacts chemically with existing vapor bubbles, depending on the pressure and temperature conditions. The size of the stability field of HSL plus vapor increases relative to that of vapor-only field with the addition of CO_2 to chloride salt-H_2O systems at magmatic temperatures (Bowers and Helgeson, 1983a;b; Heinrich, 2007; Aranovich et al., 2017), and it has been well demonstrated that flushing of CO_2-

charged vapor through melt occurs in natural systems (Moore, 2008; Humphreys et al., 2009; Blundy et al., 2010). It is difficult, therefore, to identify with confidence all likely fluids in the natural systems discussed in this study without information on the respective CO_2 contents of each magmatic system, and improved experimental constraints on CO_2-H_2O-M_xCl_y-melt phase equilibria (where M represents cations). Thus, in summary, while such a CO_2-flushing process may force HSL condensation in the first instance and/or it may increase the mass of HSL that condenses, the reader should be aware that the limitations in the current experimental and natural dataset do not allow for quantitative modeling of this process.

5.1 SUMMARY & CONCLUSIONS

We collated geochemical data for >3500 melt inclusions and matrix glasses spanning 64 separate magmatic systems to assess how effectively fractional crystallization, magma mixing, and fluid-melt component exchange processes can be deciphered through the use of the newly developed solubility-normalized Cl contents of the samples. Our extensive analysis leads to the following conclusions:

1. With progressive melt evolution, the maximum Cl concentrations of melts (represented by melt inclusions and matrix glasses) increase from dacite to rhyodacite and subsequently decrease from rhyodacite to rhyolite, while minimum Cl contents generally decrease from dacite to rhyolite. These trends reflect partial sequestration of Cl by vapor with or without HSL during fractional crystallization ± magma ascent.
2. Importantly, plots of the Cl[Me/Mo] (measured Cl concentration in melt/modeled 200-MPa solubility of Cl in melt) versus the Larsen melt evolution index for these 64 systems provide new insights into processes of magma evolution and fluid exsolution, and constrain the role of Cl in these processes. The relative contributions of these magmatic processes are largely

obscured when only the simple total Cl concentrations are used to interpret data from natural systems.

3. Nine of the volcanic systems include some glass compositions that are consistent with equilibration of the melt with HSL ± vapor for modeling of S-poor magmas at 20 MPa. When modeled for 100 MPa, glasses from 4 of the plutonic systems involve melts that likely exchanged Cl with HSL ± vapor. Magmatic brines are therefore more active, and important, than is generally understood.
4. If the strong influence of oxidizing magmatic sulfur on Cl partitioning between melt and fluid(s) is accounted for, 10 additional eruptive magmas at 20 MPa and 1 additional plutonic system at 100 MPa contain Cl contents that are consistent with saturation of their melt in HSL ± vapor.
5. The Cl concentrations, bulk glass compositions, and computed Cl solubilities of the magmatic systems support estimation of the pressures at which melt would have been in equilibrium with HSL ± vapor at pressures ranging from 20 to as high as 600 MPa.
6. Most Cl contents of the glasses of these magmatic systems are consistent with our modeling of Cl behavior that occurs during melt evolution dominated by fractional crystallization of fluid(s)-saturated systems that are characterized by increasing Cl contents of residual melt, essentially no change of Cl in melt, or decreasing Cl contents of aliquots of residual melt. Glass Cl contents from several of the 64 magmatic systems are consistent with modeled Cl behavior expressing melt evolution dominated by fractional crystallization of fluid-absent magma.
7. Steep, near-vertical curves expressed by Cl[Me/Mo] plotted against the Larsen melt evolution index are observed for some magmatic systems. These relationships may represent fluid-absent magma crystallization for melt compositions ranging from dacite to rhyolite or these curves may

signify the exchange of Cl between fluid(s) and melt for more highly evolved rhyolitic melt compositions.

8. Some magmatic systems show minimal dispersion for less-evolved dacitic melts and increasing dispersion with melt evolution to rhyolitic compositions in plots of Cl[Me/Mo] versus the Larsen melt index. The increasing dispersion may be a consequence and indication of either equilibrium to non-equilibrium assimilation of an alkali or alkaline earth HSL.
9. Equilibrium Cl concentrations computed for S-poor magmatic fluids at 200 MPa vary with the fluid/melt mass ratio, and small masses of incipient fluid may be extremely Cl enriched. Chlorine contents range from 0.3 to nearly 70 wt.% at fluid/melt ratios of 2.0×10^{-3}, and from 0.3 to only 11 wt.% Cl at fluid/melt ratios of 4.17×10^{-2}. Conversely, Cl contents of fluids will be higher for magmatic systems containing several wt.% of oxidized sulfur in fluid.

We have shown that this new approach to interpreting the concentrations of Cl measured in MI and MG offers great promise for modeling fluid exsolution and estimating Cl concentrations of fluids and coexisting melts during Cl exchange between both phases. To facilitate this approach further, we conclude with a recommendation for the collection of more experimental data on fluid-melt Cl partitioning for mid- to shallow-crustal pressures other than 200 MPa, and particularly further work to better quantify the strong influences of oxidized magmatic sulfur, and fluid/melt CO_2 concentrations, on Cl partitioning.

ACKNOWLEDGEMENTS

We appreciate thoughtful and instructive discussions with J. Gardner, C. Huber, and O. Bachmann, and M. Humphreys. We also acknowledge constructive reviews by J. Gardner, H. Balcone-Boissard, and editorial handling by W. van Westrenen. We also express our thanks to Keiji Hammond for assistance with data management. This research was partially supported by NSF award EAR-

1219484 to JDW, and NSF award EAR-1219480 and the University of Auckland Faculty Research Development Fund 2013 award to MCR. Supplementary info/data associated with this article can be found, in the online version, at http…..

REFERENCES

Acosta-Vigil A., London D., Morgan VI G.B. and Dewers T.A. (2003) Solubility of excess alumina in hydrous granitic melts in equilibrium with peraluminous minerals at 700-800°C and 200 MPa, and applications of the aluminum saturation index. *Contrib. Mineral. Petrol.* **146**, 100-119.

Aiuppa A., Baker D.R. and Webster J.D. (2009) Halogens in volcanic systems. *Chem. Geol.* **263**, 1-18.

Alletti M., Baker D.R., Scaillet B., Aiuppa A., Moretti R. and Ottolini L. (2009) Chlorine partitioning between a basaltic melt and H_2O-CO_2 fluids at Mount Etna. *Chem. Geol.* **263**, 37-50.

Alletti M., Burgisser A., Scaillet, B. and Oppenheimer C. (2014) Chloride partitioning and solubility in hydrous phonolites from Erebus volcano: A contribution towards a multi-component degassing model. *GeoResJ* **3-4**, 27-45.

Anderson A.T. (1976) Magma mixing: Petrological process and volcanological tool. *J. Volcanol. Geotherm. Res*. **1**, 3-33.

Andreeva I.A. and Kovalenko V.I. (2011) Evolution of the trachydacite and pantellerite magmas of the bimodal volcanic association of Dzarta-Khuduk, central Mongolia: investigation of inclusions in minerals. *Petrol.* **19**, 348-369.

Aranovich L.Y. (2017) The role of HSLs in high-temperature metamorphism and granitization. Petrol. DOI: 10.1134/S0869591117050022.

Aranovich L.Y., Zakirov I.V., Sretenskaya N.G. and Gerya T.V. (2010) Ternary system H_2O-CO_2-NaCl at high T-P parameters: An empirical mixing model. *Geochem. Internat.* **48**, 446-455.

Atlas Z.D., Dixon J.E., Sen G., Finny M. and Martin-Del Pozzo A.L. (2006) Melt inclusions from Volcán Popocatépetl and Volcán de Colima Mexico: Melt evolution due to vapor-saturated crystallization during ascent. *J. Volcan. Geotherm. Res.* **153**, 221-240.

Audétat A. (2015) Compositional evolution and formation conditions of magmas and fluids related to porphyry Mo mineralization at Climax, Colorado. *J. Petrol.* 1-27, doi: 10.1093/petrology/egv044.

Audétat A. and Li W. (2017) The genesis of Climax-type porphyry Mo deposits: Insights from fluid inclusions and melt inclusions. *Ore Geol. Rev.* **88**, 436-460.

Audétat A. and Lowenstern J.B. (2014) Melt inclusions. In *Geochemistry of Mineral Deposits Treatise on Geochemistry* (ed. S.D. Scott). 2nd edition, Elsevier, pp. 143-173.

Audétat A., Pettke T., Heinrich C.A. and Bodnar, R.J. (2008). The composition of magmatic-hydrothermal fluids in barren and mineralized intrusions. *Econ. Geol*. **103,** 877–908.

Bachmann O., Wallace P.J. and Bourquin J. (2010) The melt inclusion record from the rhyolitic Kos Plateau Tuff (Aegean Arc). *Contrib. Mineral. Petrol.* **159**, 187-202.

Bai T.B. and Koster van Groos A.F. (1994) Diffusion of chlorine in granitic melts. *Geochim. Cosmochim. Acta* **58**, 113-123.

Baker D.R. and Alletti M. (2012) Fluid saturation and volatile partitioning between melts and hydrous fluids in crustal magmatic systems: The contribution of experimental measurements and solubility models. *Earth-Sci. Rev.* **114**, 298-324.

Baker D.R. and Balcone-Bloissard H. (2009) Halogen diffusion in magmatic systems: Our current state of knowledge. *Chem. Geol.* **263**, 82-88.

Baker D.R., Freda C., Brooker R.A. and Scarlato P. (2005) Volatile diffusion in silicate melts and its effects on melt inclusions. An*nal. Geophys.* **48**, 699-717.

Balcone-Boissard H., Boudon G., Cioni R., Webster J.D., Zdanowicz G., Orsi G. and Civetta L. (2016) Chlorine as a geobarometer for alkaline magmas: Evidence from a systematic study of the eruptions of Mount Somma-Vesuvius. *Nature* DOI: 10.1038/srep21726.

Bao B., Webster J.D., Zhang D., Goldoff B. and Zhang R. (2016) Compositions of biotite, amphibole, apatite and silicate melt inclusions from the Tongchang mine, Dexing porphyry deposit, SE China: implications for the behavior of halogens in this mineralized porphyry system. *Ore Geol. Rev.* **79**, 443-462.

Barclay J., Riley D.S. and Sparks R.S.J. (1995) Analytical models for bubble growth during decompression of high viscosity magma. *Bull. Volcanol*. **57**, 422-431.

Barclay J., Carroll M.R., Houghton B.F. and Wilson C.J.N. (1996) Pre-eruptive volatile content and degassing history of an evolving peralkaline volcano. *J. Volcanol. Geotherm. Res.* **74**, 75-87.

Barnes J.D., Prather T.J., Cisneros M., Befus K., Gardner J.E. and Larson T.E. (2014) Stable chlorine isotope behavior during volcanic degassing of H_2O and CO_2 at Mono Craters, CA. *Bull. Volcanol.* **76**, 805-818.

Beermann O. (2010) The solubility of sulfur and chlorine in H_2O-bearing dacites of Krakatau and basalts of Mt. Etna. Ph.D. thesis, Hannover, Germany, 109 p.

Bégué F. (2014) Magmatic volatiles: A melt inclusion study of Taupo Volcanic Zone rhyolites, NZ. Ph.D. thesis, University of Canterbury, NZ, 188 p.

Bégué F., Gravley D.M., Chambefort I., Deering C.D. and Kennedy B.M. (2015) Magmatic volatile distribution as recorded by rhyolitic melt inclusions in the Taupo Volcanic Zone, NZ. *Geol. Soc. Lond. Spec. Pub.* **410**, 71-94.

Beier C., Bach W., Turner S., Niedermeier D., Woodhead J., Erzinger J. and Krumm S. (2015) Origin of silicic magmas at spreading centers-an example from the South East Rift, Manus Basin. *J. Petrol.* **56**, 255-272.

Berlo K., Blundy J., Turner S., Cashman K., Hawkesworth C. and Black S. (2004) Geochemical precursors to volcanic activity at Mount St. Helens, USA. *Science* **306**, 1167–1169.

Blundy J. and Cashman K. (2001) Ascent-driven crystallisation of dacite magmas at Mount St. Helens, 1980–1986. *Contrib. Mineral. Petrol.* **140(no.6)**, 631–650, doi:10.1007/s004100000219.

Blundy J. and Cashman K. (2005) Rapid decompression-driven crystallization recorded by melt inclusions from Mount St. Helens volcano. *Geol.* **33(no.10)**, 793–796, doi:10.1130/G21668.1.

Blundy J., Cashman K.V. and Berlo K. (2008) Evolving magma storage conditions beneath Mount St. Helens inferred from chemical variations in melt inclusions from the 1980–1986 and current (2004–2006) eruptions. (Eds.) Sherrod, D.R., Scott, W.E., and Stauffer, P.H., A Volcano Rekindled; The Renewed Eruption of Mount St. Helens, 2004–2006. *U.S. Geol. Surv. Prof. Pap*. **1750**, 755-790.

Blundy J., Cashman K.V., Rust A. and Witham F. (2010) A case for CO_2-rich arc magmas. *Earth Planet. Sci. Lett.* **290**, 289-301.

Bodnar R.J., Burnham C.W. and Sterner S.M. (1985) Synthetic fluid inclusions in natural quartz. III. Determination of phase equilibrium properties in the system H_2O-NaCl to 1000° C and 1500 bars. *Geochim. Cosmochim. Acta* **49**, 1861-1873.

Borisova A.Y., Pichavant M., Beny J.-M., Rouer O. and Pronost J. (2005) Constraints on dacite magma degassing and regime of the June 15, 1991, climactic eruption of Mount Pinatubo (Philippines): New data on melt and crystal inclusions in quartz. *J. Volcanol. Geotherm. Res.* **145**, 35-67.

Borisova A.Y., Pichavant M., Polve M., Wiedenbeck M., Freydier R. and Candaudap F. (2006) Trace element geochemistry of the 1991 Mt. Pinatubo silicic melts, Philippines: Implications for ore-forming potential of adakitic magmatism. *Geochim. Cosmochim. Acta* **70**, 3702-3716.

Borisova A.Y., Toutain J.-P., Dubessy J., Pallister J., Zwick A. and Salvi S. (2014) H_2O-CO_2-S fluid triggering the 1991 Mount Pinatubo climactic eruption (Philippines). *Bull. Volcanol.* ***76***, DOI 10.1007/s00445-014-0800-3.

Borisova A.Y., Martel C., Gouy S., Pratomo I., Sumarti S., Toutain J.-P., Bindeman I.N., de Parseval P., Mexatian J.-P. and Surono (2013) Highly explosive 2010 Merapi eruption: Evidence for shallow-level crustal assimilation and hybrid fluid. *J. Volcanol. Geotherm. Res.* **261**, 193-208.

Botcharnikov R.E., Holtz F. and Behrens H. (2007) The effect of CO_2 on the solubility of H_2O-Cl fluids in andesitic melt. *Eur. J. Mineral.* **19**, 61-68.

Botcharnikov R.E., Holtz F., Behrens H., Sato H. and Koepke J. (2002) Experimental study of sulfur and chlorine solubility in rhyodacite and andesite melts of Unzen volcano, Japan. *EMPG IX conf. Zurich*, abstract 7, 17.

Botcharnikov R.E., Behrens H., Holtz F., Koepke J. and Sato H. (2004) Sulfur and chlorine solubility in Mt. Unzen rhyodacite melt at 850°C and 200 MPa. *Chem. Geol.* **213**, 207-225.

Bowers T.S. and Helgeson H.C. (1983a) Calculation of the thermodynamic and geochemical consequences of nonideal mixing in the system H_2O-CO_2-NaCl on phase relations in geological systems: Equation of state for H_2O-CO_2-NaCl fluids at high pressures and temperatures. *Geochim. Cosmochim. Acta* **47**, 1247-1275.

Bowers T.S. and Helgeson H.C. (1983b) Calculation of the thermodynamic and geochemical consequences of nonideal mixing in the system H_2O-CO_2-NaCl on phase relations in geological systems: Metamorphic equilibria at high pressures and temperatures. *Am. Mineral.* **68**, 1059-1075.

Bucholz C.E., Gaetani G.A., Behn M.D. and Shimizu N. (2013) Post-entrapment modification of volatiles and oxygen fugacity in olivine-hosted melt inclusions. *Earth Planet. Sci. Lett.* **374**, 145-155.

Candela P.A. (1997) A review of shallow, ore-related granites: Textures, volatiles, and ore metals. *J. Petrol.* **38(12),** 1619-1633.

Carroll M.R. (2005) Chlorine solubility in evolved alkaline magmas. *Ann. Geophys.* **48**, 619-631.

Carroll M.R. and Webster J.D. (1994) Solubilities of sulfur, noble gases, nitrogen, chlorine, and fluorine in magmas. In *Volatiles in Magmas* (eds. M.R. Carroll and J.R. Holloway). *Min. Soc. Am.* **30**, pp. 231-279.

Chambefort I., Bégué F., Heinrich C., Walle M. and Dilles J. (2014) From magma to mudpool: linking arc volatiles and active geothermal systems (abs). 2014 Gold. Conf., Sacramento California, 8-13 June.

Chamberlain K.J., Barclay J., Preece K., Brown R.J., Davidson J.P. and EIMF (2016) Origin and evolution of silicic magmas at ocean islands: Perspectives from a zoned fall deposit on Ascension Island, South Atlantic. *J. Volcanol. Geotherm. Res.* **327**, 349-360.

Castro J.M. and Dingwell D.B. (2009) Rapid ascent of rhyolitic magma at Chaitén volcano, Chile. *Nature* **461**, 780-784.

Chesner C.A. and Luhr J.F. (2010) A melt inclusion study of the Toba Tuffs, Sumatra, Indonesia. *J. Volcanol. Geotherm. Res.* **197**, 259-278.

Chevychelov V.Y. and Chevychelova T.K. (1997) Partitioning of Pb, Zn, W, Mo, Cl, and major elements between aqueous fluid and melt in the systems granodiorite (granite, leucogranite)-H_2O-NaCl-HCl. *Neues Jahr. Mineral*. **172**, 101-115.

Chevychelov V.Y. and Suk N.I. (2003) Influence of the compositions of magmatic melt on the solubility of metal chlorides at pressures of 0.1-3.0 kbar. *Petrol.* **11**, 62-74.

Chiodini G., Cioni R. and Marini L. (1993) Reactions governing the chemistry of crater fumaroles from Vulcano Island, Italy, and implications for volcanic surveillance. *App. Geochem.* **8**, 357-371.

Chiodini G., Marini L. and Russo M. (2001) Geochemical evidences of high-temperature hydrothermal HSLs at Vesuvio Volcano (Italy). *Geochim. Cosmochim. Acta* **65**, 2129-2147.

Christensen B.W. (2000) Geochemistry of fluids associated with the 1995-1996 eruption of Mt. Ruapehu, New Zealand: signatures and processes in the magmatic-hydrothermal system. In: Varekamp J.C. and Rowe G.L. (eds.), *Crater Lakes. J. Volcanol. Geotherm.* **97**, 1-30.

Cline J.S. and Bodnar R.J. (1991) Can economic porphyry copper mineralization be generated by a typical calc-alkaline melt? *J. Geophys. Res.* **96(B5)**, 8113-8126.

Congdon R.D. and Nash W.P. (1988) High-fluorine rhyolite: An eruptive pegmatite magma at the Honeycomb Hills, Utah. *Geology* **16**, 1018-1021.

Coombs M.L., Sisson T.W. and Kimura J.-I. (2004) Ultra-high chlorine in submarine Kilauea glasses: Evidence for direct assimilation of brine by magma. *Earth Planet. Sci. Lett.* **217**, 297-313.

Costa F., Andreastuti S., de Maisonneuve C.B. and Pallister J.S. (2013) Petrological insights into the storage conditions, and magmatic processes that yielded the centennial 2010 Merapi explosive eruption. *J. Volcanol. Geotherm. Res.* **261**, 209-235.

Costa A., Gottsmann J., Melnick O. and Sparks R.S.J. (2011) A stress-controlled mechanism for the intensity of very large magnitude explosive eruptions. *Earth Planet Sci. Lett.* **310**, 161-166.

Cottrell E., Gardner J.E. and Rutherford M.J. (1999) Petrologic and experimental evidence for the movement and heating of the pre-eruptive Minoan rhyodacite (Santorini, Greece). *Contrib. Mineral Petrol.* **135**, 315-331.

Dalou C., Mysen B. and Foustoukos, D. (2015). In-situ measurements of fluorine and chlorine speciation and partitioning between melts and aqueous fluids in the Na_2O-Al_2O_3-SiO_2-H_2O system. *Am. Mineral.* **100**, 47-58.

Davidson P. and Kamenetsky V.S. (2001) Immiscibility and continuous felsic melt-fluid evolution within the Rio Blanco porphyry system, Chile: Evidence from inclusions in magmatic quartz. *Econ. Geol*. **96(8),** 1921-1929.

Davidson P. and Kamenetsky V.S. (2007) Primary aqueous fluids in rhyolitic magmas: melt inclusion evidence for pre- and post-trapping exsolution. *Chem. Geol.* **237**, 372-383.

De Rosa R., Donato P., Gioncada A., Masetti M. and Santacroce R. (2003) The Monte Guardia eruption (Lipari, Aeolian Islands): an example of a reversely zoned magma mixing sequence. *Bull. Volcanol.* **65**, 530-543.

Devine J.D., Sigurdsson H., Davis A.N., Self S. (1984) Estimates of sulfur and chlorine yield to the atmosphere from volcanic eruptions and potential climatic effects. *J. Geophys. Res*. **89(B7)**, 6309-6325.

Doherty A.L., Webster J.D., Goldoff B.A. and Piccoli P.M. (2014) Partitioning behavior of chlorine and fluorine in felsic melt-fluid(s)-apatite systems at 50 MPa and 850-950°C. *Chem. Geol.* **384**, 94-109.

Dolejs D. and Zajacz Z. (2018) Halogens in silicic magmas and their hydrothermal systems. In: Harlov D., Aranovich L.Y. (eds.), The Role of Halogens in Terrestrial and Extraterrestrial Geochemical Processes: Surface, Crust and Mantle. Springer Lectures in Geology Series. pp.?

Driesner T. (2007) The system H_2O-NaCl. Part II: Correlations for molar volume, enthalpy, and isobaric heat capacity from 0 to 1000°C, 1 to 5000 bars, and 0 to 1 X_{NaCl}. *Geochim. Cosmochim. Acta* **71**, 4902-4919.

Driesner T. and Heinrich C.A. (2007) The system H_2O-NaCl. Part. I: correlation formulae for phase relations in temperature-pressure-composition space from 0 to 1000°C, 0 to 5000 bar, and 0 to 1 X_{NaCl}. *Geochim. Cosmochim. Acta* **71**, 4880-4901.

Duffield W.A. and Du Bray E.A. (1990) Temperature, size, and depth of the magma reservoir for the Taylor Creek Rhyolite, New Mexico. *Am. Mineral.* **75**, 1059-1070.

Dunbar N.W. and Hervig R.L. (1992a) Petrogenesis and volatile stratigraphy of the Bishop Tuff: Evidence from melt inclusion analysis. *J. Geophys. Res.* **97B11**, 15129-15150.

Dunbar N.W. and Hervig R.L. (1992b) Volatile and trace element composition of melt inclusions from the Lower Bandelier Tuff: Implications for magma chamber processes and eruptive style. *J. Geophys. Res.* **97B11**, 15151-15170.

Edmonds M., Pyle D. and Oppenheimer C. (2002) HCl emissions at Soufriere Hills Volcano, Montserrat, West Indies, during a second phase of dome building: November 1999 to October 2000. *Bull. Volcanol.* **64**, 21-30.

Edmonds M., McGee K.A. and Doukas, M.P. (2008) Chlorine degassing during the lava dome-building eruption of Mount St. Helens, 2004–2005, c-1506.hap. 27 *of* Sherrod, D.R., Scott, W.E., and Stauffer, P.H., eds., A volcano rekindled; the renewed eruption of Mount St. Helens, 2004–2006. *U.S. Geol. Surv. Prof. Pap*. **1750**, 573-589.

Fournier R.O. (1987) Conceptual models of brine evolution in magmatic-hydrothermal systems. *U.S. Geol. Surv. Prof. Pap. 1350* **2**, 1487

Frezzotti M.-L. (1992) Magmatic immiscibility and fluid phase evolution in the Mount Genis granite (southeastern Sardinia, Italy). *Geochim. Cosmochim. Acta* **56**, 21-33.

Frezzotti M.-L. (2001) Silicate-melt inclusions in magmatic rocks: applications to petrology. *Lithos* **55**, 273-299.

Frezzotti M.-L., Peccerillo A., Zanon V. and Nikogosian I. K. (2004) Silica-rich melts in quartz xenoliths from Vulcano island and their bearing on processes of crustal anatexis and crust-magma interaction beneath the Aeolian Arc, Southern Italy. *J. Petrol.* **45**, 3-26.

Gavigan T.H., Nash W.P. and Webster J.D. (1991) Volatile content of the silicic magma chamber of the Honeycomb Hills, Utah: Complications associated with melt inclusion entrapment and redistribution (abs). *Geol. Soc. Amer. Abs. Prog.* **23**, p. A44a.

Gerlach T.M., Westrich H.R., Casadevall T.J. and Finnegan D.L. (1994) Vapor saturation and accumulation in magmas of the 1989– 1990 eruption of Redoubt Volcano, Alaska. *J. Volcanol. Geotherm. Res.* **62**, 317–337.

Giggenbach W.F. and Glover R.B. (1975) The use of chemical indicators in the surveillance of volcanic activity affecting the crater lake on Mt. Ruapehu, New Zealand. *Bull. Volcanol.* **39**, 70-81.

Giggenbach W.F., Shinohara H., Kusakabe M. and Ohbam T. (2003) Formation of acid volcanic HSLs through interaction of magmatic gases, seawater, and rock within the White Island volcanic-hydrothermal system, New Zealand. In: Simmons S.F. and Graham I. (eds.), Vo*lcanic, Geothermal, and Ore-forming Fluids: Rulers and Witnesses of Processes Within the Earth. Soc. Econ. Geol. Spec. Pub*. **10**, pp. 19-40.

Gioncada A. and Landi P. (2010) The pre-eruptive volatile contents of recent basaltic and pantelleritic magmas at Pantelleria (Italy). *J. Volcan. Geotherm. Res.* **189**, 191-201.

Gioncada A., Clocchiatti R., Sbrana A., Bottazzi P., Massare D. and Ottolini L. (1998) A study of melt inclusions at Vulcano (Aeolian Islands, Italy): Insights on the primitive magmas and on the volcanic feeding system. *Bull. Volcanol.* **60**, 286-306.

Guglielminetti M. (1986) Mofete geothermal field. *Geothermom.* **15**, 781-790.

Guiffrida M., Viccaro M. and Ottolini L. (2018) Ultrafast syn-eruptive degassing and ascent trigger high-energy basic eruptions. *Nature Scientific Reports* **8, 147** DOI:10.1038/s41598-017-18580-8.

Gurenko A.A., Trumbull R.B., Thomas R. and Lindsay J.M. (2005) A melt inclusion record of volatiles, trace elements and Li-B isotope variations in a single magma system from the Plat Pays Volcanic Complex, Dominica, Lesser Antilles. *J. Petrol.* **46(12)**, 2495-2526.

Hansteen T.H. and Lustenhouwer W.J. (1990) Silicate melt inclusions from a mildly peralkaline granite in the Oslo paleorift, Norway. *Mineral. Mag.* **54**, 195-205.

Harris C. (1986) A quantitative study of magmatic inclusions in the plutonic ejecta of Ascension Island. *J. Petrol.* **27**, 251-276.

Heinrich W. (2007) Fluid immiscibility in metamorphic rocks, In: Leibscher, A., Heinrich, C. (eds.), *Fluid-Fluid Equilibria in the Crust. Mineralogical Society of America* **65**, pp. 389-430.

Hofstra A.H., Todorov T.I., Mercer C.N., Adams D.T. and Marsh E.E. (2013) Silicate melt inclusion evidence for extreme pre-enrichment and post-eruptive depletion of lithium in silicic volcanic rocks of the western United States: Implications for the origin of lithium-rich HSLs. *Econ. Geol.* **108**, 1691-1701.

Horn S. (1997) Magmatische evolution und volatile emission der ca. 1000 AD eruption des Baitoushan vulkans (China/North Korea). Ph.D. diss. Christian-Albrechts-Universitat zu Kiel. Tectum, Marburg, 210 p.

Horn S. and Schmincke H.-U. (2000) Volatile emission during the eruption of Baitoushan volcano (China/North Korea) ca. 969 ad. *Bull. Volcanol.* **61**, 537-555.

Huber C., Bachmann O., Vigneresse J.-L., Dufek J. and Prmigiani A.A. (2012) A physical model for metal extraction and transport in shallow magmatic systems. *Geochem. Geophys. Geosys.* **13**, A08003.

Humphreys M.C.S., Blundy J.D. and Sparks R.S.J. (2008) Shallow-level decompression crystallization and deep magma supply at Shiveluch volcano. *Contrib. Mineral. Petrol.* **155**, 45-61.

Humphreys M.C.S., Kearns S.L. and Blundy J.D. (2006) SIMS investigation of electron-beam damage to hydrous, rhyolitic glasses: Implications for melt inclusion analysis. *Am. Mineral.* **91**, D**OI:** https://doi.org/10.2138/am.2006.1936.

Humphreys M.C.S., Edmonds M., Christopher T. and Hards V. (2009) Chlorine variations in the magma of Soufriére Hills Volcano, Montserrat: Insights from Cl in hornblende and melt inclusions. *Geochim. Cosmochim. Acta* **73**, 5693-5708.

Humphreys M.C.S., Edmonds M., Christopher T., Hards V. (2010) Magma hybridization and diffusive exchange recorded in heterogeneous glasses from Soufriére Hills Volcano, Montserrat. *Geophys. Res. Lett.* **37,** DOI: 10.1029/2009GL041926.

Iacovino K., Ju-Song K., Sisson T., Lowenstern J., Kuk-Hun R., Jong-Kam J., Kun-Ho S., Song-Hwan H., Oppenheimer C., Hammond J.O.S., Donovan A., Liu K.W. and Kum-Ran, R. (2016) Quantifying gas emissions from the "Millenium Eruption" of Paektu volcano, Democratic People's Republic of Korea/China. *Sci. Adv*. **2(11**), e1600913, DOI: 10.1126/sciadv.1600913.

Iveson A.A., Webster J.D., Rowe M.C. and Neill, O.K. (2017). Major Element and Halogen (F, Cl) Mineral–Melt–Fluid Partitioning in Hydrous Rhyodacitic Melts at Shallow Crustal Conditions. *J. Petrol.* 58, 2465–2492.

Iveson A.A., Webster J.D., Rowe M.C. and Neill, O.K. (2019). Fluid-melt trace-element partitioning behaviour between evolved melts and aqueous fluids: Experimental constraints on the magmatic-hydrothermal transport of metals. *Chem. Geol.* **516**, 18-41.

Johnson E.R., Kamenetsky V.S. and McPhie J. (2013). The behavior of metals (Pb, Zn, As, Mo, Cu) during crystallization and degassing of rhyolites from the Okataina volcanic center, Taupo volcanic zone, New Zealand. *J. Petrol.* **54**, 1641–1659.

Johnson E.R., Kamenetsky V.S., McPhie J. and Wallace P.J. (2011). Degassing of the H_2O-rich rhyolites of the Okataina Volcanic Center, Taupo Volcanic Zone, New Zealand. *Geology* **39**, 311–314.

Johnson E.R., Wallace P.J., Cashman K.V. and Delgado Granados H. (2010) Degassing of volatiles (H_2O, CO_2, S, Cl) during ascent, crystallization, and eruption at mafic monogenetic volcanoes in central Mexico. *J. Volcanol. Geochem. Res.* **19**7, 225-238.

Johnston D.A. (1978) Volatiles, magma mixing, and the mechanism of eruption of Augustine Volcano, Alaska. Ph.D. diss., University of Washington, 177 p.

Kamenetsky V.S. (2006) Melt inclusion record of magmatic immiscibility in mantle and crustal magmas. In: Webster J.D. (ed.), *Melt Inclusions in Plutonic Rocks. MAC Short Course* **36**, pp. 81-98.

Kasai K., Sakagawa Y., Komatsu R., Sasaki M., Akuku K. and Uchida T. (1998) The origin of hypersaline liquid in the Quaternary Kakkonda granite, samples from well WD-1a, Kakkonda geothermal system, Japan. *Geotherm.* **27**, 631-645.

Kent A.J.R., Peate D.W., Newman S., Stolper E.M. and Pearce J.A. (2002) Chlorine in submarine glasses from the Lau Basin: Seawater contamination and constraints on the composition of slab-derived fluids. *Earth Planet. Sci. Lett.* **202**, 361-377.

Khorzinskiy M.A., Tkachenko S.I., Bulgarov R.F. and Shmulovich K.I. (1996) Condensate composition and native metals in sublimates of high temperature gas streams of Kudriavy volcano, Iturup, Kurile Islands. *Geochim. Internat*. **34**, 1057-1064.

Kilgour G., Blundy J., Cashman K. and Mader H.M. (2013) Small volume andesite magmas and melt-mush interactions at Ruapehu, New Zealand: Evidence from melt inclusions. *Contrib. Mineral. Petrol.* **166**, 371-392.

Koleszar A.M. (2011) Controls on eruption style and magma compositions at Mount Hood, Oregon. Ph.D. Diss. Oregon State University, 199 p.

Koleszar A.M., Kent A.J.R., Wallace P.J. and Scott W.E. (2012) Controls on long-term low explosivity at andesitic arc volcanoes: Insights from Mount Hood, Oregon. *J. Volcanol. Geotherm. Res.* **219-220**, 1-14.

Kravchuk I.F. and Keppler H. (1994) Distribution of chloride between aqueous fluids and felsic melts at 2 kbar and 800°C. *Eur. J. Mineral.* **6**, 913-923.

Kutterolf S., Hansteen T.H., Appel K., Freundt A., Krüger K., Pérez W. and Wehrmann H. (2013) Combined bromine and chlorine release from large explosive volcanic eruptions: A threat to stratospheric ozone? *Geology* **41(6)**, 717-710.

Lanzo G., Landi P. and Rotolo S.G. (2013) Volatiles in pantellerite magmas: A case study of the Green Tuff plinian eruption (Island of Pantelleria, Italy). *J. Volcan. Geotherm. Res.* **262**, 153-163.

Larsen E.S. (1938) Some New Variation Diagrams for Groups of Igneous Rocks. *J.Geol.* **46**, 505-520.

Larsen J.F., Nye C.J., Coombs M.L., Tilman M., Izbekov P. and Cameron C. (2010) Petrology and geochemistry of the 2006 eruption of Augustine volcano. In: Power, J., Coombs, M.L., Freymueller, J. (Eds.), The 2006 Eruption of Augustine Volcano. *U. S. Geol. Surv. Prof. Pap.* **1769**, pp. 335-382.

Lassiter J.C., Hauri E.H., Nikogosian I.K. and Barsczus H.G. (2002) Chlorine-potassium variations in melt inclusions from Raivavae and Rapa, Austral Islands: Constraints on chlorine recycling in the mantle and evidence for brine-induced melting of oceanic crust. *Earth Planet. Sci. Lett.* **202**, 525-540.

Lecumberri-Sanchez P., Steele-MacInnis M. and Bodnar R.J. (2015) Synthetic fluid inclusions XIX. Experimental determination of the vapor-saturated liquidus of the system H_2O-NaCl-$FeCl_2$. *Geochim. Cosmochim. Acta* **148**, 34-49.

Le Roux P.J., Shirey S.B., Hauri E.H., Perfit M.R. and Bender J.F. (2006) The effects of variable sources, processes and contaminants on the composition of northern EPR MORB (8-10°N and 12-14 N): Evidence from volatiles (H_2O, CO_2, S) and halogens (F, Cl). *Earth Planet. Sci. Lett.* **251**, 209–231.

Liberto V.D., Nuccio P.M. and Paonita A. (2002) Genesis of chlorine and sulfur in fumarolic emissions at Vulcano Island (Italy): assessment of pH and redox conditions in the hydrothermal system. *J. Volcan. Geotherm. Res.* **116**, 137-150.

Liu Y., Anderson A.T., Wilson C.J.N., Davis A.M. and Steele I.M. (2006) Mixing and differentiation in the Oruanui rhyolitic magma, Taupo, New Zealand: Evidence from volatiles and trace elements in melt inclusions. *Contrib. Mineral. Petrol.* **151**, 71-87.

Lowenstern J.B. (1993) Evidence for a copper-bearing fluid in magma erupted at the Valley of Ten Thousand Smokes, Alaska. *Contrib. Mineral. Petrol.* **114**, 409-421.

Lowenstern J.B. (1994) Chlorine, fluid immiscibility, and degassing in peralkaline magmas from Pantelleria, Italy. *Am. Mineral.* **79**, 353-369.

Lowenstern J.B. (2000) A review of the contrasting behavior of two magmatic volatiles: chlorine and carbon dioxide. *J. Geochem. Explor.* **69**, 287-290.

Lukanin O.A. (2015) Chlorine partitioning between melt and aqueous chloride fluid during granite magma, degassing I. Decompression-induced melt degassing. *Geochem. Internat*. **53**, 786-810.

Lukanin O.A. (2016) Chlorine partitioning between melt and aqueous chloride fluid during granite magma, degassing. Part II. Crystallization-induced degassing of melts. *Geochem. Internat*. **54**, 660-680.

Malinin S.D., Kravchuk I.F. and Delbove F. (1989) Chloride distribution between phases in hydrated and dry chloride-aluminosilicate melt systems as a function of phase composition. *Geochem. Internat.* **26**, 32-38.

Mandeville C.W., Carey S.N. and Sigurdsson, H. (1996) Magma mixing, fractional crystallization, and volatile degassing during the 1883 eruption of Krakatau Volcano, Indonesia. *J. Volcan. Geotherm. Res*. **74**, 243-274.

Mandeville C.W., Webster J.D., Tappen C., Taylor B.E., Timbal A., Sasaki A., Hauri E., Bacon C.R. (2009) Stable isotopic and petrologic evidence for open-system degassing during the climactic and pre-climactic eruptions of Mt. Mazama, Crater Lake, Oregon. *Geochim. Cosmochim. Acta* **73**, 2978-3012.

Mandon, C.L. (2017) Volatile Transport Of Metals In The Andesitic Magmatic-Hydrothermal System Of White Island. Ph.D. diss. Victoria University of Wellington, 221 p.

Mann C.P., Wallace P.J. and Stix J. (2013) Phenocryst-hosted melt inclusions record stalling of magma during ascent in the conduit and upper magmat reservoir prior to vulcanian explosions, Soufriére Hills volcano, Montserrat, West Indies. *Bull. Volcanol.* **75**, 687-703.

Mathez, E.A. and Webster, J.D.W. (2005) Partitioning behavior of chlorine and fluorine in the system apatite–silicate melt–fluid. *Geochim. Cosmochim. Acta* **69**, 1275-1286.

Mercer C.N., Hofstra A.H., Todorov T.I., Roberge J., Burgisser A., Adams D.T. and Cosca M. (2015) Pre-eruptive conditions of the Hideaway Park topaz rhyolite: insights into metal source and evolution of magma parental to the Henderson porphyry molybdenum deposit, Colorado. *J. Petrol.* **56**, 645-679.

Métrich N. and Rutherford M.J. (1992) Experimental study of chlorine behavior in hydrous silicic melts. *Geochim. Cosmochim. Acta* **56**, 607-616.

Métrich N., Schiano P., Clocchiatti R. and Maury R.C. (1999) Transfer of sulfur in subduction settings: An example from Bataan Island (Luzon volcanic arc, Philippines). *Earth Planet. Sci. Lett.* **167**, 1-14.

Michael P.J. and Schilling J.-G. (1989) Chlorine in mid-ocean ridge magmas: Evidence for assmilation of seawater-influenced components. *Geochim. Cosmochim. Acta* **53(12),** 3131–3143.

Michaud V., Clocchiatti R. and Sbrana S. (2000) The Minoan and post-Minoan eruptions, Santorini (Greece), in the light of melt inclusions: Chlorine and sulphur behavior. *J. Volcanol. Geotherm. Res.* **99**, 195-214.

Moore G. (2008) Interpreting H_2O and CO_2 contents in melt inclusions: Constraints from solubility experiments and modeling. *Rev. Mineral. Geochem.* **69**, 333-361.

Morgan G.B. and London D. (1996) Optimizing the electron microprobe analysis of hydrous alkali aluminosilicate glasses. *Am. Mineral.* **81**, **DOI:** https://doi.org/10.2138/am-1996-9-1016.

Nadeau O., Stix J. and Williams-Jones A.E. (2013) The behavior of Cu, Zn and Pb during magmatic-hydrothermal activity at Merapi volcano, Indonesia. *Chem. Geol.* **342**, 167-179.

Nadeau P.A., Webster J.D., Mandeville C.W., Goldoff B.A., Shimizu N. and Monteleone B. (2015) A glimpse into Augustine volcano's Pleistocene past: Insight from the petrology of a massive rhyolite deposit. *J. Volcanol. Geotherm. Res.* **304**, 304-323.

Naumov V.B., Tolstykh M.L., Grib E.N., Leonov V.L. and Kononkova N.N. (2008) Chemical compositions, volatile components and trace elements in melts of the Karymskii volcanic center, Kamchatka, and Golovnina volcano, Kunashir Island: Evidence from inclusions in minerals. *Petrol.* **16**, 1-18.

Naumov V.B., Prokofiev V.Y., Kovelenker V.A., Tolstykh M.L., Damian G. and Damian F. (2013) Unusual acid melts in the area of the unique Rosia Montana gold deposit, Apuseni Mountains, Romania: Evidence from inclusions in quartz. *Geochem. Internal.* **51**, 876-888.

Neave D.A., Fabbro G., Herd R.A., Petrone C.M. and Edmonds M. (2012) Melting, differentiation and degassing at the Pantelleria volcano, Italy. *J. Petrol.* **53**, 637-663

Newman S. and Lowenstern J.B. (2002) VolatileCalc: a silicate melt-H_2O-CO_2 solution model written in Visual Basic for Excel. *Comp. Geosci.* **28**, 597-604.

Norling B., Rowe M.C., Chambefort I., Tepley III F.J. and Morrow S. (2016) Volatile behavior and trace metal transport in the magmatic-geothermal system at Putauaki (Mt. Edgecumbe), NZ. *J. Volcanol. Geotherm. Res*. **318**, 27-44.

Park J.-W., Campbell I.H., Kim J. and Moon J.-W. (2015) The role of late sulfide saturation in the formation of a Cu- and Au-rich magma: Insights from the platinum group element geochemistry of Niuatahi-Motutahi lavas, Tonga rear arc. *J. Petrol.* **56**, 59-81.

Parmigiani A., Huber C., Chopard B. and Bachmann O. (2011) Pore-scale mass and reactant transport in multiphase porous media flows. *J. Fluid. Mech.* **686**, 40-76.

Parmigiani A., Farough S., Huber C., Bachmann O. Su Y. (2016) Bubble accumulation and its role in the evolution of magma reservoirs in the upper crust. *Nature* **532**, 492-495.

Pintea I. (2014) The magmatic immiscibility between silicate-, HSL-, and Fe-S-O melts from the porphyry (Cu-Au-Mo) deposits in the Carpathians (Romania): A review. *Rom. J. Earth Sci.* **87**, 1-32.

Pokrovski, G.S. Borisova, A.Y. and Bychkov, A.Y. (2013). Speciation and transport of metals and metalloids in geological vapors. *MSA Rev. Min. Geochem*. **76**, 165–218.

Portnyagin M., Hoernle K., Storm S., Mironov N., van den Bogaard C. and Botcharnikov R. (2012) H_2O-rich melt inclusions in fayalitic olivine from Hekla volcano: Implications for phase relationships in silicic systems and driving forces of explosive volcanism on Iceland. *Earth Planet. Sci. Lett*. **357-358**, 337-346.

Preece K., Gertisser R., Barclay J., Berlo K. and Herd R.A. (2014) Pre- and syn-eruptive degassing and crystallization processes of the 2010 and 2006 eruptions of Merapi volcano, Indonesia. *Contrib. Mineral. Petrol.* **168**, DOI 10.1007/s00410-014-1061-z.

Rapien M.H. (1998) Geochemical evolution at White Island, NZ. M.S. thesis, Virginia Polytechnic Institute and State University. 59 p.

Rapien M.H., Bodnar R.J., Simmons S.F., Szabo C. and Sutton S.R. (2003) The embryonic porphyry copper system at White Island, NZ. *Soc. Econ. Geol. Spec. Pub.* **10**, 41-59.

Roedder E. (1992) Fluid inclusion evidence for immiscibility in magmatic differentiation. *Geochim. Cosmochim. Acta* **56**, 5-20.

Roedder E. and Coombs D.S. (1967) Immiscibility in granitic melts, indicated by fluid inclusions in ejected granitic blocks from Ascension Island. *J. Petrol.* **8**, 417-451.

Roman D.C., Cashman K.V., Gardner C.A., Wallace P.J. and Donovan J.J. (2006) Storage and interaction of compositionally heterogeneous magmas from the 1986 eruption of Augustine volcano, Alaska. *Bull. Volcanol.* **68**, 240-254.

Rottier B., Kouzmanov K., Bouvier A.-S., Baumgartner L.P., Wälle M., Rezeau H., Bendezú, R. and Fontboté L. (2016) Heterogeneous melt and hypersaline liquid inclusions in shallow porphyry type mineralization as markers of the magmatic-hydrothermal transition (Cerro de Pasco district, Peru). *Chem. Geol.* **447**, 93-116.

Rouwet D. and Ohba T. (2015) Isotope fractionation and HCl partitioning during evaporative degassing from active crater lakes. Volcanic Lakes: Advances in Volcanology. (Eds.) Rouwet D., Christenson B., Tassi F., Vandemeulebrouck J., pp. 179-200.

Ruprecht P. and Bachmann O. (2010) Pre-eruptive reheating during magma mixing at Quizapu volcano and the implications fort he explosiveness of silicic arc volcanoes. *Geology* **38**, 919-922.

Saito G., Kazahaya K., Shinohara H., Stimac J. and Kawanabe Y. (2001) Variation of volatile concentration in a magma system of Satsuma-Iwojima volcano deduced from melt inclusion analyses. *J. Volcanol. Geotherm. Res.* **108**, 11-31.

Saunders K.E., Baker J.A. and Wysoczanski R.J. (2010) Microanalysis of large volume silicic magma in continental and oceanic arcs: melt inclusions in Taupo volcanic zone and Kermadec arc rocks, South West Pacific. *J. Volcanol. Geotherm. Res.* **190**, 203-218.

Schmidt A.K., Trumbull R.B., Dulski P. and Emmermann R. (2002) Zr-Nb-REE mineralization in peralkaline granites from the Amis Complex, Brandberg (Namibia): Evidence for magmatic pre-enrichment from melt inclusions. *Econ. Geol.* **97**, 399-413.

Self S. and King A.J. (1996) Petrology and sulfur AD chlorine emissions of the 1963 eruption of Gunung Agung, Bali, Indonesia. *Bull. Volcanol.* **58,** 263-285.

Shinohara H. (1994) Exsolution of immiscible vapor and liquid phases from a crystallizing silicate melt: implications for chlorine and metal transport. G*eochim. Cosmochim. Acta* **58**, 5215-5221.

Shinohara H., Ilyama J.T. and Matsuo S. (1989) Partition of chlorine compounds between silicate melt and hydrothermal solutions: I. Partition of NaCl-KCl. G*eochim. Cosmochim. Acta* **53**, 2617-2630.

Shmulovich K.I. and Churakov S.V. (1998) Natural fluid phases at high temperatures and low pressures. *J. Geochem. Explor*. **62**, 183-191.

Shmulovich K.I. and Graham C.M. (2004) An experimental study of phase equilibria in the systems H_2O-CO_2-$CaCl_2$ and H_2O-CO_2-NaCl at high pressures and temperatures (500-800 °C, 0.5-0.9 GPa): geological and geophysical applications. *Contrib. Mineral. Petrol.* **146**, 450-462.

Signorelli S. and Carroll M.R. (2000) Solubility and fluid–melt partitioning of Cl in hydrous phonolitic melts. *Geochim. Cosmochim. Acta* **64**, 2851– 2862.

Signorelli S. and Carroll M.R. (2002) Experimental study of Cl solubility in hydrous alkaline melts: Constraints on the theoretical maximum amount of Cl in trachytic and phonolitic melts. *Contrib. Mineral. Petrol.* **143**, 209-218.

Sisson T.W. and Layne G.D. (1993) H_2O in basalt and basaltic andesite glass inclusions from four subduction-related volcanoes. *Earth Planet. Sci. Lett.* **117**, 619-635.

Sparks S.R.J., Sigurdsson H. and Wilson L. (1977) Magma mixing: A mechanism for triggering acid explosive eruptions. *Nature* **267**, 315-318.

Steele-MacInnis M., Lecumberri-Sanchez P. and Bodnar R.J. (2015) Synthetic fluid inclusions XX. Critical *PTx* properties of H_2O-$FeCl_2$ fluids. *Geochim. Cosmochim. Acta* **148**, 50-61**.**

Sterner S.M., Hall D.L. and Bodnar R.J. (1988) Synthetic fluid inclusions. V. Solubility relations in the system NaCl-KCl-H2O under vapor-saturated conditions. *Geochim. Cosmochim. Acta* **52**, 989-1005.

Stewart A.-M. and Castro J.M. (2016) P-T-X evolution of the 1280 AD Quilotoa dacite. J. *Volcanol. Geotherm. Res*. **313**, 29-43.

Stewart R.B., Price R.C. and Smith I.E.M. (1996) Evolution of high-K arc magma, Egmont volcano, Taranaki, New Zealand: evidence from mineral chemistry. *J. Volcan. Geotherm. Res.* **74**, 275-295.

Stix J. and Layne G.D. (1996) Gas saturation and evolution of volatile and light lithophile elements in the Bandelier magma chamber between two caldera-forming eruptions. *J. Geophys. Res.* **101B11**, 125181-25196.

Straub S.M. and Layne G.D. (2003) The systematics of chlorine, fluorine, and water in Izu arc front volcanic rocks: Implications for volatile recycling in subduction zones. *Geochim. Cosmochim. Acta* **67**, 4179-4203.

Streck M.J. and Wacaster S. (2006) Plagioclase and pyroxene hosted melt inclusions in basaltic andesites of the current eruption of Arenal volcano, Costa Rica. *J. Volcanol. Geotherm. Res.* **157**, 236-253.

Student J.J. and Bodnar R.J. (2004) Silicate melt inclusions in porphyry copper deposits: Identification and homogenization behavior. *Can. Mineral.* **42**, 1583-1599.

Sun W.D., Binns R.A., Fan A.C., Kamenetsky V.S., Wysoczanski R., Wei G.J., Hu Y.H. and Arculus R.J. (2007) Chorine in submarine volcanic glasses from the eastern Manus basin. *Geochim. Cosmochim. Acta* **71**, 1542-1552.

Tappen C., Webster J.D., Roderick D. and Mandeville C.W. (2009) Petrology and geochemistry of ca. 2100 -1000 a.B.P. magmas of Augustine volcano, Alaska. *J. Volcan. Geotherm. Res.* **183**, 42-62.

Taran Y.A., Connor C.B., Shapar V.N., Ovsyannikov A.A. and Bilichenko A.A. (1997) Fumarolic activity of Avachinsky and Koryaksky volcanoes, Kamchatka, from 1993 to 1994. *Bull. Volcanol.* **58**, 441-448.

Thomas R. and Davidson P. (2016) Revisiting complete miscibility between silicate melts and hydrous fluids, and the extreme enrichment of some elements in the supercritical state – Consequences for the formation of pegmatites and ore deposits. *Ore Geol. Rev.* **72**, 1088-1101.

Thomas R. and Webster J.D. (2000) Strong tin enrichment in a pegmatite-forming melt. *Mineral. Depos.* **35**, 570-582.

Thomas R., Webster J.D. and Heinrich W. (2000) Melt inclusions in pegmatite quartz: complete miscibility between silicate melts and hydrous fluids at low pressure. *Contrib. Mineral. Petrol.* **139**, 394-401.

Thomas R., Förster H.-J., Rickers K. and Webster J.D. (2005) Formation of extremely F-rich hydrous melt fractions and hydrothermal fluids during differentiation of highly evolved tin-granite magmas: A melt/fluid-inclusion study. *Contrib. Mineral. Petrol.* **148**, 582-601.

Tolstykh M.L., Naumov V.B., Ozerov A. Y. and Kononkova N.N. (2001) Composition of magmas of the 1996 eruption at the Karymskii volcanic center, Kamchatka: evidence from melt inclusions. *Geochem. Int.* **39**, 447-458.

Tolstykh M.L., Naumov V.B., Babanskii A.D., Bogoyavlenskaya G.E. and Khubunaya S.A. (2003) Chemical composition, volatile components, and trace elements in andesitic magmas of the Kurile-Kamchatka region. *Petrol.* **11**, 407-425.

Tolstykh M.L., Naumov V.B., Babanskii A.D., Khubanaya S.A. and Kononkova N.N. (2000) Chemical composition, trace elements, and volatile components of melt inclusions in minerals from andesites of the Shiveluch volcano, Kamchatka. *Geochim. Inter.* **38**, 123-132.

Varekamp J.C., Pasternack G.B. and Rowe G.L., Jr. (2000) Volcanic lake systematics II. Chemical constraints. In: Varekamp J.C. and Rowe G.L. (Eds.), *Crater Lakes. J. Volcan. Geotherm. Res.* **97**, pp. 161-179.

Villemant B. and Boudon G. (1999) H_2O and halogen (F, Cl, Br) behavior during shallow magma degassing processes. *Earth Planet. Sci. Lett.* **168**, 271-286.

Villemant B., Mouatt J. and Michel A. (2008) Andesitic magma degassing investigated through H2O vapour-melt partitioning of halogens at Soufriére Hills Volcano, Montserrat (Lessar Antilles). *Earth Planet. Sci. Lett*. **269**, 212-229.

Wade J.A., Plank T., Melson W.G., Soto G.J. and Hauri E.H. (2006) The volatile content of magmas from Arenal volcano. *J. Volcanol. Geotherm. Res.* **157**, 94-120.

Wahrenberger C.M. (1997) Some aspects of the chemistry of volcanic gases. Ph.D. diss., Swiss Federal Institute of Technology, Zurich.

Wallace P.J. (2005) Volatiles in subduction zone magmas: concentrations and fluxes based on melt inclusion and volcanic gas data. *J. Volcan. Geotherm. Res.* **140**, 217-240.

Wallace P.J., Anderson Jr. A.T. and Davis A.M. (1995) Quantification of pre-eruptive exsolved gas contents in silicic magmas. *Nature* **377**, 612-616.

Wallace P.J., Anderson Jr. A.T. and Davis A.M. (1999) Gradients in H_2O, CO_2, and exsolved gas in a large-volume silicic magma system: Interpreting the record preserved in melt inclusions from the Bishop Tuff. *J. Geophys. Res.* **104(B9)**, 20097-20122.

Wanless V.D., Perfit M.R., Ridley W.I., Wallace P.J., Grimes C.B. and Klein E.M. (2011) Volatile abundances and oxygen isotopes in basaltic to dacitic lavas on mid-ocean ridges: The role of assimilation at spreading centers. *Chem. Geol.* **287**, 54-65.

Watson E.B. (1991) Diffusion of dissolved CO_2 and Cl in hydrous silicic to intermediate magmas. *Geochim. Cosmochim. Acta* **55**, 1897-1902.

Webster J.D. (1992a) Water solubility and Cl partitioning in Cl-rich granitic systems: Effects of melt composition at 2 kbar and 800° C. *Geochim. Cosmochim. Acta* **56**, 659-678.

Webster J.D. (1992b) Fluid-melt interactions involving Cl-rich granites: Experimental study from 2 to 8 kbar. *Geochim. Cosmochim. Acta* **56**, 679-687.

Webster J.D. (2004) The exsolution of magmatic hydrosaline chloride liquids. *Chem. Geol.* **210**, 33-48.

Webster J.D. and De Vivo B. (2002) Experimental and modeled solubilities of chlorine in aluminosilicate melts, consequences of magma evolution, and implications for exsolution of hydrous chloride melt at Mt. Somma-Vesuvius. *Am. Mineral.* **87**, 1046-1061.

Webster J.D. and Duffield W.A. (1991) Volatiles and lithophile elements in Taylor Creek Rhyolite: constraints from glass inclusion analysis. *Am. Mineral.* **76**, 1628-1645.

Webster J.D. and Duffield W.A. (1994) Extreme halogen abundances in tin-rich magma of the Taylor Creek Rhyolite, New Mexico. *Econ. Geol.* **89**, 840-850.

Webster J.D. and Mandeville C.W. (2007) Fluid immiscibility in volcanic systems. In: A. Leibscher, C. Heinrich, eds., *Fluid-Fluid Equilibria in the Crust, Reviews in Mineralogy and Geochemistry* **65**, 313-362.

Webster J.D. and Rebbert C.R. (2001) The geochemical signature of fluid-saturated magma determined from silicate melt inclusions in Ascension Island granite xenoliths. *Geochim. Cosmochim. Acta* **65**, 123–136.

Webster J.D., Baker D.R. and Aiuppa, A. (2018) Halogens in mafic and intermediate-silica content magmas. In: Harlov D., Aranovich L.Y. (eds.), The Role of Halogens in Terrestrial and Extraterrestrial Geochemical Processes: Surface, Crust and Mantle. Springer Lectures in Geology Series, pp. 307-430.

Webster J.D., Burt D.M. and Aguillon R.A. (1996) Volatile and lithophile trace-element geochemistry of Mexican tin rhyolite magmas deduced from melt inclusions. *Geochim. Cosmochim. Acta* **60**, 3267-3283.

Webster J.D., De Vivo B. and Tappen C. (2003) Volatiles, magmatic degassing and eruptions of Mt. Somma-Vesuvius: Contraints from silicate melt inclusions, Cl and H_2O solubility experiments and modeling. In: Melt Inclusions in Volcanic Systems: Methods, Applications and Problems (B. De Vivo & R. J. Bodnar, Eds). *Developments in Volcanology* **5**. Elsevier, Amsterdam, pp. 207-226.

Webster, J.D., Kinzler, R.J., and Mathez, E.A. (1999) Chloride and water solubility in basalt and andesite liquids and implications for magmatic degassing. *Geochim. Cosmochim. Acta* **63**, 729-738.

Webster J.D., Taylor R.P. and Bean C. (1993) Pre-eruptive melt composition and constraints on degassing of a water-rich pantellerite magma, Fantale volcano, Ethiopia. *Contrib. Mineral. Petrol.* **114**, 53-6

Webster J.D., Goldoff B.A., Flesch R. and Silbert, Z.W. (2017) Hydroxyl, Cl, and F partitioning between high-silica rhyolitic melt-apatite-fluid(s) at 50-200 MPa and 700-1000°C. *Am. Mineral.* **102**, 61-74.

Webster J.D., Mandeville C.W., Goldoff B., Coombs M.L. and Tappen C. (2010) Augustine volcano, Alaska: The influence of volatile components in magmas erupted AD 2006 to 2100 years before present. In: Power, J., Coombs, M.L., Freymueller, J. (Eds.), The 2006 Eruption of Augustine Volcano. *U. S. Geol. Surv. Prof. Pap.* **1769**, pp. 383-423.

Webster J.D., Sintoni M.F., Goldoff B., De Vivo B. and Shimizu N. (2014) C-O-H-S-Cl-F volatile component solubilities and partitioning in phonolitic-trachytic melts and aqueous-carbonic vapor ± saline liquid at 200 MPa. *J. Petrol.* **55(11),** 2217-2248.

Webster J.D., Thomas R., Rhede D, Förster H.-J. and Seltmann R. (1997) Melt inclusions in quartz from an evolved peraluminous pegmatite: geochemical evidence for strong enrichment in fluorine-rich and phosphorus-rich residual melts. *Geochim. Cosmochim. Acta* **61**, 2589-2604.

Webster J.D., Thomas R., Förster H.-J., Seltmann R. and Tappen C. (2004) Geochemical evolution of halogen-enriched granite magmas and mineralizing fluids of the Zinnwald tin-tungsten mining district, Erzgebirge, Germany. *Mineral. Deposit.* **39**, 452-472.

Webster J.D., Vetere F., Botcharnikov R.E., Goldoff B., McBirney A. and Doherty A.L. (2015) Experimental and modeled chlorine solubilities in aluminosilicate melts at 1 to 7000 bars and 700 to 1250C: Applications to magmas of Augustine volcano, Alaska. *Am. Mineral.* **100**, 522-535.

Werner C., Hurwitz S., Evans W.C., Lowenstern J.B., Bergfeld D., Heasler H., Jaworowski C. and Hunt A. (2008) Volatile emissions and gas geochemistry of Hot Spring Basin, Yellowstone National Park, USA. *J. Volcanol. Geotherm.* Res. **178**, 751-762.

Whitaker M.L., Nekvasil H., Lindsley D.H. and McCurry M. (2008) Can crystallization of olivine tholeiite give rise to potassic rhyolites? – an experimental investigation. *Bull. Volcanol.* **70**, 417-434.

Wilson C.J.N., Blake S., Charlier B.L.A. and Sutton A.N. (2006) The 26.5 ka Oruanui eruption, Taupo volcano, NZ: development, characteristics and evacuation of a large rhyolitic magma body. *J. Petrol*. **47**, 35-69.

Witham F. (2011) Conduit convection, magma mixing, and melt inclusion trends at persistently degassing volcanoes. *Earth Planet. Sci. Lett.* **301**, 345-352.

Wittenbrink J. (2006) Geochemische, metallogenetische und bor-isotopen untersuchungen an schmelzeinschlüssen und gesteinen bolivianischer und chilenischer porphyry-lagerstätten der zentralen Anden. Ph.D. Diss., Technischen Universität Clausthal, Germany, 220 p.

Wittenbrink J., Lehmann B., Wiedenbeck M., Wallianos A., Dietrich A. and Palacios C. (2009) Boron isotope composition of melt inclusions from porphyry systems of the Central Andes: A reconnaissance study. *Ter. Nova* **21**, 111-118.

Wright H.M., Bacon C.R., Vazquez J.A. and Sisson T.W. (2012) Sixty thousand years of magmatic volatile history before the caldera-forming eruption of Mount Mazama, Crater Lake, Oregon. *Contrib. Mineral. Petrol.* **164**, 1027-1052.

Yang K. (1997) Glass inclusions in quartz phenocrysts of rhyolites, Mt. Jang, Pusan, Korea. *Geosci. J.* **1**, 50-56.

Yang K. and Scott S.D. (2002) Magmatic degassing of volatiles and ore metals into a hydrothermal system on the modern sea floor of the eastern Manus back-arc basin, Western Pacific. *Econ. Geol.* **97**, 1079-1100.

Yang K. and Scott S.D. (2005) Vigorous exsolution of volatiles in the magma chamber beneath a hydrothermal system on the modern sea floor of the eastern Manus back-arc basin, western Pacific: Evidence from melt inclusions. *Econ. Geol.* **100**, 1085-1096.

Zajacz Z., Candela P.A., Piccoli P.M. and Sanchez-Valle C. (2012) The partitioning of sulfur and chlorine between andesitic melts and magmatic volatiles and the exchange coefficients of major cations. *Geochim. Cosmochim. Acta* **89**, 81-101.

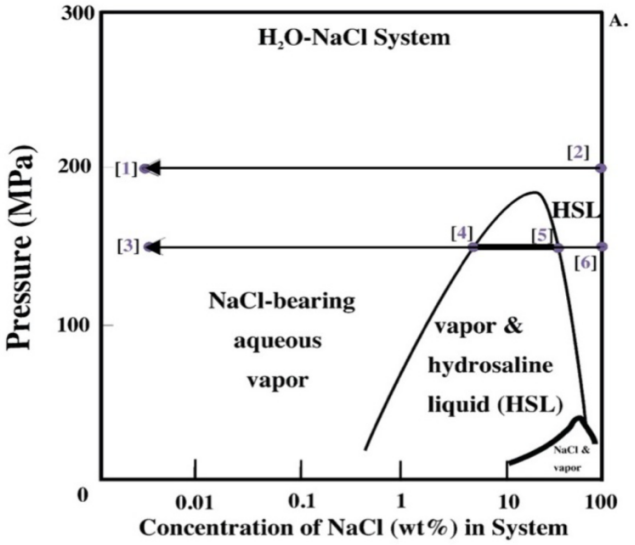

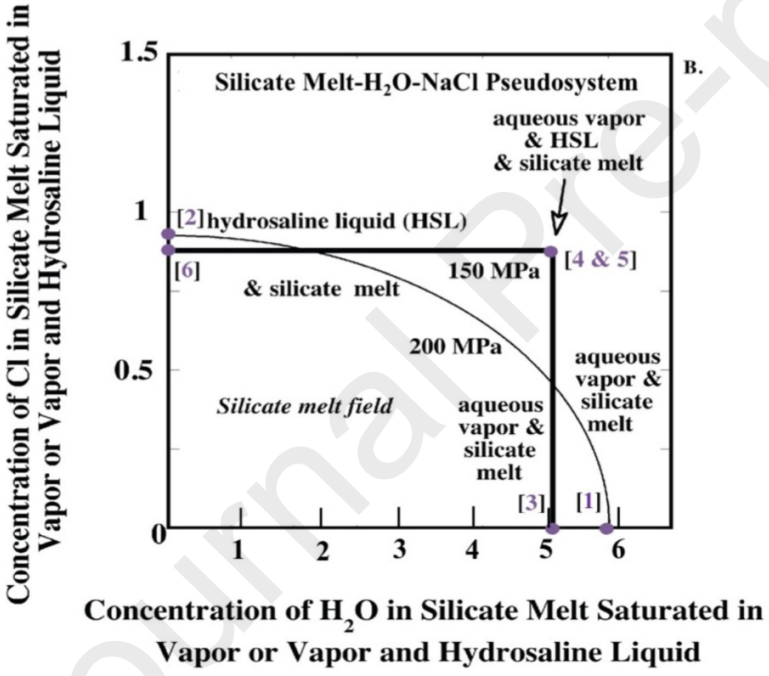

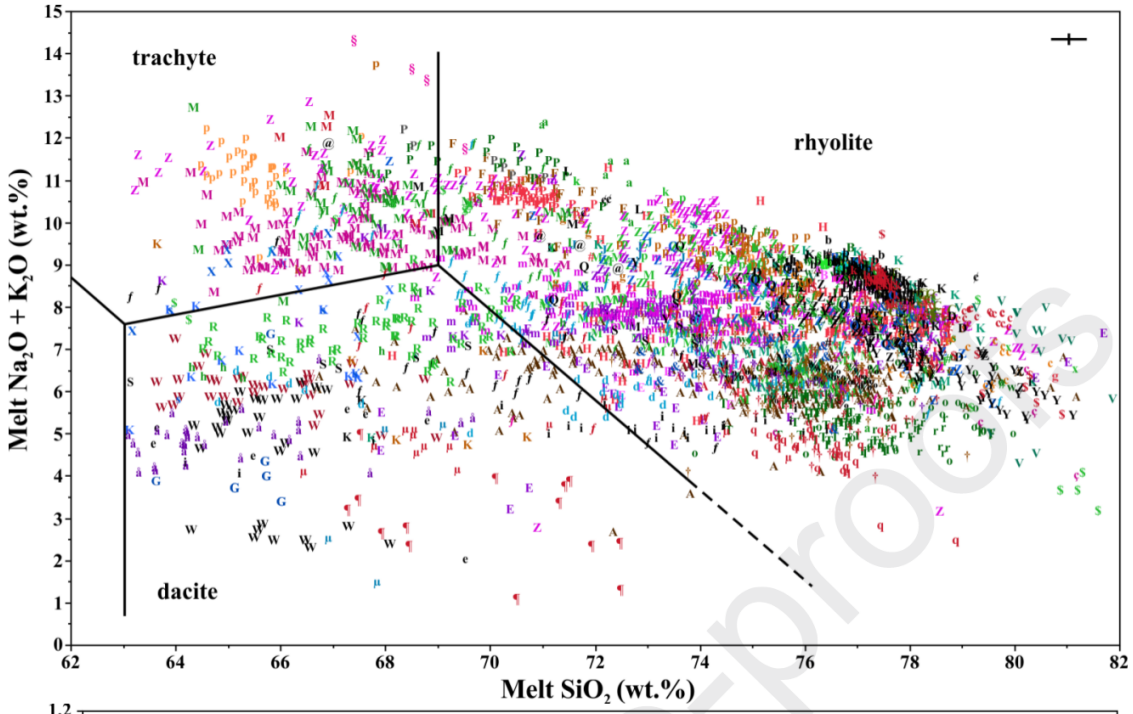

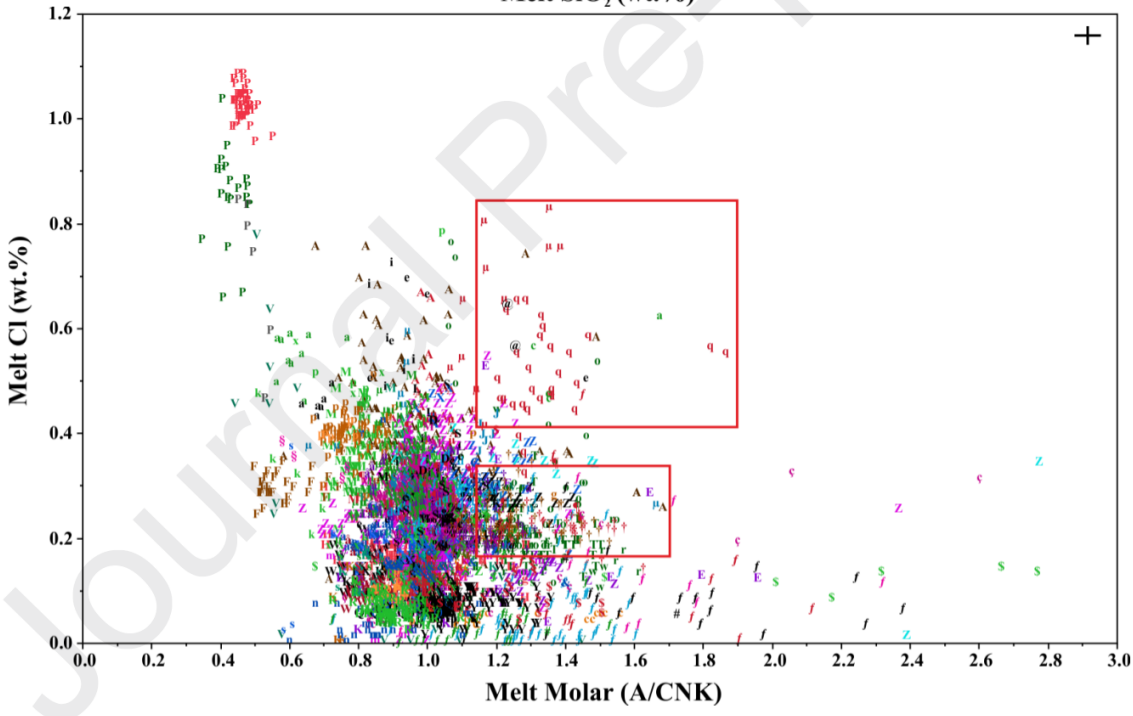

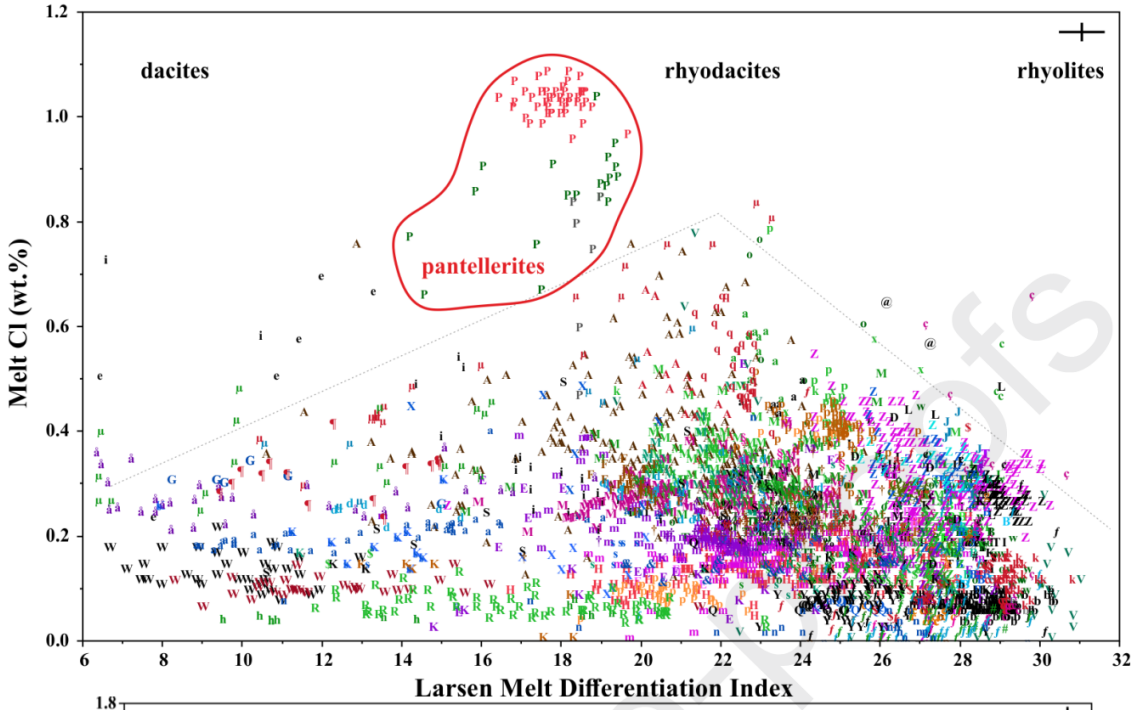

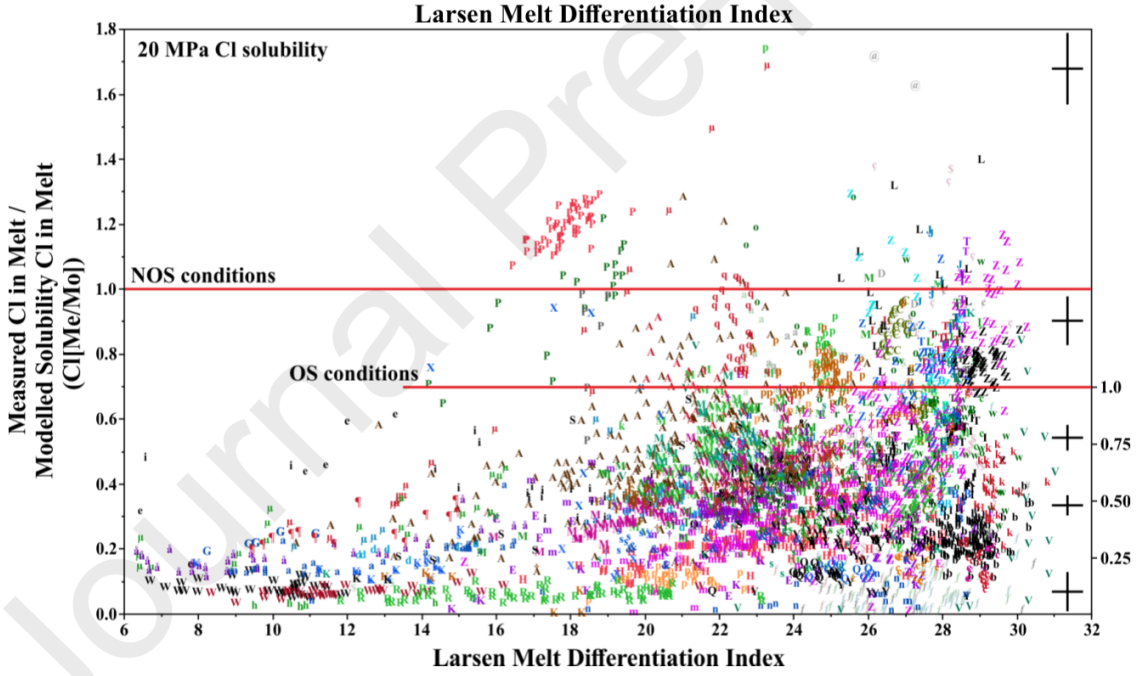

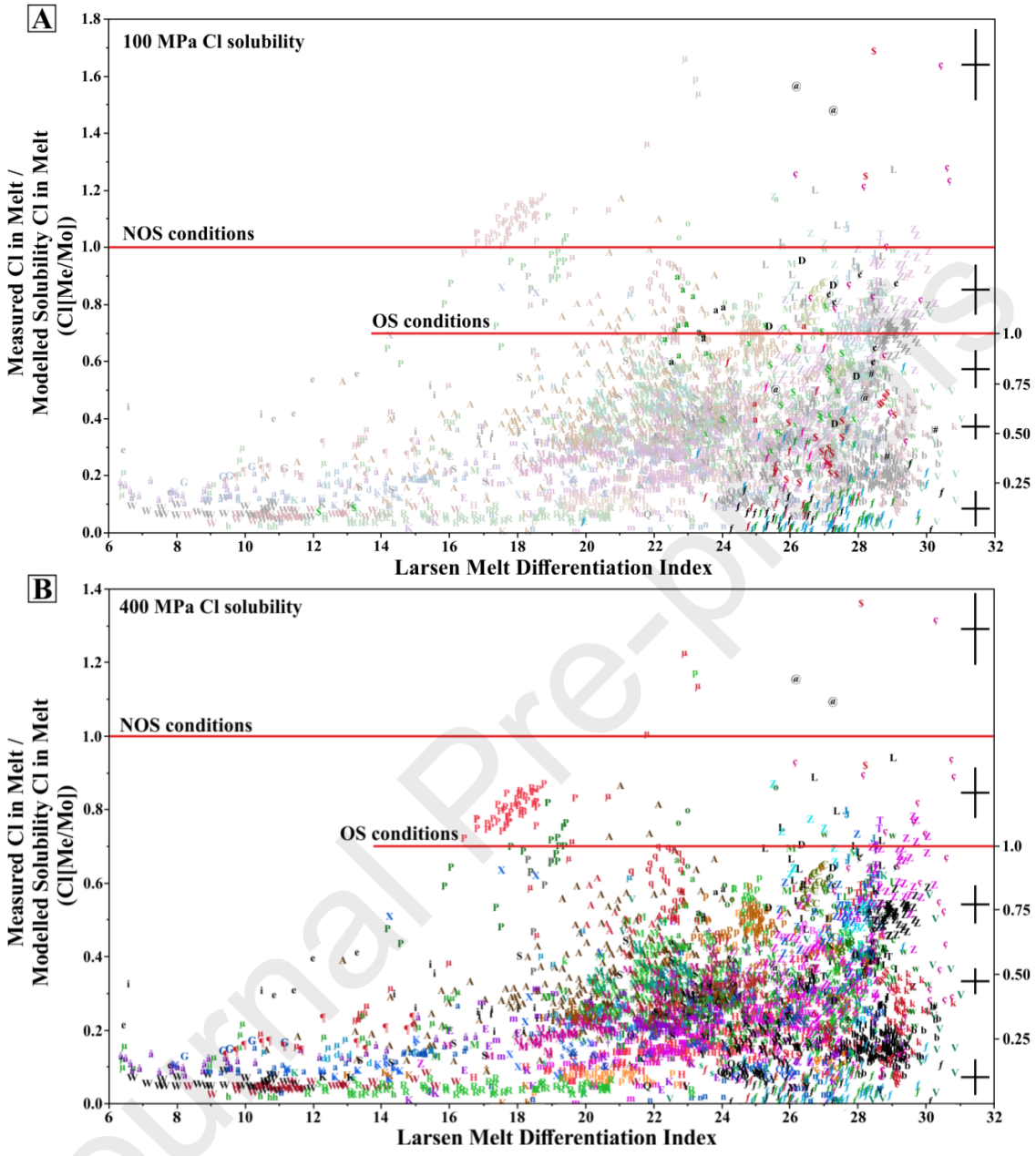

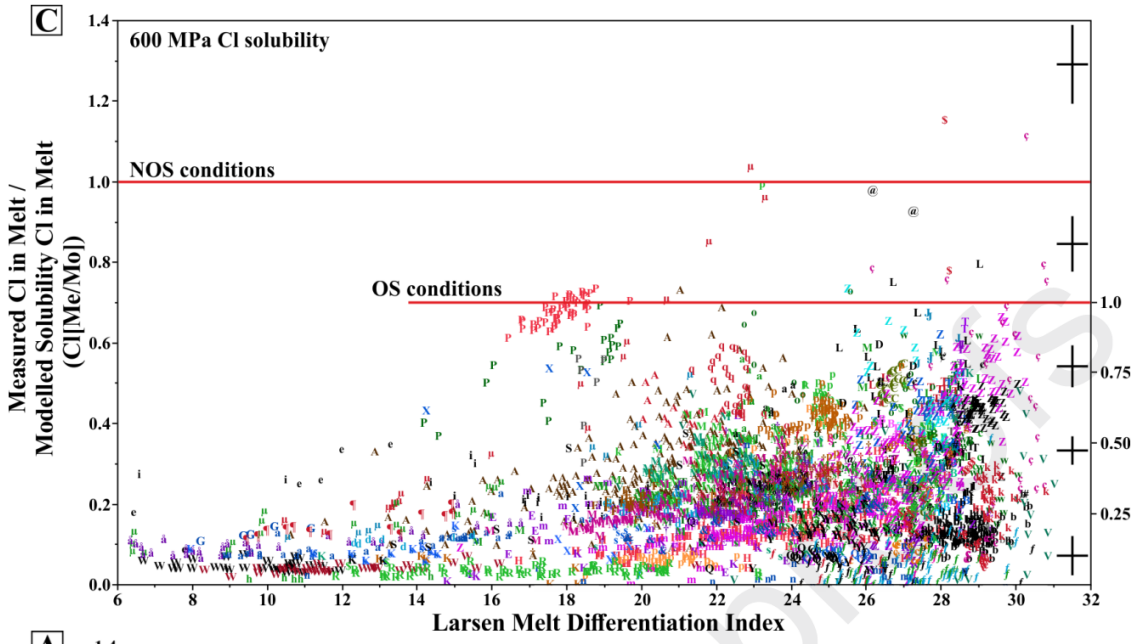

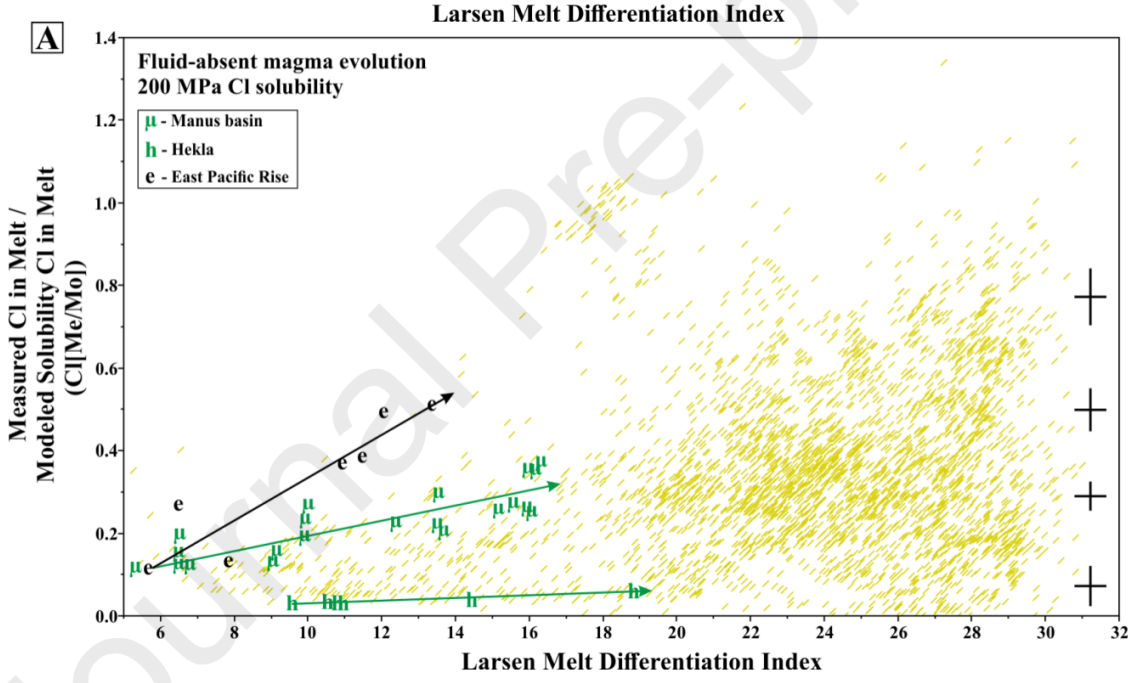

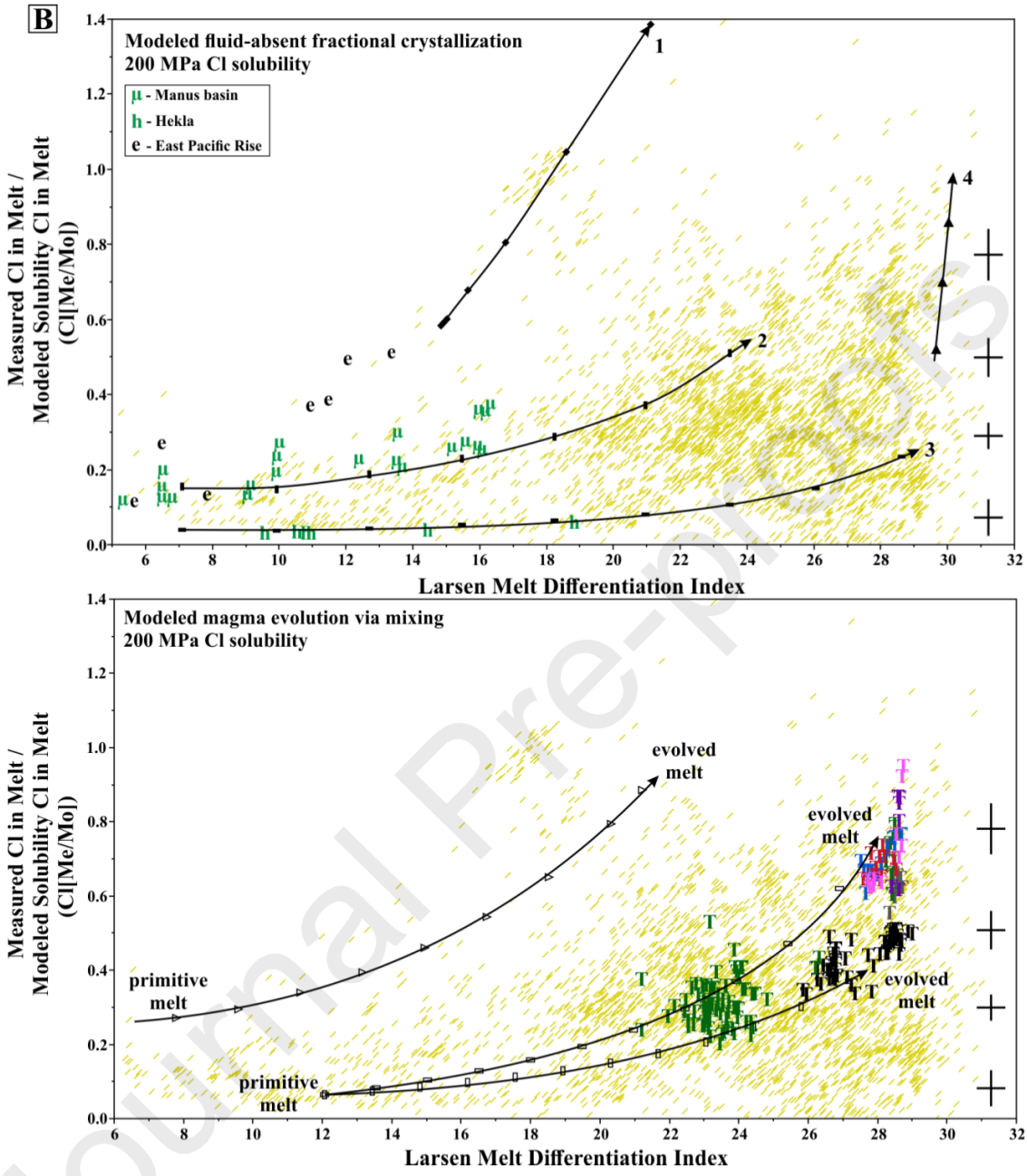

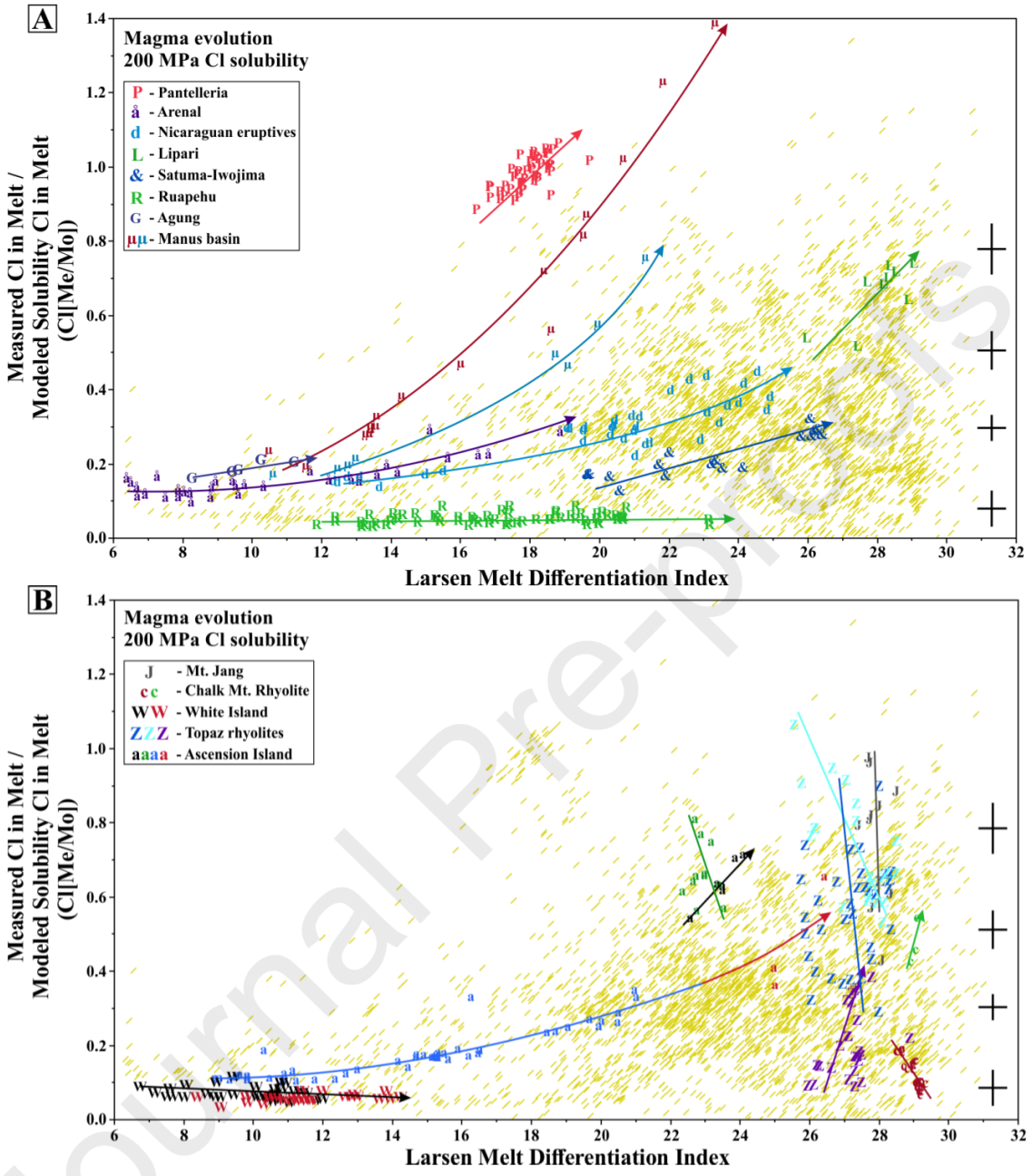

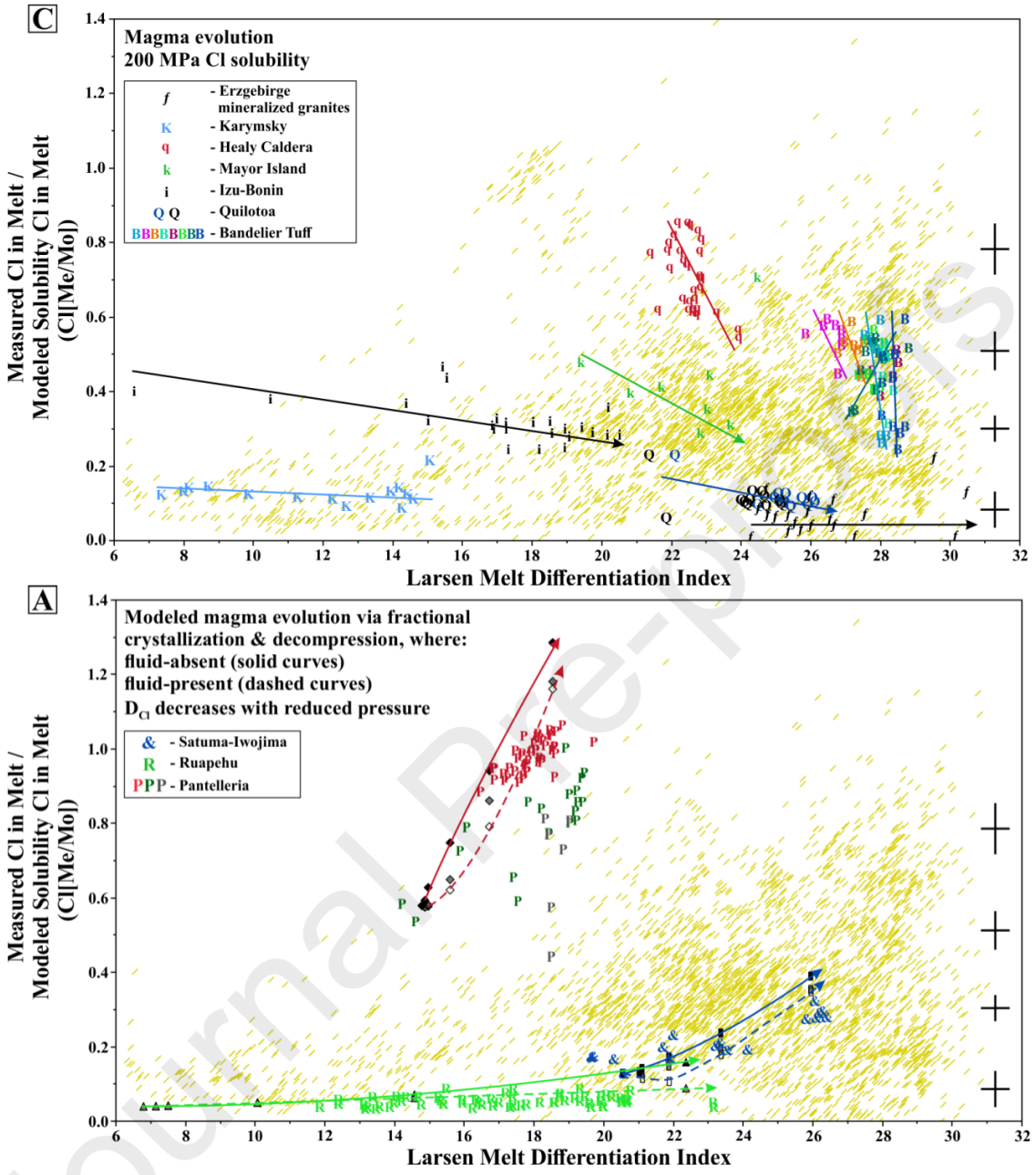

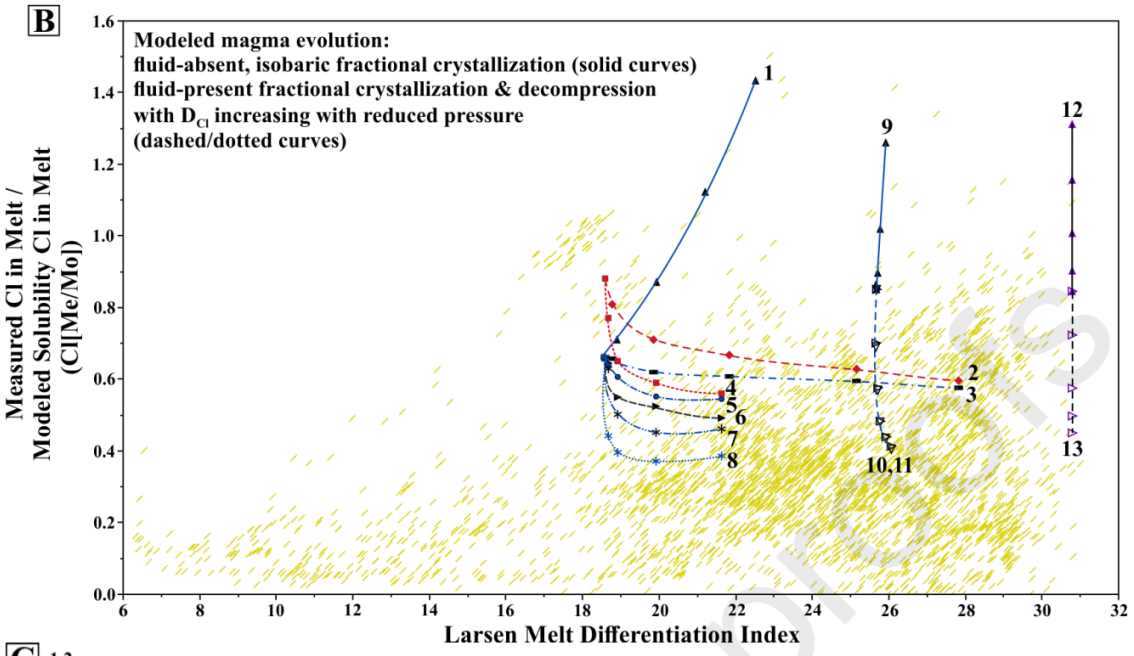

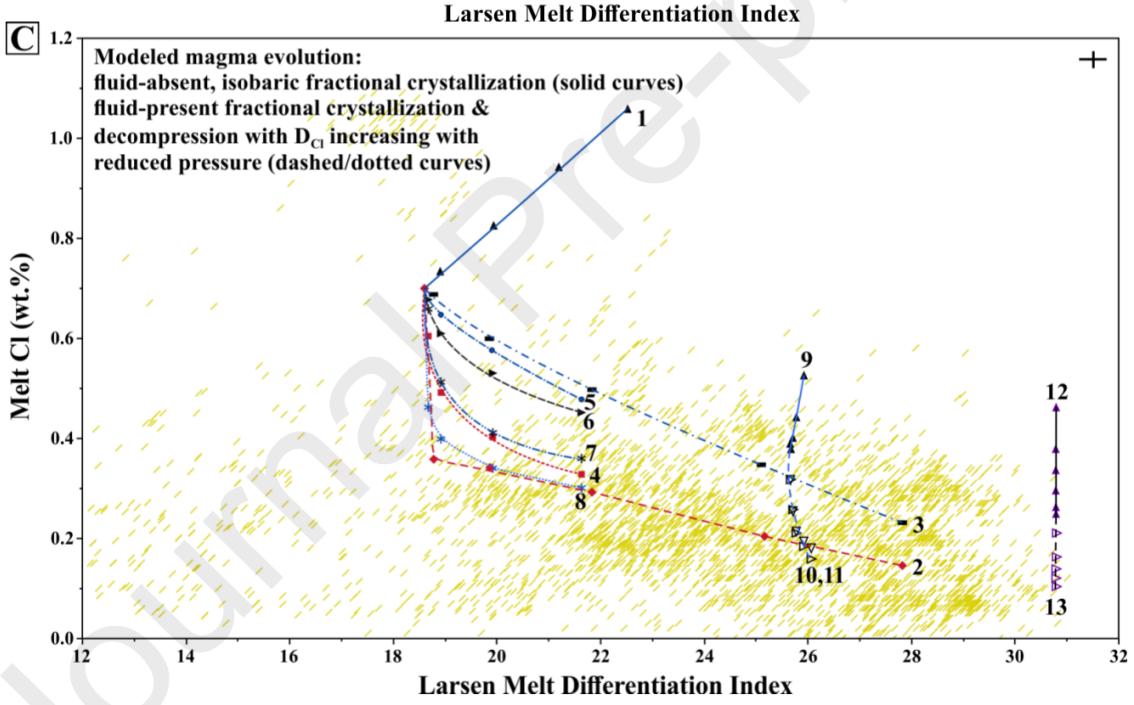

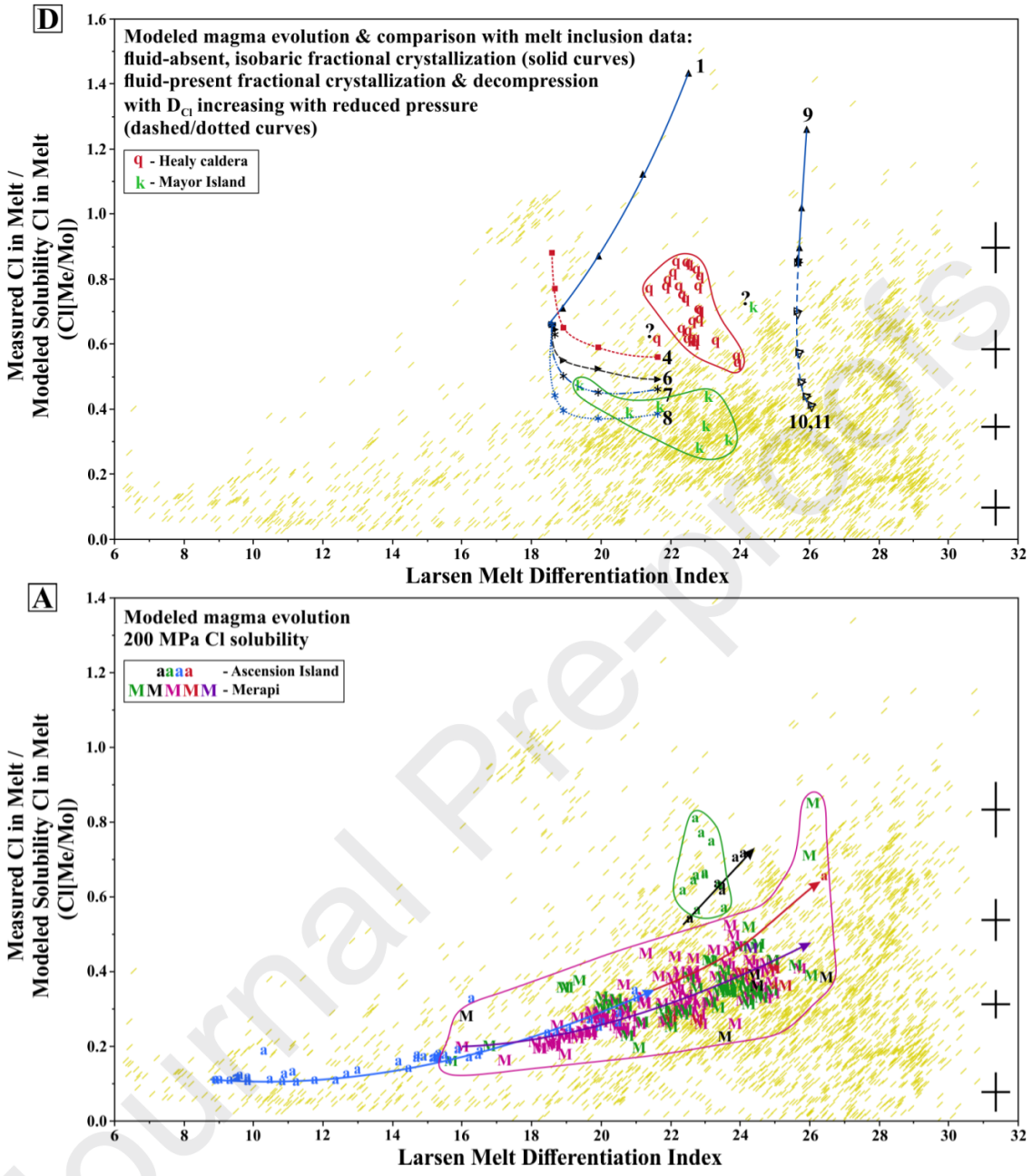

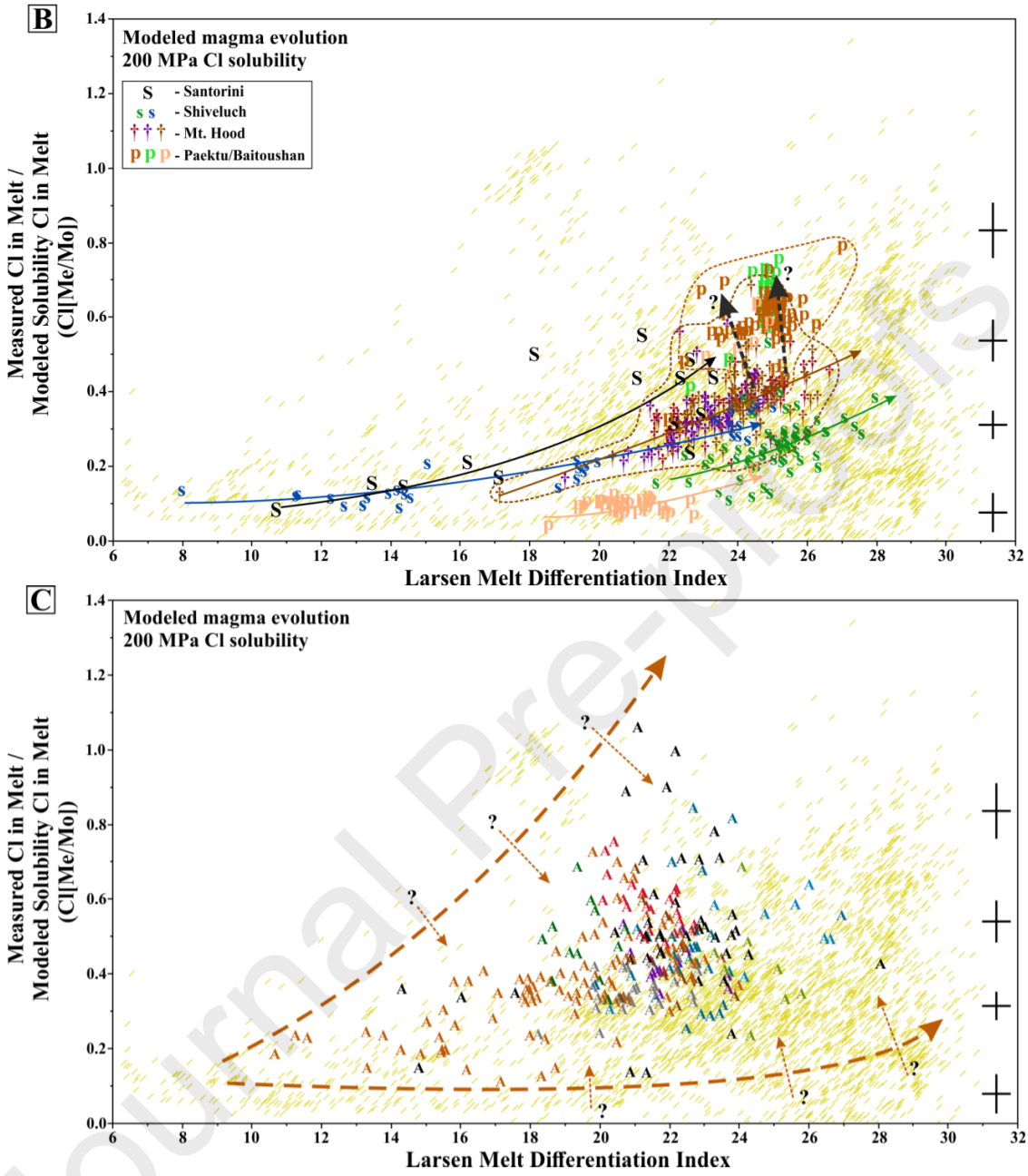

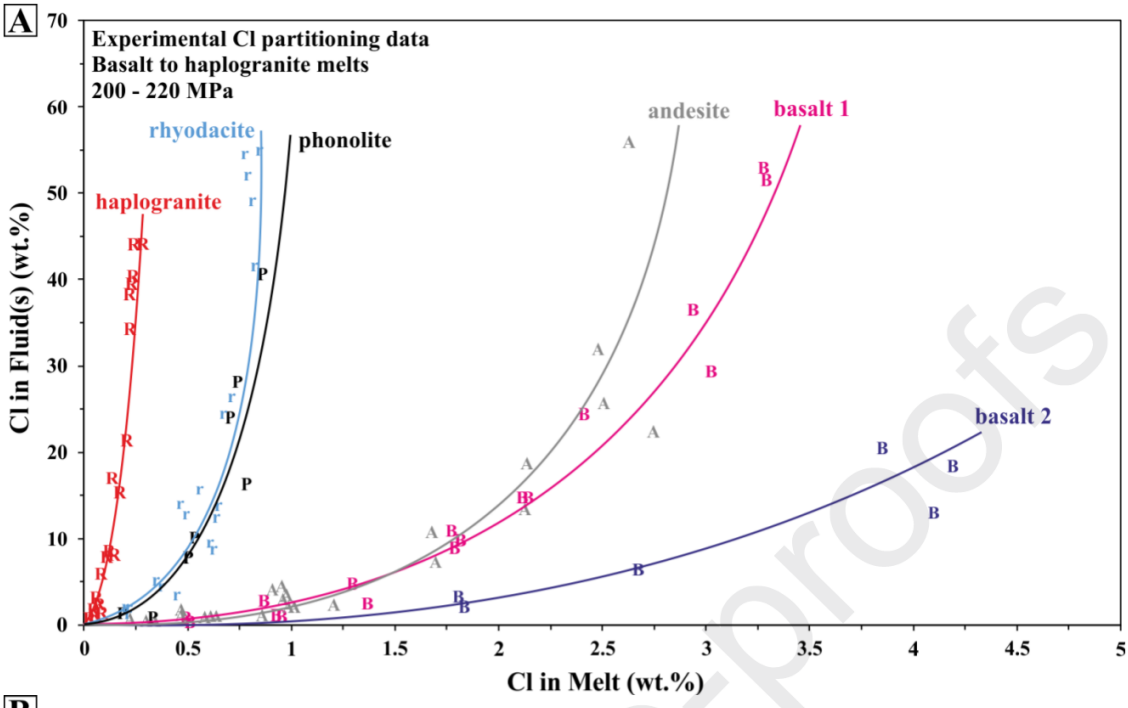

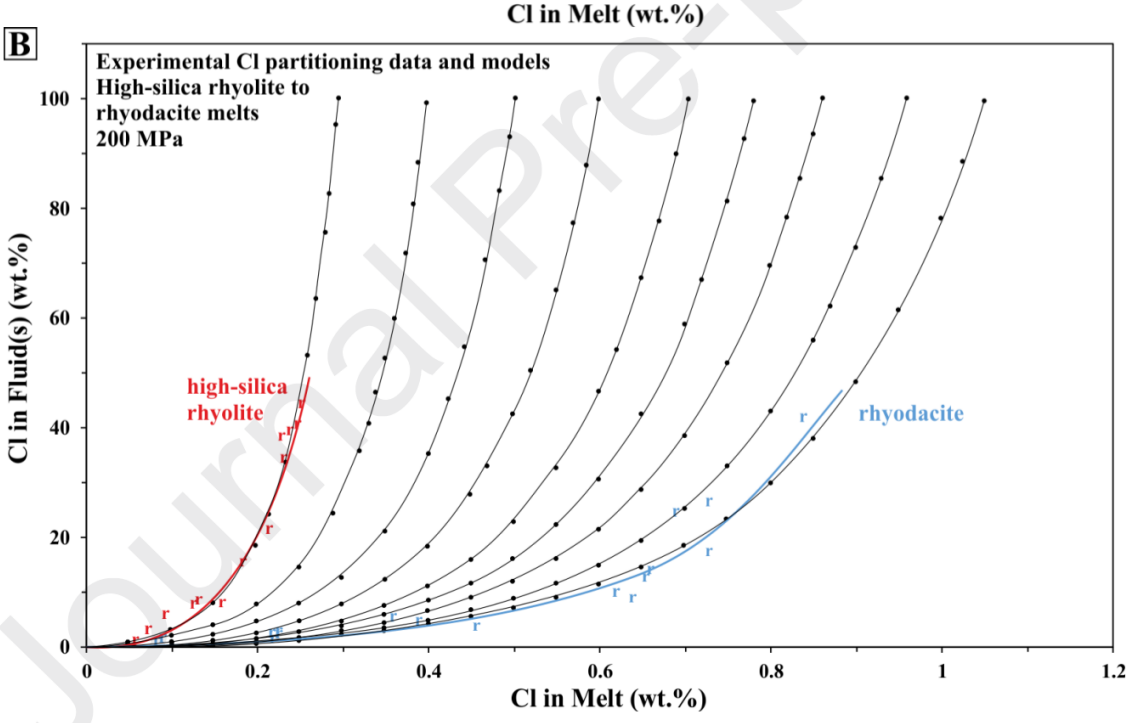

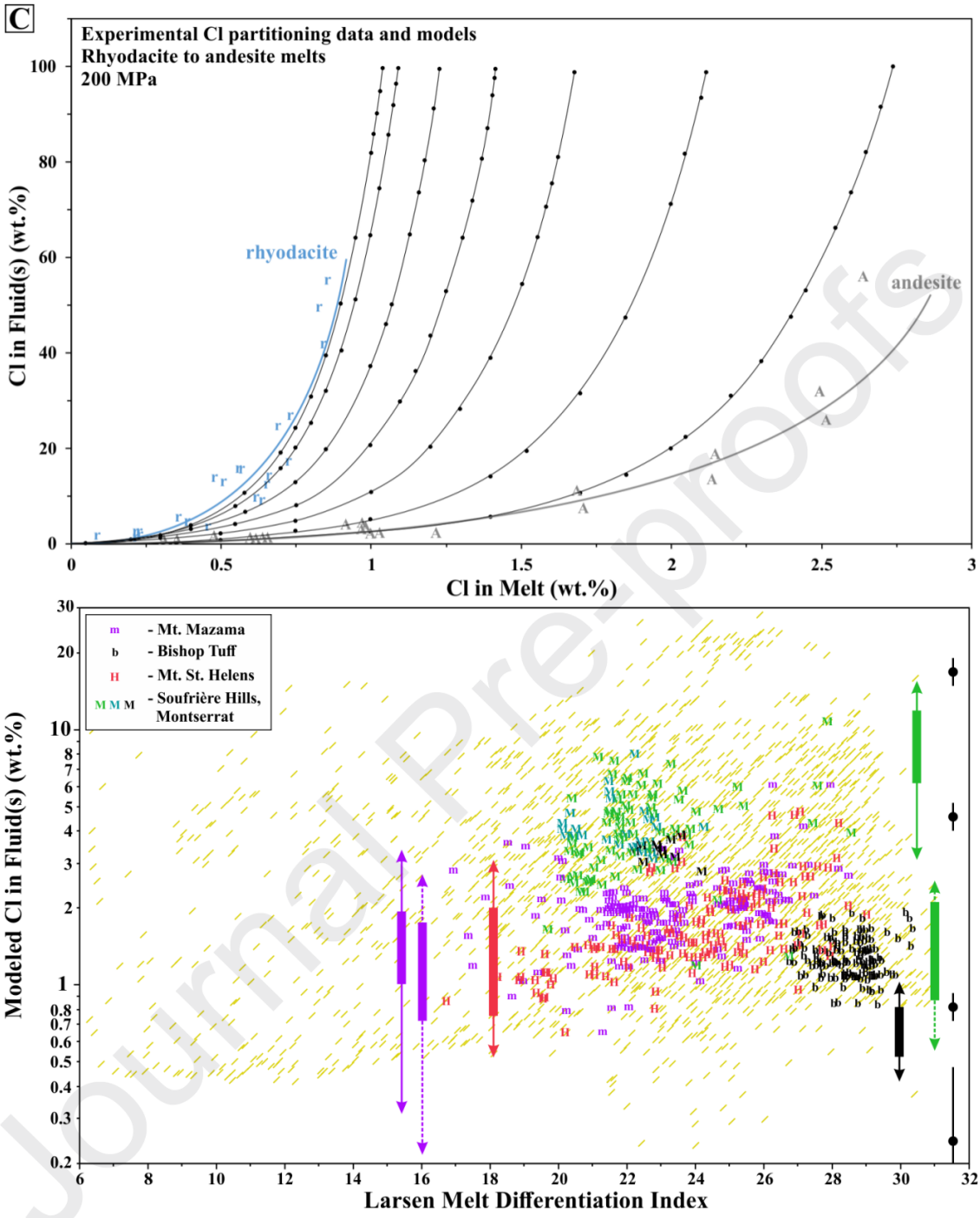

FIGURE CAPTIONS

Fig.1. Schematic diagram detailing the phase relations of the binary NaCl-H_2O and pseudo-ternary silicate melt-NaCl-H_2O systems. (A.) Plot of pressure versus log concentration of NaCl in the system. Line 1 to 2 shows single fluid phase behavior above the vapor-hydrosaline liquid (HSL = brine) solvus; whereas line 3 to 6 expresses the transition from vapor to vapor plus HSL to HSL only with increasing NaCl in system. (B). Corresponding plot of concentrations of Cl versus H_2O in silicate melt when in equilibrium with single fluid (curve 1 to 2) or with vapor only, vapor plus HSL, or HSL only (lines 3 to 4, and 5 to 6). Note that vapor plus HSL field (between 4 and 5 in plot A) corresponds to point (4 & 5) in plot B. See text for discussion.

Fig.2. Graph plotting the total alkali oxide ($Na_2O + K_2O$) versus silica concentrations, on an anhydrous basis, for the > 3500 individual silicate melt inclusion glass and matrix glass compositions of this study. All glasses contain at least 63 wt.% SiO_2. Most of the data plot in the rhyolite, dacite, and trachyte fields, but other more-rare glasses include pantelleritic and comenditic compositions. Figure symbols are described and sources of data for each data set are provided in Table 1. Maximum representative errors shown as cross in upper right corner.

Fig.3. Graph plotting the weight percent Cl versus the A/CNK ratio (i.e., the molar $Al_2O_3/[CaO+Na_2O+K_2O]$) of the >3500 glasses of this study. The data display a weak negative hyperbolic correlation with the highest Cl concentrations occurring in the most alkaline glasses and the lowest values in metaluminous to peraluminous glass compositions. Most glasses are characterized by A/CNK ratios of 0.8 to 1.3 and contain < 0.5 wt.% Cl. Maximum Cl concentrations rarely exceed 1 wt.%. See text for additional details, but some analytical data

for comparatively small melt inclusions likely involve artificially low Na_2O (± K_2O) concentrations; and correspondingly high molar A/CNK ratios. Examples of such compositional realms are enclosed by the 2 rectangles. Figure symbols and sources of data are provided in Table 1. Maximum representative errors shown as cross in upper-right corner.

Fig.4. Graph plotting the Cl concentration versus the Larsen melt differentiation index (wt.% values of [(SiO_2/3 + K_2O) – (CaO+MgO+FeO)]) for the > 3500 melt inclusion and matrix glasses of this study. Maximum Cl concentrations in non-pantelleritic felsic melts increase with the Larsen index from 6 to ca. 22 (for rhyodacitic melts) where maximum values ca. 0.8 wt.% are achieved, and as the Larsen index continues to increase the maximum Cl contents decrease largely due to sequestration by fluids. See text for further discussion. Figure symbols and sources of data are provided in Table 1. Pantelleritic glasses noted with red outlining. Maximum representative errors shown as cross in upper-right corner.

Fig.5. Graph plotting the Cl solubility-normalized ratios (Cl[Me/Mo] for a given pressure and temperature) versus the Larsen melt differentiation index (wt.% values of [(SiO_2/3 + K_2O) - (CaO+MgO+FeO)]) for the > 3500 melt inclusion and matrix glasses of this study(plutonic samples have been made transparent, relative to the volcanic samples). Chlorine solubilities calculated at 20 MPa for both NOS (negligible oxidized S in system) and OS (significant oxidized S in system) conditions. The horizontal red lines illustrate where measured Cl contents are equivalent to the modeled Cl solubility of the melt, for the respective sulfur condition (note the different y-axis scales). For any glass composition on each line, the corresponding melts would be saturated in HSL with or without aqueous vapor if they ascended to this pressure at

equilibrium. For glasses lying above each line, the melts would be saturated in HSL with or without aqueous vapor at some greater pressure. See text for further discussion. Figure symbols and data sources are provided in Tables 1 and 2. Representative, maximum errors (varying as a function of Cl[Me/Mo]) shown as crosses on right-hand side of plots.

Fig.6. Graphs plot the Cl solubility-normalized ratios (Cl[Me/Mo])) versus the Larsen melt differentiation index (wt.% values of [(SiO_2/3 + K_2O) - (CaO+MgO+FeO)] as a function of varying magmatic pressure. Chlorine solubilities calculated for (A) 100 MPa, (B) 400 MPa, and (C) 600 MPa at NOS (negligible oxidized S in system applying to data on left-hand side of graph) and OS (significant oxidized S in system applying to data on right-hand side of graph) conditions. In (A), volcanic samples have been made transparent, to highlight the plutonic samples . The red lines highlight where measured Cl contents are equivalent to modeled Cl solubility of melts (Cl[Me/Mo] =1) for magmas that ascend through this depth and pressure. For any glass composition on the line, the corresponding melts would have been saturated in HSL with or without aqueous vapor for equilibrium at this pressure. For glasses lying above the line, the melts saturate in HSL with or without aqueous vapor at some greater pressure. See text for discussion; figure symbols and data sources are provided in Tables 1 and 2. Representative, maximum errors (varying as a function of Cl[Me/Mo]) shown as crosses on right-hand side of plots.

Fig.7. Graph (A) plots the Cl solubility-normalized ratios Cl[Me/Mo] at 200 MPa) versus the Larsen melt differentiation index (wt.% values of [(SiO_2/3 + K_2O) - (CaO+MgO+FeO)] for dacitic to rhyodacitic glasses from the Manus Basin (μ) (Beier et al., 2015), East Pacific rise (e)

(Wanless et al., 2011), and Hekla volcano, Iceland, (h) (Portnyagin et al., 2012). The curves are best fits to these data sets.All remaining data shown as faint yellow hash marks. These investigations report no evidence of magma being saturated in fluid during magma evolution and while the melt inclusions and matrix glasses formed. The curves in graph (B) express the modeled increases in Cl[Me/Mo] versus increasing Larsen index for two dacitic starting compositions (curves 2, 3), one pantelleritic starting composition (curve 1), and one highly evolved, high-silica starting composition (curve 4) as a result of fractional crystallization at 200 MPa *at fluid-absent conditions*. Modeled results for curves 2 and 3 are compatible with glass compositions Manus basin and Hekla. See Appendix A for details on fractional crystallization modeling. Representative, maximum errors for glasses (varying as a function of Cl[Me/Mo]) shown as crosses on right-hand side of plots.

Fig.8. Graph plots the Cl solubility-normalized ratios (Cl[Me/Mo]) versus the Larsen melt differentiation index (wt.% values of [(SiO_2/3 + K_2O) - (CaO+MgO+FeO)] for melt inclusions from 8 different rhyolitic eruptive units of Taupo and Ohakuri, NZ (T = symbol; Saunders et al., 2010; Begue, 2014).Allremaining data shown as faint yellow hash marks. . The curves express the modeled effects of magma mixing at fluid-absent conditions with no crystallization at 200 MPa (see Appendix B) for details). Representative, maximum errors for glasses (varying as a function of Cl[Me/Mo]]) shown as crosses on right-hand side of plot.

Fig. 9. Graphs plotting the Cl solubility-normalized ratios (Cl[Me/Mo]) versus the Larsen melt differentiation index (wt.% values of [(SiO_2/3 + K_2O) - (CaO+MgO+FeO)] for melt inclusions and matrix glasses exhibiting generally low dispersion, and both positive (A) and negative slopes

(B, C) for magmatic systems that were likely saturated in fluid prior to eruption (Table 2). Curves are best fit lines to each dataset; horizontal to negative slopes in the fits to data reflect Cl sequestration by fluid(s) during magma differentiation and ascent. The magmatic systems include:

(A) Ruapehu (R; Kilgour et al., 2013), Pantelleria (P; Lanzo et al., 2013), Manus Basin (µ; Yang and Scott, 2005; Sun et al., 2007); Lipari, Italy (L; De Rosa et al., 2003; this study), Arenal, Costa Rica (å; Streck and Wacaster, 2006; Wade et al., 2006), Nicaraguan eruptives (d; Kutterolf et al., 2013), Agung, Indonesia (G; Self and King, 1996), Satsuma-Iwojima (&; Saito et al., 2001);

(B) Ascension Island (a; Harris, 1986; Webster and Rebbert, 2001; Chamberlain et al., 2016), White Island, NZ (W; Rapien, 1998; Mandon (2017)), topaz rhyolites (Z; Honeycomb Hills, Utah; Congdon and Nash, 1988; Gavigan et al., 1991; Spor Mountain, Utah; Hofstra et al. (2013); this study), Mt. Jang, Korea (J; Yang, 1997), Chalk Mtn. Rhyolite near Climax, CO (c; Audétat, 2015);

(C) Healy caldera, Kermadec arc (q; Saunders et al., 2010), Quilotoa dacite, Ecuador (Q; Stewart and Castro, 2016), Izu-Bonin arc (i; Straub and Layne, 2003), Bandelier Tuff, NM (B; Dunbar and Hervig, 1992b), Mayor Island (k; Barclay et al., 1996), Erzgebirge, Germany Sn-Mo-W mineralized granites (*f*; Webster et al., 1997; Thomas et al. 2005), and Karymsky volcano, Kamchatka (K; Tolstykh et al., 2001).

Remaining data shown as faint yellow hash marks. See text for discussion. Representative, maximum errors for glasses (varying as a function of Cl[Me/Mo]) shown as crosses on right-hand side of plots.

Fig.10. Graphs plotting the Cl solubility-normalized ratios (Cl[Me/Mo]) or Cl concentration in melt versus the Larsen melt differentiation index (wt.% values of [(SiO_2/3 + K_2O) -

(CaO+MgO+FeO)] for melt inclusions exhibiting positive to negative trends; comparisons with modeled results are also included.

Graph (A) models the geochemical evolution of fluid-absent (solid curves) and fluid-saturated (dashed curves; open symbols for open-system and filled grey symbols for closed-system conditions) magma through fractional crystallization and magma ascent (decompression), for melt inclusions from Pantelleria, Italy (P; Giondada and Landi, 2010; Neave, 2012; Lanzo et al., 2013), Ruapehu, NZ (R; Kilgour et al., 2013), and Satsuma-Iwojima (&; Saito et al., 2001). The fluid/melt partition coefficient for Cl is modeled to *decrease* with decreasing pressure (see Sections 2.3 and 4.3.1 for further details).

Graph (B) displays model results for up to 46 wt.% isobaric fractional crystallization of fluid-absent, felsic magmas at 200 MPa (solid curves 1, 9, and 12). Other modeling, shown as dashed and dot-dash curves, represents fluid-saturated melts as they evolve via fractional crystallization at either fixed pressure or decreasing pressure during ascent towards surface. Here, the fluid/melt partition coefficient for Cl is modeled to *increase* with decreasing pressure as described in text (see Sections 2.3 and 4.3.1 for further details, and Appendix C).

Curve 2 = 80 wt.% crystallization of closed-system fluid-saturated rhyodacitic melt at 200 MPa and S-enriched, OS conditions;

Curve 3 = 80 wt.% crystallization of closed-system fluid-saturated rhyodacitic melt at 200 MPa and S-poor, NOS conditions;

Curves 4 to 8 = up to 40 wt.% fractional crystallization accompanied by decompression of rhyodacitic melts for conditions of: S-enriched OS closed-system (curve 4), NOS open-system (curve 5), NOS closed-system (curve 6), NOS closed-system with excess fluid mass of 2 wt.% (curve 7), and NOS closed-system with excess fluid mass of 4 wt.% (curve 8).

Curves 10 and 13 = rhyolitic melts at closed-system NOS conditions and fixed 200 MPa pressure

Curve 11 = rhyolitic melt ascent at closed-system NOS conditions.

The increments in modeled pressure for magma decompression are 200, 190, 150, 100, 50, and 10 MPa.

Graph (C) shows the same model results as graph (B), except that (C) shows the measured melt Cl (wt.%) only, and does not involve computed Cl solubility.

Graph (D) compares melt inclusion compositions for Mayor Island (k; Barclay et al., 1996),) and Healy caldera, Kermadec arc (q; Saunders et al., 2010) with modeled curves 1, 4, 6, 7, 8, 9, 10, and 11 from Fig. (B).

All remaining data shown as faint yellow hash marks. All modeling for fluid-saturated melts returns slopes that are horizontal to negative; these slopes become increasing vertical with increasing Larsen index. See Appendix A for details on fractional crystallization modeling and Appendix C for modeling of Cl exchange between fluids and melts. Representative, maximum error bars for glasses (varying as a function of Cl[Me/Mo]) shown as crosses on right-hand side of plots.

Fig.11. Graphs plotting the Cl solubility-normalized ratios (Cl[Me/Mo]) versus the Larsen melt differentiation index (wt.% values of [(SiO_2/3 + K_2O) - (CaO+MgO+FeO)] for melt inclusion sets exhibiting small to larger dispersion. The solid-arrowed curves represent schematically interpreted, primary-evolution trends for melts; the curves are dashed where the interpretations are less certain, and remaining data shown as faint yellow hash marks. Many of the sets show larger dispersion at higher Larsen indices (highlighted by outlining data), and some exhibit distinct shifts of data to higher Cl[Me/Mo] with increasing dispersion and increasing Larsen

index; this is likely due to fluid-melt interactions. Dashed arrows with question marks represent potential paths of evolution with increasing or decreasing Cl[Me/Mo] and Larsen indices reflecting Cl gain or loss from melt.

Graph (A) shows data for Ascension Island (a; Harris, 1986; Webster and Rebbert, 2001; Chamberlain et al., 2016) and Merapi, Indonesia (M; Nadeau et al., 2013; Preece et al., 2014).

Graph (B) displays melt inclusions for Santorini (S; Michaud et al., 2000), Shiveluch (s; Humphreys et al., 2008; Naumov et al., 2008), Mt. Hood (†; Koleszar et al., 2012), Paektu/Baitoushan (p; Horn, 1997; Iacovino et al., 2016).

Graph (C) displays melt inclusions from >12 eruptive units of Augustine volcano, Alaska (A; Roman et al., 1986; Tappen et al., 2009; Webster et al., 2010; Nadeau et al., 2015; Webster et al., 2015). See text for discussion. Representative, maximum errors for glasses (varying as a function of Cl[Me/Mo]) shown as crosses on right-hand side of plots.

Fig. 12. A comparison of experimentally determined and modeled Cl partitioning behavior between silicate melt and vapor, vapor plus HSL, or HSL at pressures of 200-220 MPa for various melt compositions. Experimental data sources are as follows: basaltic melts [B] – Webster et al. (1999), Webster and De Vivo (2002), Mathez and Webster (2005); andesitic melts [A] – Botcharnikov et al. (2007), Zajacz et al. (2012); phonolitic melts [P] – Webster et al. (2014); rhyodacitic melts [r] – Botcharnikov et al. (2004), Webster et al. (2009), Iveson et al. (2017; 2019); haplogranitic melts [R] – Webster et al. (1992), Kravchuk and Keppler (1994).

Graph (A) shows fits to experimental data on equilibrium fluid-melt Cl partitioning relevant to haplogranite, rhyodacite, phonolite, andesite, and basalt melt compositions. Chlorine partitioning varies strongly with the bulk Cl content of the system and the melt. Similarity in these curves is

the basis for modeling the partitioning of Cl between fluid(s) and melt described in the text and Appendix C.

Graph (B) shows experimentally determined Cl partitioning behavior for high-silica rhyolite or haplogranite (red curve; data of Webster et al., 1992; Kravchuk and Keppler, 1994) and rhyodacite (blue curve; data of Botcharnikov et al., 2004; Webster et al., 2009; Iveson et al., 2017; 2019) melts and vapor, vapor plus HSL, HSL at 200 MPa. Black curves represent modeling of Cl partitioning for these melts and other intermediate melt compositions ranging between haplogranite (high-SiO_2) and rhyodacite melts. Modeled curves based on Appendix equations C.2-C.9.

Graph (C) shows experimentally determined Cl partitioning behavior for rhyodacite (blue curve; data of Botcharnikov et al., 2004; Webster et al., 2009; Iveson et al., 2017; 2019) and andesite (grey curve; Botcharnikov et al., 2007; Zajacz et al., 2012) melts and vapor, vapor plus HSL, HSL at 200 MPa. Black curves represent modeling of Cl partitioning for other melt compositions ranging between rhyodacite to andesite melts. Modeled curves based on Appendix equations C.2-C.6 and C.9-C.12.

Fig. 13. Graph plotting the Cl concentration of fluid(s) (calculated for 200 MPa) versus the Larsen index using methods of this investigation for melt inclusions (shown as individual data points) from Soufriere Hills, Montserrat (M); the Bishop Tuff (b); Mt. St. Helens (H); and Mt. Mazama (m); remaining data shown as faint yellow hash marks. The melt inclusion-calculated Cl contents of 1 wt.% of vapor are compared with constraints from prior research; values of $D_{Cl}^{fluid/melt}$ from prior work were used to compute the Cl concentrations of vapors coexisting with these melt inclusion Cl contents (expressed by arrows). Solid arrows involved either singular or

higher values of $D_{Cl}^{fluid/melt}$, and dashed arrows applied lower values of $D_{Cl}^{fluid/melt}$ to compute Cl in vapor if a range in $D_{Cl}^{fluid/melt}$ was involved. Arrows are thickened where the bulk of the data plot. Data: violet arrows represent Mt. Mazama, black for Bishop Tuff, red for Mt. St. Helens, and green for Soufriere hills, Montserrat. See text for discussion; methods of computing Cl contents of fluids described in Appendix C. Figure symbols and sources of data are provided in Table 1. Representative, maximum errors for the Cl concentration of fluids shown on right-hand side of plots.

Table 1

Magmatic systems of this study, number of melt inclusion and matrix glass samples from each system, and

VOLCANIC SYSTEMS				
Magmatic System No.	**Symbol, and colour used in figures**	**No. of glass samples**	**Magmatic System Name and Location**	**Data Sources**
1	G, blue	10	Agung, Indonesia	Self & King (1996)
2	å, blue, brown	34	Arenal, Costa Rica	Streck & Wacaster (2006); Wade et al. (2006)
3	A, multicolored	264	Augustine volcano, AK USA	Roman et al. 2006; Tappen et al. (2009); Webster et al. (2010); Nadeau et al. (2015)
4	p, green, brown	128	Baitoushan or Paektu, China, North Korea	Horn (1997); Horn & Schmincke (2000); Iacovino et al. (2016)
5	X, blue	14	Bataan, Philippines	Métrich et al. (1999)
6	K, purple	14	Bezymianny, Kamchatka, Russia	Tolstykh et al. (2003)
7	b, gray, black	156	Bishop Tuff, CA USA	Wallace et al. (1999); Dunbar & Hervig (1992a)
8	Z, green	35	Cerro el Lobo, Cerro el Pajaro, Mexico	Webster et al. (1996)
9	d, blue	51	Chiltepe/Apoyo volcanic complex, Nicaragua	Kutterolf et al. (2013)
10	c, multicolored	67	Climax-related igneous rocks, Climax, CO USA	Audétat (2015); Audétat & Li (2017)
11	K, green	11	Dikii greben, Kamchatka, Russia	Tolstykh et al. (2003)
12	§, violet	4	Dzarta-Khuduk, Mongolia	Andreeva & Kovalenko (2011)
13	F, brown	29	Fantale, Ethiopia	Webster et al. (1993)
14	q, red	30	Healy Caldera, Kermadec arc, Pacific Ocean	Saunders et al. (2010)
15	h, green	6	Hekla, Iceland	Portnyagin et al. (2012)
16	Z, black	49	Hideaway Park topaz rhyolite, Red Mtn., CO USA	Mercer et al. (2015)
17	Z, violet	25	Honeycomb Hills, UT USA	Congdon & Nash (1988); Gavigan et al. (1991)
18	i, black	25	Izu arc front, Pacific Ocean	Straub & Layne (2003)
19	K, blue	12	Karymsky, Kamchatka, Russia	Tolstykh et al. (2001; 2003)
20	k, red	32	Kos plateau tuff, Greece	Bachmann et al. (2010)
21	K, brown	7	Kudryavyi, Kamchatka, Russia	Tolstykh et al. (2003)
22	L, multicolored	34	Lipari, Italy	DeRosa et al. (2003); Webster, Frezzotti, DiMartino (Supp. Data)
23	g, brown	7	Llallagua, Bolivia	Wittenbrink (2006); Wittenbrink et al. (2009)

24	B=Bandeleier, C=Cerro Toledo, multicolored	115	Lower Bandelier Tuff and Cerro Toledo rhyolite, NM USA	Dunbar & Hervig (1992b); Stix & Layne (1996)
25	k, green	8	Mayor Island, NZ	Barclay et al. (1996)
26	µ, multicolored	49	Manus back-arc basin, Pacific Ocean	Yang & Scott (2002); Sun et al. (2007); Beier et al. (2015)
27	M, violet, green, blue	178	Merapi, Indonesia	Nadeau et al. (2013); Preece et al. (2014); Borisova et al. (2013); Costa et al. (2013)
28	e, black	7	MOR dacite, East Pacific Rise	Wanless et al. (2011)
29	†, multicolored	186	Mt. Hood, OR USA	Koleszar (2011); Koleszar et al. (2012)
30	J, blue	10	Mt. Jang, Korea	Yang (1997)
31	(m, violet, pink)	198	Mt. Mazama, OR USA	Mandeville et al. (2009); Wright et al. (2012)
32	Y, black	58	Mt. Pinatubo, Philippines	Borisova et al. (2005; 2006; 2014)
33	E, violet, pink	47	Mt. Putauaki (Mt. Edgecomb), NZ	Norling et al. (2016)
34	H, red	156	Mt. St. Helens, WA USA	Blundy & Cashman (2001; 2005); Blundy et al. (2008); Berlo et al. (2004); Edmonds et al. (2008)
35	¶, red	14	Niuatahi-Motutahi lavas, Tonga arc, Pacific Ocean	Park et al. (2015)
36	P, multicolored	71	Pantelleria, Italy	Lowenstern (1994); Neave et al. (2012); Lanzo et al. (2013); Gioncada & Landi (2010)
37	%, black	22	Plat Pays, Dominica Lesser Antilles, Caribbean Sea	Gurenko et al. (2005)
38	Q, black, blue	23	Quilotoa, Ecuador	Stewart & Castro (2016)
39	n, blue	25	Rosia Montana-related dacites, Romania	Naumov et al. (2013)
40	R,, green	64	Ruapehu, NZ	Kilgour et al. (2013)
41	S, black, blue	21	Santorini, Greece	Michaud et al. (2000); Cottrell et al. (1999)
42	&, blue	17	Satuma-Iwojima, Japan	Saito et al. (2001)
43	s, green, blue	97	Shiveluch, Russia	Humphreys et al. (2008); Naumov et al. (2008); Tolstykh et al. (2000)
44	M, multicolored	126	Soufriere Hills volcano, Montserrat	Humphreys et al. (2009; 2010); Mann et al. (2013); Edmonds et al. (2002)
45	Z, light blue, dark blue	55	Spor Mountain, UT USA	Hofstra et al. (2013); Webster & Rebbert (Supp. Data)

46	T=Taupo, w=Whakamaru, o=Oruanui, r=Rotorua; multicolored	342	Taupo V.Z., North Island, NZ	Bégué (2014); Bégué et al. (2015); Saunders et al. (2010); Johnson et al. (2011; 2013); Chambefort et al. 2014)
47	Z, pink	169	Taylor Creek, NM USA	Webster & Duffield (1991; 1994); Duffield & Du Bray (1990)
48	I, black	15	Toba, Indonesia	Chesner & Luhr (2010)
49	K, black	17	Unidentified, East. Volcanic Front, Russia	Tolstykh et al. (2003)
50	V, turquoise	32	Vulcano, Italy	Gioncada et al. (1998); Frezzotti et al. (2004)
51	W, black, red	69	White Island, New Zealand	Rapien (1998); Rapien et al. (2003); Mandon (2017)

PLUTONIC SYSTEMS

Magmatic System No.	Symbol, and colour used in figures	Number of glass samples	Magmatic System Name and Location	Data Sources
52	x, green	15	Amix Zr-Nb-REE mineralized complex, Namibia	Schmidt et al. (2002)
53	a, multicolored	71	Ascension Island, Atlantic Ocean	Roedder & Coombs (1967); Harris (1986); Webster & Rebbert (2001); Chamberlain et al. (2016)
54	ç, violet	27	Cerro de Pasco Zn-Pb-Ag-Cu-Bi mineralized granites, Peru	Rottier et al. (2016)
55	#, black	3	Cerro Rico de Potosi silver deposit, Bolivia	Wittenbrink (2006); Wittenbrink et al. (2009)
56	#, red	1	Chorolque tin porphyry, Bolivia	Wittenbrink (2006); Wittenbrink et al. (2009)
57	¢, black	6	Deva Cu-Au porphyry, Romania	Pintea (2014)
58	D, black	5	Dexing Cu-Mo-Au porphyry, China	Bao et al. (2016)
59	*f*, black, violet, red	47	Ehrenfriedersdorf granites, Germany	Webster et al. (1997); Thomas et al. (2000)
60	#, green	3	El Salvador Cu porphyry, Chile	Wittenbrink (2006); Wittenbrink et al. (2009)
61	@, black	4	Olso rift granites, Norway	Hansteen & Lustenhouwer (1990)
62	$, green	16	Red Mountain Cu porphyry, AZ USA	Student & Bodnar (2004)
63	$, red	21	Tyrone Cu porphyry, NM USA	Student & Bodnar (2004)
64	*f*, blue, green	88	Zinnwald Sn-W granites, Germany	Thomas et al. (2005); Webster et al. (2004)

Table 2

Igneous systems (filtered from Table 1) exhibiting geochemical ± textural evidence of exsolved pre-eruptive o
sources

VOLCANIC SYSTEMS

Magmatic System									
Number (from Table 1)	**Location**	**Composition range (based on MI or MG)**	**Range of Cl (wt. %) in MI or MG**	**Range of (measured Cl/modeled Cl) of MI or MG @ NOS conditions**	**Magmatic components used to constrain, chemically, the presence of exsolved brine (HSL) or vapor?**	**Range of SO_2 (wt. %) in MI ± MG**	**Range of (measured Cl/modeled Cl) of MI or MG @ OS conditions**	**Textural ± chemical evidence of magmatic brine (± vapor) ?†**	**References: those discussing *potential* role of brine (HSL) in system are listed in bold font**
3	Augustine, AK USA	rhyodacite to rhyolite	0.14-1.35	0.13-1.30	**YES**: Cl, H_2O, CO_2	bdl-0.14	0.19-1.86	Yes	Roman et al. (2006); Tappen et al. (2009); **Webster et al. (2010);** Nadeau et al. (2015); **Webster et al. (2015); this study for 20 MPa**
4	Baitoushan/Paektu, China, North Korea	comendite, trachyte & rhyolite	0.08-0.8	0.03-1.75	**YES:** Cl, CO_2, H_2O, S, F	bdl-0.06	0.07-2.6	Yes	Horn (1997); Horn & Schminke (2000); **Iacovino et al. (2016); this study for 20 MPa**
5	Bataan, Philippines	rhyolite	0.09-0.49	0.04-0.95	**YES:** Cl, S	0.07-0.08	0.06-1.35	Yes	Metrich et al. (1999); **this study for 20 MPa OS conditions**
7	Bishop Tuff , CA USA	rhyolite	0.04-0.11	0.12-0.40	**YES**: H_2O, CO_2 ± Cl, Li, Be, B	< 0.01	0.17-0.57	No	Wallace et al. (1999); Dunbar & Hervig (1992a)

8	Cerro el Lobo, Cerro el Pajaro, Mexico	topaz rhyolite	0.09-0.27	0.21-0.54	**YES**: Cl, H_2O, Be, B	n.d.	0.3-0.77	No	Webster et al. (1996)
9	Chiltepe/ Apoyo volcanic complex, Nicaragua	dacite, rhyodacite & rhyolite	0.08-0.38	0.03-0.69	**YES:** Br, Br/Cl	n.d.	0.05-0.98	No	Kutterolf et al. (2013)
10	Climax-related igneous rocks, Climax, CO USA	rhyolite	0.04-0.57	0.08-0.67	**YES:** Mo	bdl-0.02	0.12-0.95	Yes	**Audétat (2015); Audétat & Li (2017)**
12	Dzarta-Khuduk, Mongolia	pantellerite & trachydacite	0.32-0.68	0.23-0.36	**YES:** F brine, Li	bdl-0.02	0.58-0.91	No	Andreeva & Kovalenko (2011)
14	Healy Island, Kermadec arc	rhyolite	0.33-0.66	0.67-1.05	**NO:** not in published work,	n.d.	0.96-1.50	Yes	Saunders et al. (2010); **this study for 20 MPa**
16	Hideaway Park, Red Mtn., CO USA	topaz rhyolite	0.23-0.35	0.44-0.88	**YES**: H_2O, CO_2, Cl, (and δD in mica)	bdl-0.03	0.62-1.27	Yes	Mercer et al. (2015); **this study for 20 MPa OS conditions**
18	Izu arc front, Pacific Ocean	rhyo-dacite to rhyolite	0.21-0.73	0.3-0.57	**YES:** Cl, H_2O, S, F	n.d.	0.42-0.81	No	Straub & Layne (2003)
20	Kos plateau tuff, Greece	rhyolite	0.07-0.17	0.22-0.53	**YES:** CO_2, H_2O	bdl-0.08	0.31-0.75	No	Bachmann et al. (2010)

22	Lipari, Italy	rhyolite	0.18-0.49	0.5-1.4	**NO:** not in prior published work	bdl-0.02	0.7-2.0	Yes	DeRosa et al., 2003; Webster, Frezzotti, DiMartino unpub. Data; **this study for 20 MPa**
24	Lower Bandelier Tuff and Cerro Toledo rhyolite, NM USA	rhyolite	0.1-0.31	0.3-0.97	**YES**: Cl, H_2O	< 0.01	0.43-1.39	Yes	Dunbar and Hervig (1992b); **Stix & Layne (1996)**
25	Major Island, NZ	alkaline rhyolite	0.21-0.48	0.2-0.5	**YES:** Cl, H_2O	n.d.	0.5-1.25	Yes	Barclay et al. (1996); **this study for 20 MPa OS conditions**
26	Manus back-arc basin, Pacific Ocean	dacite to rhyolite	0.09-0.84	0.03-1.82	**YES:** Cl, H_2O, S ± F	0.02-0.24	0.04-2.62	Yes	Yang & Scott (2002); Sun et al. (2007); Beier et al. (2015); **this study for 20 MPa**
27	Merapi, Indonesia	dacite & trachydacite	0.21-0.7	0.14-0.62	**YES:** Cl, H_2O, Li	0.07-0.08	0.19-0.88	Yes	Nadeau et al. (2013); **Preece et al. (2014); Borisova et al. (2013);** Costa et al. (2013)
29	Mt. Hood, OR USA	rhyodacite to rhyolite	0.15-0.36	0.08-0.47	**YES:** Cl, CO_2, H_2O	<0.01	0.21-1.18	Yes	**Koleszar (2011); Koleszar et al. (2012)**
30	Mt. Jang, Korea	rhyolite	0.19-0.44	0.48-1.08	**YES:** H_2O	n.d.	0.68-1.55	No	Yang (1997); **this study for 20 MPa**

31	Mt. Mazama, OR USA	rhyodacite to rhyolite	0.02-0.4	0.01-0.75	**YES**: Cl, S, F, H_2O, CO_2, Li, Be, B	bdl-0.10	0.02-1.08	Yes	Mandeville et al. (2009); **Wright et al. (2012); this study for 20 MPa OS conditions**
32	Mt. Pinatubo, Philippines	rhyolite	0.02-0.13	0.06-0.38	**YES:** CO_2, S, Cl	n.d.	0.08-0.54	No	Borisova et al. (2005; 2006; 2014)
33	Mt. Putauaki, NZ	dacite to rhyolite	0.04-0.53	0.11-0.74	**YES**: Cl ± Li, Cu	0.01-0.09	0.07-1.06	Yes	Norling et al. (2016); **this study for 20 MPa OS conditions**
34	Mt. St. Helens, WA USA	rhyolite	0.05-0.3	0.08-0.62	**YES**: Cl, H_2O, CO_2, Li	bdl-0.15	0.11-0.89	No	Blundy & Cashman (2001; 2005); **Blundy et al. (2008); Berlo et al. (2004);** Edmonds et al. (2008)
35	Niuatahi-Motutahi lavas, Tonga arc	dacite to rhyolite	0.26-0.42	0.20-0.36	**YES:** Cl, S	0.01-0.06	0.29-0.51	No	Park et al. (2015)
36	Pantelleria, Italy	pantellerite	0.47-1.09	0.54-1.3	**YES:** Cl, CO_2, H_2O, S	bdl-0.08	0.77-1.85	Yes	**Lowenstern (1994); Neave et al. (2012);** Lanzo et al. (2013); Gioncada & Landi (2010); **this study for 20 MPa**
38	Quilotoa, Ecuador	rhyolite	0.06-0.2	0.07-0.28	**YES:** H_2O	0.01-0.05	0.11-0.40	No	Stewart & Castro (2016)

42	Satuma-Iwojima, Japan	rhyolite	0.11-0.18	0.16-0.4	**YES:** H_2O	0.018-0.046	0.22-0.56	No	Saito et al. (2001)
43	Shiveluch, Russia	dacite & rhyolite	0.03-0.38	0.01-0.65	**YES:** H_2O, Li	bdl-0.44	0.02-0.92	No	**Humphreys et al. (2008);** Naumov et al. (2008); Tolstykh et al. (2000)
44	Soufriere Hills volcano, Montserrat	rhyolite	0.11-0.52	0.17-0.84	**YES**: Cl, H_2O, CO_2	n.d.	0.24-1.45	Yes	Humphreys et al. (2009; 2010); Mann et al. (2013); Edmonds et al. (2002); **this study for 20 MPa OS conditions**
45	Spor Mtn., Utah, USA	topaz rhyolite	0.17-0.47	0.37-1.29	**NO:** not in prior published work	n.d.	0.51-1.86	Yes	Unpub. data J. Webster; unpub. data C. Mercer et al. (2013); **this study for 20 MPa**
46	Taupo Volcanic Zone, NZ	rhyolite	0.09-0.77	0.21-1.29	**YES**: Cl, H_2O, CO_2	bld-0.01	0.31-1.84	Yes	**Bégué (2014);** Bégué et al. (2015); Saunders et al. (2010); **Johnson et al.** (2011; **2013**); Chambefort et al. 2014); **this study for 20 MPa**
47	Taylor Creek, NM USA	topaz rhyolite	0.02-0.55	0.03-1.18	**NO:** not in prior published work	n.d.	0.03-1.66	Yes	Webster & Duffield (1991; 1994) Duffield & Du Bray (1990); **this study**

									for 20 MPa
48	Toba, Indonesia	rhyolite	0.13-0.21	0.32-0.57	**YES**: Cl, H_2O, CO_2	n.d.	0.46-0.81	No	Chesner & Luhr (2010)
50	Vulcano, Italy	comenditic rhyolite	0.01-0.78	0.02-0.85	**YES:** H_2O, S	n.d.	0.02-1.21	Yes	Gioncada et al. (1998); Frezzotti et al. (2004); **this study for 20 MPa OS conditions**
51	White Island, NZ	alkaline dacite	0.07-0.22	0.06-0.14	**YES**: CO_2	n.d.	0.08-0.19	No	Rapien (1998); Rapien et al. (2003); M. Rowe, unpub. data ; Student & Bodnar (2004)

PLUTONIC SYSTEMS

Magmatic System		**Composition range (based on MI or MG)**	**Range of Cl (wt. %) in MI or MG**	**Range of (measured Cl/modeled Cl) of MI or MG @ NOS conditions**	**Magmatic components used to constrain, chemically, the presence of exsolved brine (HSL) or vapor?**	**Range of SO_2 (wt. %) in MI ± MG**	**Range of (measured Cl/modeled Cl) of MI or MG @ OS conditions**	**Textural ± chemical evidence of magmatic brine (± vapor) ?†**	**References: those discussing *potential* role of brine (HSL) in system are listed in bold font**
Number (from Table 1)	**Location**								
52	Amix Zr-Nb-REE mineralized complex, Namibia	alkaline granite	0.11-0.58	0.2-0.8	**YES:** REE behavior	n.d.	0.28-1.15	No	Schmidt et al. (2002) **; this study for 100 MPa OS conditions**

53	Ascension Island, Atlantic Ocean	granite, F-rich granite	0.25-0.63	0.4-0.8	**YES**: Cl, H_2O, Be, B, Li	n.d.	0.58-1.29	Yes	**Roedder & Coombs (1967); Webster & Rebbert (2001);** Harris (1986); Chamberlain et al. (2016); **this study for 20 MPa OS conditions**
54	Cerro de Pasco Zn-Pb-Ag-Cu-Bi mineralized granites, Peru	syenite/trachyte/ granite	0.06-0.67	0.33-2.8	**YES:** Cl	n.d.	0.4-4.2	Yes	**Rottier et al. (2016); this study for 100 MPa**
57	Deva Cu-Au porphyry, Romania††	granite	0.19-0.36	0.38-0.57	**YES:** Cl	n.d.	0.86-1.3	Yes	**Pintea (2014) ; this study for 100 MPa OS conditions**
58	Dexing Cu-Mo-Au porphyry, China	granite	0.15-0.43	0.24-0.6	**YES:** Cl, S	bdl-0.028	0.55-1.39	Yes	**Bao et al. (2016); this study for 100 MPa OS conditions**
59	Ehrenfriedersdorf granites, Germany	syenite to granite	0.01-0.59	0.01-0.65	**YES:** H_2O, F, P, B, Cl	n.d.	0.02-0.93	No	Webster et al. (1997); Thomas et al. (2000)
61	Oslo rift, Norway	syenite to granite	0.19-0.65	0.47-1.57	**YES:** Cl, S	bdl-0.04	0.68-2.24	Yes	**Hansteen & Lustenhouwer 1990; this study for 100 MPa**
62	Red Mountain Cu porphyry, AZ USA	granite	0.09-0.14	0.23-0.7	**YES:** EPMA H_2O "by difference"	n.d.	0.33-1.01	No	Student & Bodnar (2004)

63	Tyrone Cu porphyry, AZ	granite	0.05-0.58	0.18-1.8	**NO:** not in prior published work	n.d.	0.27-2.6	Yes	Student & Bodnar (2004); **this study for 100 MPa**
64	Zinnwald, Germany Sn-W granites	syenite to granite	0.01-0.59	0.01-0.34	**YES:** H_2O, Li, Cl, F	n.d.	0.01-0.49	No	Webster et al. (2004); Thomas et al. (2005)

MI = melt inclusion, MG = matrix glass
Cl solubility calculated for 20 MPa for eruptive systems and 100 MPa for plutons
n.d. = no data; bdl = below detection limit.
†Physical evidence includes fluid inclusions in phenocrysts, salt crystals in phenocrysts, coexisting melt and fluid inclusions in same growth zones of phenocrysts, systematic variation in melt inclusion bubble volumes, unidirectional solidification textures in rocks, or miarolitic cavities in rocks.
††Na2O values were increased until molar (A/CNK) ratios achieved values similar to those of other porphyritic granites.
If 20 MPa calculated values of Cl[Me/Mo] ≥ 1, then brine ± vapor exsolution indicated for NOS conditions.